

Application of Stiffness/Strength Corrector and Cellular Automata  
in Predicting Response of Laterally Loaded Masonry Panels

Guang Chun Zhou

A thesis submitted to the University of Plymouth for the degree of  
Doctor of Philosophy

School of Civil and Structural Engineering  
Faculty of Technology

January 2002

APPLICATION OF STIFFNESS/STRENGTH CORRECTOR AND CELLULAR  
AUTOMATA IN PREDICTING RESPONSE OF LATERALLY LOADED MASONRY  
PANELS by GUANGCHUN ZHOU

**ABSTRACT**

This research has introduced a new concept, "stiffness/strength corrector", which more accurately models variation in masonry properties at various locations (zones) within a masonry wall panel. Derivation of these correctors was based on a closer mapping of the laboratory experimental results to those obtained from a non-linear finite element analysis of full-scale masonry panels subjected to a uniformly distributed lateral load.

In this research only one panel, which was tested in a previous research, was used as the "base panel" and correctors for new panels with and without openings with various boundary conditions were derived by matching similar regions and zones between the new panel and the base panel.

The research has also derived the concept of zone similarity between the base panel and any new panel. It was discovered that the types of panel boundaries surrounding specific regions within the two panels govern zone similarity. At first, a manual method for matching zone similarity was proposed based on careful visual inspection to identify similar regions within the two panels. It was found that this method is difficult to implement as the user needs to have a deep knowledge of the behaviour of the panel to be able to accurately locate similar regions/zones. As it was established that the zone similarity was mainly related to the panel boundaries, this knowledge was used to derive appropriate rules for matching zone similarity. These rules were implemented in a cellular automata model which was able to automatically locate similar zones between the base panel and a new panel and assign appropriate corrector values to zones within the new panel.

The stiffness/strength corrector values were used to modify global material properties of the panel. A specialised non-linear FEA program for masonry panels was used to analyse a number of panels provided by CERAM with modified rigidities or tensile strength values. Comparison of results with laboratory experimental values shows that with this new method an average 18% improvement in the prediction of failure load, in comparison with the non-linear FEA results with smeared masonry properties, was possible. The failure patterns for the majority of panels with or without openings, having various sizes and boundary conditions, were much closer to the experimental results.

The results of case studies using the new method clearly show that the proposed method is a much better representation of the true behaviour of the masonry panels which models variation in masonry properties and the boundary effects more accurately. The corrector values for any type of new panel are derived from a single base panel in which there was not sufficient data available at different locations on the panel, particularly near the panel boundaries. Thus, in some cases it uses a crude approximation of the boundary types to establish corrector values for a new panel. If sufficient data points were available more accurate results would have been possible to achieve.

## TABLE OF CONTENTS

LIST OF FIGURES.....	VII
LIST OF TABLES.....	XI
SYMBOLS AND NOTATION.....	XII
GLOSSARY.....	XIII
ACKNOWLEDGEMENTS.....	XIV
AUTHOR'S DECLARATION.....	XV
TRAINING.....	XVI
TEACHING WORK.....	XVI
FUNDING.....	XVI
<b>1. INTRODUCTION .....</b>	<b>1</b>
1.1. Tasks Accomplished in the Research.....	1
1.2. Results Achieved in the Research.....	3
1.3. Scope of This Thesis.....	5
<b>2. A HISTORICAL OVERVIEW OF RESEARCH INTO LATERALLY LOADED MASONRY PANELS.....</b>	<b>8</b>
2.1. Introduction.....	8
2.2. The First Period (1950-1968).....	8
2.3. The Second Period (1969-1978).....	10
2.4. The Third Period (1979-1989).....	16
2.5. The Present Period (1990-present).....	20
2.6. Issues Arising from Review of Previous Research.....	26
2.6.1. Facts and Goals.....	26
2.6.2. Issues.....	26
<b>3. TECHNIQUES OF FINITE ELEMENT ANALYSIS FOR MASONRY.....</b>	<b>30</b>
3.1. Introduction.....	30
3.2. The FEA Using Biaxial Stress Failure Criterion.....	30
3.2.1. Development of the FEA Model.....	30

3.2.2. Stress-Strain Models.....	31
3.2.3. Biaxial Stress Failure Criterion.....	32
3.2.4. Modelling of Cracking and Crushing.....	33
3.2.5. Masonry Representation.....	35
3.2.6. Integration Rules.....	36
3.2.7. Non-Linear Algorithms.....	37
3.2.8. Convergence Criteria.....	37
3.2.9. Termination of the Analysis.....	37
<b>3.3. The FEA Using Homogeneous Technique.....</b>	<b>38</b>
3.3.1. Application of Experimental Data.....	38
3.3.2. Homogenisation Technique.....	38
3.3.3. First Stage of Homogenisation-Equivalent Properties of Masonry.....	39
3.3.4. Second Stage of Homogenisation-Modelling of Cracking Masonry.....	40
<b>4. INTRODUCTION OF CONCEPT OF STIFFNESS/STRENGTH CORRECTOR.....</b>	<b>44</b>
<b>4.1. Introduction.....</b>	<b>44</b>
<b>4.2. Significance and Functions of Correctors.....</b>	<b>45</b>
<b>4.3. Introducing Corrector <math>\psi_i</math>.....</b>	<b>46</b>
<b>4.4. Characteristics of Stiffness Corrector.....</b>	<b>49</b>
<b>4.5. Summary.....</b>	<b>52</b>
<b>5. MODELLING SIMILARITY OF ZONES BETWEEN AND WITHIN PANELS</b>	<b>54</b>
<b>5.1. Introduction.....</b>	<b>54</b>
<b>5.2. Similarity of Zones.....</b>	<b>55</b>
5.2.1. Distribution of Correctors on Experimental Panels.....	55
5.2.2. Regions with Similar Corrector Distribution.....	56
<b>5.3. Modelling Similarity of Zones between Two Panels.....</b>	<b>60</b>
5.3.1. Boundary Conditions.....	60
5.3.2. Material Properties.....	61
5.3.3. Load.....	62

5.4. Rules for Matching Similar Zones.....	62
5.5. Procedure for Applying Rules for Matching Similar Zones.....	64
5.6. Summary.....	67
<b>6. APPLICATION OF CELLULAR AUTOMATA IN MODELLING SIMILAR ZONES WITHIN PANELS.....</b>	<b>69</b>
6.1. Introduction.....	69
6.2. Modelling Boundary Effect Using Cellular Automata.....	71
6.2.1. Cellular Automata Model.....	71
6.2.2. Modelling Boundary Effect by Cellular Automata.....	72
6.2.3. Application of CA to Determine Correctors.....	76
6.3. Rules of Matching Zone Similarity .....	76
6.3.1. Pre-Conditions.....	77
6.3.2. Development of Rules for Matching Similar Zones.....	77
6.4. Analysis of Equations for Matching Similar Zones.....	78
6.4.1. Effect of Neighbourhood Orientation in Developing Rules for Matching Similar Zones.....	78
6.4.2. Division of Regions and Method for Matching Their Similarity.....	81
6.4.2.1. Solid Panels.....	82
6.4.2.2. Panels with Openings.....	85
6.5. Investigation into Values of Boundary Parameters and Transition Coefficient.....	89
6.5.1. Characteristics of Transition Function Related to Boundary Parameters and Transition Coefficient.....	89
6.5.2. Parametric Study for Matching Similar Zones Using Different Initial Boundary Parameter Values.....	92
6.5.3. CA Matching Similar Zones of Panels with Openings Using Panel SB02 as the Base Panel.....	97
6.6. Further Improvement of Matching Similarity Method.....	102
6.7. Summary.....	110

<b>7. EFFECT OF CORRECTORS ON DISPLACEMENT PREDICTED USING CORRECTORS.....</b>	<b>112</b>
<b>7.1. Introduction.....</b>	<b>112</b>
<b>7.2. Methods for Improving the FEA of Masonry Panels.....</b>	<b>113</b>
<b>7.3. Improved Panel Displacement Using Correctors.....</b>	<b>114</b>
<b>7.4. Investigation into Effect of Introducing Noise at Local Zones within the Panel.....</b>	<b>119</b>
7.4.1. Changes in Displacement Pattern Due to Introducing Noise.....	120
7.4.2. Effect of Region Size.....	122
7.4.3. Analytical Summary.....	123
<b>7.5. Comparison of Experimental and Analytical Displacements on Panels with and without Openings.....</b>	<b>123</b>
<b>7.6. Summary.....</b>	<b>130</b>
<b>8. CASE STUDY ON PREDICTING FAILURE LOAD AND FAILURE PATTERN OF MASONRY WALLS USING CORRECTORS.....</b>	<b>132</b>
<b>8.1. Introduction.....</b>	<b>132</b>
<b>8.2. Predicting the Failure Load and Failure Pattern of the Base Panel SB01..</b>	<b>134</b>
8.2.1. The FEA Result Using Biaxial Stress Failure Criterion.....	134
8.2.2. The FEA Result Using Homogeneous Technique .....	136
<b>8.3. Case Study of Predicting Failure Loads and Failure Patterns Using Correctors.....</b>	<b>137</b>
8.3.1. Panel SB06.....	138
8.3.2. Wall 1a. Control.....	141
8.3.3. Wall 2a. Control.....	144
8.3.4. Wall Case 7. Control.....	147
8.3.5. Wall 1a (ii) with Opening.....	150
8.3.6. Wall 2a (i) with Opening.....	153
8.3.7. Panel SB02 with Opening.....	155
<b>8.4. Homogeneous Technique.....</b>	<b>156</b>
8.4.1. Panel SB06.....	157

8.4.2. Wall 1a. Control.....	159
8.5. Summary.....	161
9. ONCLUSIONS AND PROPOSALS FOR FUTURE RESEARCH.....	163
9.1. Conclusions.....	163
9.2. Proposals for Future Research.....	166
REFERENCES.....	169
APPENDIX A: THE CORRECTOR DATA AND LOAD-CORRECTOR DIAGRAMS DERIVED FROM THE BASE PANEL SB01.....	175
APPENDIX B: LOAD-DISPLACEMENT CURVES.....	178
APPENDIX C: CORRECTORS SELECTED BY THE CA.....	184

## LIST OF FIGURES

3.1	The procedure of experimental and theoretical analysis using the biaxial stress failure criterion.....	31
3.2	Uniaxial stress – strain relationship.....	32
3.3	Complete biaxial failure criterion.....	34
3.4	The planes through the depth of element.....	36
3.5	The procedure of experimental and theoretical analysis using homogeneous techniques.....	38
3.6	Representation elementary volume including a crack.....	42
4.1	Procedure of producing correctors and their application.....	46
4.2	The standard panel SB01.....	50
4.3	Load – Modified Modulus $E'$ curves of Points A5-D5 on the panel SB01.....	51
4.4	Load – Modified Modulus $E'$ curves of Points B1-B5 on the panel SB01.....	51
5.1	Contour graph of correctors of Panel SB01.....	56
5.2	Contour graph of correctors of Panel SB06.....	57
5.3	Comparison of similar regions between Panels SB01 and SB06.....	58
5.4	Contour graph of correctors of Panel SB02 with opening.....	59
5.5	Similar zones between Panels A and B.....	61
5.6	Manually matching similar zones using a geometrical method.....	66
5.7	Matching similar zones using an analytical method.....	66
6.1	Cellular Automata Neighbourhoods of von Neumann and Moore.....	71
6.2	Panel is modelled as a CA system.....	73
6.3	Divided zones of Panel SB01 around every measured points.....	79
6.4	State values of Zones D2 and D8 as well as their neighborhood zones.....	80
6.5	State values of Zones C1 and C9 as well as their neighborhood zones.....	81
6.6	Example of matching similar regions.....	83
6.7	The division of regions of a new panels with opening.....	85
6.8	Similar zones between the panel with opening and solid panel SB01.....	85-86
6.9	Investigation into initial values describing boundary types.....	90
6.10	Investigation into transition coefficient.....	91
6.11	Investigation into proper boundary parameters.....	93-95



6.12	Investigation into proper boundary parameters.....	95-97
6.13	Similar zones between the base panel SB02 and a new panel.....	98
6.14	Investigation into proper boundary parameters.....	99
6.15	Investigation into proper boundary parameters.....	100-101
6.16	Investigation into proper boundary parameters.....	101-102
6.17	Case 1 : Orientation of the new panel to the base panel.....	104
6.18	Case 2 : Orientation of the new panel to the base panel.....	104
6.19	Case 3: Orientation of the new panel to the base panel.....	105
6.20	Case 4: Orientation of the new panel to the base panel.....	105
6.21	Case 5: Orientation of the new panel to the base panel.....	106
6.22	Case 6: Orientation of the new panel to the base panel.....	106
6.23	Case 7: Orientation of the new panel to the base panel.....	107
6.24	Case 8: Orientation of the new panel to the base panel.....	107
6.25	Matching similar zones using Equations (6.5) – (6.13).....	108
6.26	Matching similar zones using Equations (6.5) – (6.13).....	109
6.27	Matching similar zones using Equations (6.5) – (6.13).....	109
6.28	Matching similar zones using Equations (6.5) – (6.13).....	109
7.1	Procedure of the FEA using correctors.....	114
7.2	The two cases of zones division of Panel SB01.....	115
7.3	The displacement-load curves of Point A5 within Panel SB01.....	116
7.4	The displacement-load curves of Point B3 within Panel SB01.....	117
7.5	The displacement-load curves of Point B4 within Panel SB01.....	117
7.6	The displacement-load curves of Point B5 within Panel SB01.....	118
7.7	The displacement-load curves of Point C5 within Panel SB01.....	118
7.8	Divided zones of Panel SB01.....	119
7.9	Displacement ratio – $E$ ratio curves of Point A5 on Panel SB01.....	120
7.10	Displacement ratio – $E$ ratio curves of Point B3 on Panel SB01.....	121
7.11	Displacement ratio – $E$ ratio curves of Points A5, C5, D5 and B3 on Panel SB01 to $E$ noise at Region 1.....	121
7.12	Displacement ratio – $E$ ratio curves of Points A5, C5, D5 and B3 on Panel SB01 to $E$ noise at Region 3.....	121

7.13	Displacement ratio – $E$ ratio curves of Points A5, C5, D5 and B3 on Panel SB01 to $E$ noise at Region 2.....	122
7.14	Displacement ratio – $E$ ratio curves of Points A5, C5, D5 and B3 on Panel SB01 to $E$ noise at Region 4.....	122
7.15	Sizes of the region near the bottom support of the panel.....	122
7.16	Displacement ratio – $E$ ratio curves of Point D5 on Panel SB01 to $E$ noise and three different region sizes.....	123
7.17	Displacement ratio – $E$ ratio curves of Point A5 on Panel SB01 to $E$ noise and three different region sizes.....	123
7.18	Panel SB02 with opening.....	125
7.19	Load – displacement curves of Point B3 on Panel SB02.....	125
7.20	Panel SB05 with d.p.c.....	126
7.21	Load – displacement curves of Point A3 on Panel SB05.....	126
7.22	Panel SB06.....	127
7.23	Load – displacement curves of Point C3 on Panel SB06.....	127
7.24	Panel CB01.....	128
7.25	Panel CAV14.....	128
7.26	Load – displacement curves of Point F on Panel CAV14.....	129
7.27	Load – displacement curves of Point C on Panel CAV14.....	129
8.1	The predicted and experimental failure loads and failure patterns of Panels SB01 and SB05 (the FEA using biaxial stress failure criterion).....	135
8.2	The predicted and experimental failure loads and failure patterns of Panel SB01(the FEA using homogeneous techniques).....	137
8.3	The FEA and experimental results of Panel SB06.....	139-140
8.4	The FEA and experimental results of Panel Wall 1a. Control.....	143-144
8.5	The FEA and experimental results of Panel Wall 2a. Control.....	146-147
8.6	The FEA and experimental results of Panel Wall Case 7. Control.....	148-149
8.7	The FEA and experimental results of Panel Wall 1a (ii).....	152-153
8.8	The FEA and experimental results of Panel Wall 2a (i).....	154
8.9	The FEA and experimental results of Panel Wall 1a. Control.....	156

8.10 The failure load and failure pattern of Panel SB06 (the FEA using homogeneous techniques).....158

8.11 The failure load and failure pattern of Panel Wall 1a. Control (the FEA using homogeneous techniques).....160

## LIST OF TABLES

5.1	The correctors of Panel SB01.....	55
6.1	State values from Equations (6.2) and (6.3).....	76
6.2	State values of Panel SB01 calculated using Equation (6.3).....	80
6.3	Errors of Zone D2 to all other zones calculated using Equation (6.4).....	80
6.4	State values of Panel SB01 calculated using Equation (6.3).....	80
6.5	Errors of Zone C9 to all other zones calculated using Equation (6.4).....	81
6.6	State values of zones in and around Region A calculated using Equation (6.3).....	84
6.7	State values of zones in and around Region B calculated using Equation (6.3).....	84
6.8	Errors of Zone D2 to all zones in Regions A and B using Equation (6.4).....	85
6.9	Errors of Zone C9 to all zones in Regions A and B using Equation (6.4).....	85
6.10	State values of the new panel with opening.....	87
6.11	State values of Panel SB01.....	87
6.12	Errors of Zone B8 in the new panel to all Zones in Region B in the base panel SB01 using Equation (6.4) with considering orientation of region.....	88
6.13	Errors of Zone B8 in the new panel to all Zones in the base panel SB01 using Equation (6.4) without considering orientation of region.....	88
6.14	State values of Panel SB01.....	88
6.15	Errors of Zone A1 in the new panel to all zones in Region A in the base panel SB01 using Equation (6.4) with considering orientation of zone.....	88
6.16	Errors of Zone A1 in the new panel to all zones in the base panel SB01 using Equation (6.4) without considering orientation of zone.....	89
8.1	The correctors of Panel SB02 under load $q = 2.2 \text{ kN/m}^2$ .....	150
8.2	The correctors of Panel SB01 (the FEA using homogeneous technique).....	157

## SYMBOLS AND NOTATION

$E$	Elastic modulus
$E'$	Modified elastic modulus
$[K]$	Stiffness matrix
$\{\Delta W\}$	Vector of displacement
$\{\Delta P\}$	Vector of Load
$D$	the flexural rigidity
$\Psi_i, 1/R_i$	Corrector/stiffness corrector/strength corrector
$\sigma_x, \sigma_y$	Stresses in the directions $x, y$
$\nu$	Poisson's ratio
$\tau_{xy}, \tau_{np}$	Shear Stresses, n-normal to the crack direction, p-parallel to the crack direction
$\gamma_{xy}, \gamma_{np}$	Shear strains
$\varepsilon'_{xj}, \varepsilon'_{yj}$	Strains in the directions $x, y$ at Point $j$ from the new method in this report
$\alpha$	Angle between the maximum prescribed stress and the bed joints
$\sigma_1, \sigma_2$	Principal stresses
$\sigma_{1\alpha}, \sigma_{2\alpha}$	Principal stresses at an angle $\alpha$
$\theta$	Rotation angle
$f'$	Modified strength
$f_u, f_b$	Uniaxial tensile and compressive strengths
$x, y, z$	Co-ordinate axes
$TOD, TOR$	Convergence tolerances for iterations
$S_{ij}$	State value of a zone within a panel
$\eta$	Transition coefficient

## GLOSSARY

**arching effect:** a phenomenon like an arch which is formed in a masonry panel subjected to lateral pressure and built into a steel or concrete frame which provides non-yielding supports

**aspect ratio:** ratio of panel length to panel height

**axial:** adj. of axis

**built-in support:** a support at an edge of a wall panel that its movement normal to the surface and rotation about all axes of the wall panel are constrained

**d.p.c:** (bituminous) damp proof course

**failure load:** maximum load capacity of a wall panel

**failure pattern:** a figure formed from cracking lines on a wall panel

**free edge:** an edge which is not constrained by any support

**lateral load:** force normal to the surface of a wall panel

**panel:** an area of brickwork with defined boundaries, usually applied to walls resisting predominantly lateral loads

**perpend:** the vertical joint between brick units in the face of a wall

**region:** a specified part on a wall panel

**return:** wall or pier perpendicular to the plane of the panel

**similar zones:** some parts on a wall panel with the same corrector value

**simple support:** a support at an edge of a wall providing restraint to the movement normal to the surface of the wall, but not rotation

**stiffness/strength correctors:** parameters to model variation in masonry properties, which are related to structural factors such as boundary conditions of the masonry panel

**wallettes:** small walls which are used to test the flexural strengths in two perpendicular directions

**zone:** a small part within a region (a region could include a number of zones)

## ACKNOWLEDGEMENTS

The Author acknowledges with deep thanks the financial support given by Faculty of Technology at University of Plymouth for the study of the application of stiffness/strength corrector and cellular automata in the finite element analysis (FEA) of laterally loaded masonry panels.

The Author also would like to mention with deep thanks the following people for their excellent supervision, encouragement and contributions during the course of the research: Dr. M. Yaqub Rafiq, Dr. Guido Bugmann, Mr. Dave Easterbrook and Prof. John Menzies. Particular thanks is extended to them for the many challenging discussions held and for their academic and technical guidance. Particular acknowledgement and thanks are given to Dr. Rafiq in the introduction of stiffness/strength correctors and their application. In particular the successful application of cellular automata in this project benefits the most from Dr. Bugmann. Particular acknowledgement and thanks is also extended to Mr. Easterbrook for all his help in my study and life, together with other supervisors of mine.

During my study, Mr. C. Southcombe, Prof. J. Menzies, Prof. G. Edgell, Prof. S. J. Lawrence provide their experimental materials and results of theoretical analysis, and Mr. C. Southcombe, Prof. G. N. Pande and his Ph.D student H. S. Shin offer their computer programmes FEAMN.FOR and STRUMAS for masonry structures. The author acknowledges their contribution to my study with sincere thanks.

Besides, the deep thanks is given for Dr. C. Williams, head of the school, to offer all the necessary supports in my English improvement and research work together with my supervisors.

Finally, particular thanks is extended to my wife, Jing Lee, my parents, and other relatives of mine whose love, encouragement and help is gratefully acknowledged. My lovely daughter, Mo Zhou, is also an important driving force of my study.

## AUTHOR'S DECLARATION

The work described in this thesis was carried out in the school of Civil and Structural Engineering at the University of Plymouth. At no time during the registration for the degree of Doctor of Philosophy has the author been registered for any other University award. All the material described herein is the original work of the author unless otherwise acknowledged.

Signed Guanghui Zhou Date 8/4/2002



## **TRAINING**

The following modules from the University of Plymouth B. Sc Computer Science degree course were attended during this research:

“Neural Computation”, School of Computing (**Dr. G. Bugmann**)

## **TEACHING WORK**

Tutorial of Structural Analysis.

Experiment of Truss Structure.

## **FUNDING**

The University of Plymouth provided financial support for this research.

# 1. INTRODUCTION

## ***1.1. Tasks Accomplished in the Research***

The increasing use of masonry as a structural material, particularly in new applications such as its use as prestressed forms, and the incidents arising from improper use of masonry continually require research to provide accurate and convenient design methods involving many complex cases based on theoretical analysis and experimental results. One of these areas is the effect of lateral loads from wind forces or incidental loads such as the effect of explosion on masonry structures.

Research on masonry panels subjected to lateral loading was mainly covered from around 1970 to the present day, although initial research on the subject began in 1950s. During the 1970s and 1980s, researchers, such as Baker (1972, 1973, 1980, 1982), Lawrence (1980, 1983), West (1971, 1973, 1974, 1975, 1976, 1979) and Anderson (1984, 1985, 1987) comprehensively studied many aspects of laterally loaded masonry panels, such as aspect ratio, flexural strength, orthogonal strength ratio and other factors affecting the response of masonry panels. They proposed theoretical methods for the analysis and design of masonry panels based on many experiments on masonry units, wallettes and full-scale panels. In 1989, Fried (1989) summarised the then existing experimental and analytical results and gave a clear state of research results at that time. After 1990, the main research into laterally loaded masonry panels was the study of the behaviour of masonry panels with openings. These studies were conducted by Chong (1993), Ronald (1996) and Edgell (Edgell). The researches can be considered to consist of:

- A large number of experiments on small masonry specimens/wallettes have been tested to determine flexural strength, modulus of elasticity and other properties of masonry materials. The most important parameters for the masonry material properties were obtained from the statistical analysis of a large amount of laboratory experimental data. These parameters were then used in the design and analysis of masonry panels.
- Four methods of analysis were proposed for the design and analysis of laterally loaded masonry structures; (1) The Yield Line Theory, (2) The Fracture Line Theory, (3) The Empirical Strip Method and (4) The Finite Element Analysis. Among these methods, the FEA techniques for masonry proved to be much better in predicting both failure load and failure pattern of masonry panels (Chong 1993) (Lee et al. 1996).
- The experimental data for testing of full-scale masonry panels was used to verify the flexural strength of masonry panels and the validity of calculation methods.

Although the research in this field has achieved many important results, the inaccurate design and analysis of masonry panels continuously require the researchers to provide more accurate and reliable methodologies for the prediction of behaviour of masonry panels. These include:

- The masonry properties still need to be further modelled and verified in variable surroundings.
- The analytical methods for masonry still need to be further examined and improved in order to make the prediction of failure loads and failure patterns of masonry panels closer to their experimental results.

- The experiments on masonry specimens/wallettes/full-scale panels are still needed to support new analytical techniques.

## **1.2. Results Achieved in this Research**

This research proposed a new approach in modelling of masonry panels in order to achieve an accurate prediction of both failure load and failure pattern of laterally loaded masonry panels based on the existing experimental data, obtained from the full-scale testing of masonry panels, and the FEA modelling of masonry. In the past a great deal of research pointed towards the suggestions that an accurate prediction of failure load and failure pattern of the panel needs to consider the variation in masonry properties within a panel. The current research has established that the boundary effect, in parallel with the variation in masonry properties, has a critical effect on the behaviour of masonry panels.

In this thesis a new technique has been proposed which introduces a corrector concept that quantifies the effect of the variation in masonry properties. The corrector values are derived from the comparison between the analytical displacements at individual zones on the full-scale masonry panels with & without openings and the corresponding laboratory experimental data. Therefore the corrector values are related to the positions of various zones within the masonry panel. It was also found that boundary types closer to various zones have great influence on the corrector values. Based on this finding, this thesis has established the relationship between this quantitative variation (corrector) and the effect of boundary condition on the behaviour of the panel.

In order to apply correctors derived from a base panel (the standard experimental panel) to improve the FEA of a new panel, a definition for zone similarity was introduced that: two zones are similar if they have the same corrector value. To identify similar zones between/within panels and to quantify values of correctors for these zones, rules for matching similar zones were proposed. Based on these rules, a method was developed to manually select appropriate values of correctors from the base panel for similar zones on a new panel and then the correctors are used to modify the global flexural rigidity/tensile strength of the new panel. Finally, these modified flexural rigidities/strengths are used to improve the FEA result of the new panel.

However, the proposed method for matching similar zones was not easy to implement as mapping the division of zones within a base panel and a new panel required an in-depth understanding of the influence of boundaries on local zones. There was a need for developing a comprehensive automatic technique to divide the panel into zones, to match the similar zones between the new panel and the base panel, and to select appropriate corrector values for the FEA of the new panel.

This research has presented modelling of boundary effect using technique of Cellular Automata (CA). Based on the proposed rules for matching similar zones, the proposed CA method automatically matches similar zones between a new panel and a base panel.

In the thesis, two different specialised FEA softwares for masonry were used to predict the behaviour of the masonry panel. The non-linear FEA technique using the biaxial stress failure criterion (Chong 1993) has shown to give better results when modifying the global flexural rigidity  $D$ /modulus  $E$  at various local zones within the

panel. The FEA technique using the homogeneous technique (Lee et al. 1996) has shown to give better results when modifying the global tensile strength  $f$  at various local zones within the panel.

In total, application of correctors has proved to greatly improve the FEA prediction of both failure loads and failure patterns of laterally loaded masonry panels. Besides, introduction and application of correctors suggests further research projects on both theory and experiment in the research field.

### **1.3. Scope of This Thesis**

*Chapter 1:* It has introduced the main research results in the thesis, which includes the background of the research, the problems to solve, the methodologies of solving the problem and the result of investigation into the methodology.

*Chapter 2:* A review on research into laterally loaded masonry panels has been made to raise issues involved in the thesis. Two key factors, variation in masonry properties and boundary conditions, which greatly affect the accuracy of the FEA prediction of masonry panels, were highlighted using the existing research results in the past 30 years.

*Chapter 3:* It has reviewed two existing FEA techniques for masonry, one using the biaxial stress failure criterion and another using homogeneous techniques. These two FEA techniques were used in the following research on masonry panels subjected to lateral loading.

*Chapter 4:* Based on the issues in Chapter 2, it has proposed a new concept, corrector, which can qualify the variation in masonry properties at various local zones within a panel. Then the investigation into the characteristics of corrector has discovered that the corrector includes all relevant factors which affect the behaviour of the panel, among them, boundary effect is most important.

*Chapter 5:* It has investigated the distribution of correctors on several typical experimental panels. A characteristic has been discovered: if two zones within the panels are governed by similar boundary types and located at similar positions on the panel, the two zones have the same corrector value. Based on the finding, the rules for matching such similar zones have been proposed and a corresponding method has been developed in order to manually select correctors from the base panel for the FEA of new panels.

*Chapter 6:* To overcome the difficulty of manually matching similar zones, cellular automata were used to model the boundary effect on zones within the panel. Based on state values of various zones, calculated by the proposed CA equations, corresponding rules and the equations for automatically matching similar zones are introduced and initial values for boundary types and transition coefficient the accurate matching similar zones are verified.

*Chapter 7:* It has investigated the effect of correctors on the FEA displacement of the panel when the selected correctors were used to modify globally smeared modulus  $E$  of the masonry panel. Besides it has verified the effect of random noise, which

modifies the stiffness of a local zone within the panel, on the FEA displacement of the panel.

*Chapter 8:* It has investigated the effect of correctors on the FEA prediction of both failure load and failure pattern of laterally loaded masonry panels. Two FEA programs, one using the biaxial stress failure criterion and another using the homogeneous technique, were separately used to predict the failure load and failure pattern of the masonry panels and the corresponding results were compared. In the analysis, correctors were separately used to modify globally smeared modulus  $E$  or tensile strength  $f$ , and the corresponding FEA results were compared. Meanwhile, it has also verified the effect of correctors, selected by the manual method and the CA method, on the FEA results.

*Chapter 9:* It has made conclusions and proposals for the further research in the field.



## **2. A HISTORICAL OVERVIEW OF RESEARCH INTO LATERALLY LOADED MASONRY PANELS**

### ***2.1. Introduction***

This chapter reviews the research into laterally loaded masonry panels, both in the UK and around the world. The review is divided into four stages, 1950-1968, 1969-1978, 1979-1989 and 1990-present. The review focuses on the techniques proposed for predicting failure load and failure pattern of the masonry panel and the relevant factors affecting the predicted results. Special attention has been devoted to the FEA techniques because of their more reliably and reasonably theoretical basis. By reviewing these existing theoretical and experimental results, critical issues addressed by researchers are highlighted and major issues, which are the focus of the research in this thesis, are identified.

### ***2.2. The First Period (1950-1968)***

Before 1970, little information was available on laterally loaded masonry panels. Indeed, there was little information available on masonry structures as whole. Between 1950 - 1970, a number of research programmes were initiated to study the behaviour of masonry panels in the UK and around the world. Although results from these experiments were not conclusive to be included into the Codes of Practice for masonry structures, they marked the beginning of a wider range of useful research in this area.

In 1950, Davey and Thomas (1950) reported results of their research into laterally loaded walls supported on all four sides. They indicated that there would be no

reserve of strength left in a masonry panel after it cracked. They also stated that a pattern of cracking similar to a yield line was observed to develop.

In 1953, Thomas (1953) reported the effect of arching formation and existence of a reserve of strength due to arching formation after cracking on several laterally loaded brick walls. Plumer and Blume (1953) in the same year in the USA, discussed the common characteristics of lateral forces on panels induced by wind and explosion in general terms.

In 1961 in the USA, Fishburn (1961) and Hedstrom (1961) conducted experiments on the behaviour of concrete block masonry walls under lateral loading. They concluded that the orthogonal strength ratios of the wall varied from 2.2 – 3.6.

In 1962 in the USA, Plumer (1962) outlined a theoretical view of the resistance of brick walls to lateral loads by arching action, and the results of experiments on six wall tests demonstrated that the arching resistance of brick masonry was many times its bending resistance.

In 1964 in Sweden, Losberg and Johnsson's (1964) experiments on walls supported along all four edges showed that under the action of lateral load an initial cracking stage was followed by ultimate load, when the load remained constant under increasing deflections. Because the fracture lines resembled yield lines on a plate, yield line analysis was applied to the panels which gave reasonable predictions of the ultimate load. The authors recognised that the brittle nature of masonry would prevent true yield lines to be developed in the masonry panels.

In 1965 in Britain, Bradshaw and Entwistle (1965) presented preliminary guidelines on the wind forces on non-loadbearing brickwork panels. They emphasised the importance of good bond between brick and mortar, and proposed moment coefficients for design of walls with various edge conditions. They recommended that the permissible tensile stresses perpendicular and parallel to bed joints should be limited to  $0.07\text{N/mm}^2$  and  $0.14\text{N/mm}^2$  respectively. This gives an orthogonal strength ratio of 2.0.

In 1967 in Britain, Monk and Allen (1967) tested walls without axial compression on hollow clay blocks, using an air-bag to apply a lateral load. They discovered that the criterion for failure was the first appearance of the opening of the horizontal joint at the mid-depth.

From the above research, the basic issues, which are still relevant in the research of masonry panels today, were put forward at that time. These issues include: the magnitude of ultimate load, the orthogonal strength ratio and the criterion for failure of the panel.

### ***2.3. The Second Period (1969-1978)***

The serious research into the lateral resistance of masonry walls started after the Ronan Point accident in 1968. The accident report suggested the need for the revision of wind loads in the then Code of Practice CP3 (Hendry 1996). After 1970, a number of analytical techniques for predicting the failure load of masonry panels were proposed and critically examined in parallel research by various researchers both in the UK and other countries. These methods were based on the experiments of

masonry units, mortar and wassettes to determine the properties of masonry materials and the experiments of full-scale masonry panels to confirm the validity of the proposed analytical methods. The main analytical methods proposed, according to Fried's review (1989), were the Yield Line Method, Empirical Strip Analysis Method, Elastic Plate Theory, Fracture Line Method, Principle Stress Method and Energy Method. A precise determination of the ownership of these methods is very difficult. This review is mainly interested in the application of these analytical techniques.

In 1969 in the USA, Grenley et al. (1969) presented results of the lateral load tests on 36 walls of storey-height, constructed from three types of bricks and high-strength mortars. The relationship between compressive load and lateral load was studied in this research. It is important to note that extending the theory of failure based on the high-strength mortars is not valid in the type of walls built of conventional mortars with little tensile strength.

In 1969, both America and Australia published their first codes for brick walls on lateral loading, "Building Code Requirements for Engineered Brick Masonry" in America (Structural Clay Products Institute 1969) and Standards Association of Australia "S.A.A. Brickwork Code" in Australia (Standards Association of Australia 1969). The American code proposed design recommendations on lateral loading. The Australian code provided little guidance on lateral loading, but this code included provision for on-the-site controlled testing of tensile bond using stack-bonded piers tested as beams.

In 1970, The publication of CP111; part 1 (British Standards Inst. 1970) in the UK gave initial design guidance on the values of tensile strength of masonry, but this code discouraged its use.

In 1971 in Britain, West et al. (1971) carried out an extensive programme of experiments on over 100 walls to study the lateral-load resistance of the walls. These walls were of different lengths both with and without returns. Different brick and mortar types were examined in different constructions, including single leaf, double leaf and cavity. The results obtained in this research can be summarised as: (a) the compressive strength of the constituent bricks and mortar used had a negligible influence upon the lateral resistance of the wall; (b) the effect of returns changes the mode of failure to a yield-line pattern; (c) the three-pinned arch method of calculation is no longer applicable in this case, although it might be used as a conservative means of approximation. Among these results, the conclusion (b) implies that failure pattern is sensitive to boundary change.

In 1972 and 1973, Baker (1972, 1973) provided a simplified strip method of analysis and compared the experimental results respectively with his strip method, with elastic isotropic plate theory after the panels had cracked but not collapsed, with yield line theory and with tabulated elastic moment coefficients. His analysis showed that; elastic plate theory generally underestimated ultimate load; the elastic analysis of cracked panels was inconsistent; yield line consistently overestimated strengths; and his tabulated moment coefficients were always conservative. His empirical strip method was recommended as the most reliable method at that time, providing conservative estimates for three sided panel support and reasonable estimates of panel

strength with four sided panel supports. In 1980, Baker (1980) summarised his work on lateral loaded walls which included a slightly refined form of strip method. At the same time of Baker's research, James (1978) and Lawrence (1980) analysed the results of their tests on the panels using Baker's strip method. James found reasonable agreement for the four-sided panel but the predictions for panels supported along two or three edges were conservative. Lawrence found that this method gives inconsistent results and, in some cases was unsafe, not employing the stress averaging technique.

In 1973, Hendry (1973) reviewed the available information regarding flexural strength and lateral loading in the UK. He indicated that reasonable agreement between his test results and the yield line method could be obtained if the strength perpendicular to bed joints was taken to be the same as that parallel to bed joints. He also indicated that both yield line (if correctly applied) and elastic theory gave conservative predictions of panel strengths. His load predictions using the elastic theory agreed with Baker's findings, but the conservative predictions of the load capacity of walls using the yield line method were contrary to Baker's observations.

In 1973, West et al. (1973) presented the results of fourteen panel tests, carried out with various support conditions, materials and window openings. Haseltine and Hodgkinson (1973) used these experimental results to test the validity of both the elastic plate and yield line theories. Both were found to underestimate wall strengths contrary to the findings of Baker (1972, 1973).

In 1974, West et al. (1974) tested the lateral resistance of fifteen clay brick walls with various boundary conditions when carrying a compressive axial load. The

experimental results showed that the mortar composition is important in determining the failure load. Highest strengths were obtained when bending could take place in both the directions perpendicular to and parallel to the bed joints.

In 1975, West et al. (1975) conducted a large programme of experimental work using wallettes and full-scale walls. In this research, the relationship between lateral load resistance and wall length was studied for full-size walls and the effect of d.p.c was shown to be critical. Based on the results of the tests on twenty-six wallettes constructed from each of different brick type, it was found that the ratio of ultimate flexural strength in the two orthogonal directions varied between 1.5 to 5.0. The mean orthogonal ratio was shown to be 3.02. In this experiment, only one mortar type was used for all walls. A comparison of bending moments obtained from the yield line theory and the experimental results showed good agreement, with the yield line always being conservative by 8.0% average. This research also showed that boundary conditions are critical to the response of the panel (the effect of d.p.c).

In 1976, West (1976) and Haseltine (1976) investigated the flexural strength of brickwork normal and parallel to the bed joints. A wide variety of bricks and standard 1:1/4:3 and 1:1:6 cement: lime: sand mortars were studied. The type of mortar had no significant influence on the flexural strength normal to the bed joint, but parallel to the bed joint the stronger mortar gave the higher flexural strength. The factors by which the test results on the lateral strength of full-scale walls exceeded the design strength, calculated from the characteristic flexural strength and yield line theory, were tabulated. From this work it was shown that the yield line theory gives a realistic method of design.

In 1976, Cajdert and Losberg (1976) published results of their lateral load tests on brick panels simply supported on all four sides and the prediction of the first cracking load was made by the elastic plate theory. Hendry and Kheir (1976) found that the elastic plate theory underestimated test results by a large margin at higher aspect ratios and that yield line provided slightly conservative estimates of test strengths. Hendry and Kheir suggested that although application of the yield line method lacked rational basis, it should be used for the time being, implying the need to confirm that yield line theory could be used for all boundary conditions.

In 1978, the first version of the new limit state British Masonry Code, BS 5628: Part 1 (British Standards Institution, BS 5268: Part 1:1978, 1978. Latest update March 1985) was published. In this code, two design methods for laterally loaded walls were introduced. The first method was based on the yield line theory, assuming constant moments of resistance along yield lines, although there appears to be no justification for the use of such a theory because of the lack of ductility of masonry. The second method employs arching theory which allows a masonry panel to act as an arch between suitable rigid supports; however in practice it is often difficult to provide such support.

In 1978, Sinha (1978) proposed a modified yield line approach in which he assumed that the load was distributed in proportion to the stiffness in the two principal directions. Very good agreement between experimental results and theory using 1/3 scale bricks was obtained. Conventional yield line theory was shown to overestimate test results. He pointed out that flexural properties obtained from specimens tested



using central line loads might not reflect actual wall flexural strengths and also the moduli of elasticity were based on compression tests.

From the above research results, the most important finding in this stage was the introduction of a number of analytical methods for calculation of failure loads of masonry panels under lateral loading. The results were included in the masonry design code. Some important conclusions drawn from this stage can be summarised as:

- The compressive strength of the constituent bricks and mortar used has no effect on the lateral resistance (West et al. 1971).
- The yield line theory usually provided underestimates of load capacity of walls (Hendry 1973) (Haseltine and Hodgkinson 1973) (West et al. 1975) (West 1976) (Cajdert and Losberg 1976), but sometimes it overestimated failure loads of walls (Baker 1972, 1973) (Sinha 1978).
- Boundary conditions have strong effect on the lateral load resistance of the panel (West et al. 1971) (West et al. 1975).

These conclusions provided the background for the further research in laterally loaded masonry panels.

#### ***2.4. The Third Period (1979-1989)***

The publication of BS 5628 in 1978 undoubtedly stimulated the substantial research into laterally loaded masonry panels, because researchers further found that the yield line theory proposed in BS 5628 predicted failure loads of masonry panels inaccurately, when compared with the corresponding experimental results. At the same time, two new analytical methods, Principle Stress Method (Baker 1982) and Energy Method (Candy 1988), were developed.

In 1979, West et al (1979a) investigated the behaviour of calcium silicate and clay brickwork panels supported along three sides but free along one vertical side. In this experiment, flexural properties were obtained using the test data from wallettes. In this study, strength values obtained from wallette tests were used in the yield line technique to make reasonable predictions of wall failure loads. This research showed that the yield line predictions overestimated actual wall strengths at low aspect ratios, and reasonably predicted wall strengths if partial rotation restraint along the supported panel side was included.

In 1980, Cajdert (1980), in an extensive study of many aspects of masonry, recommended the use of the yield line techniques for the prediction of the ultimate load of masonry panels and the use of elastic plate theory for predicting the first cracking load. Both techniques gave reasonable estimates for the masonry panels presented in his research.

In 1982, Baker (1982a, b) developed a principal stress method to predict the lateral load capacity of brick walls based on the principal moments in the panel, and on a partially plastic failure criterion. The theory also makes allowance for variable joint strengths in the panel. Baker compared his theoretical predictions with test results. He found that his theory generally overestimated experimental cracking loads but that the prediction of ultimate load for the particular case of panels supported along all four sides was reasonably accurate.

In 1983, Gairns (1983) compared load predictions obtained using the principal stress method with test results using concrete blockwork and found out that the load predictions underestimated test results. In the same year, Lawrence (1983) compared clay brick wall test results with the predictions using the principal stress method and found that for panels supported along four edges, the predicted cracking loads were not generally in agreement with the test results. Lawrence also observed that predicting cracking loads using elastic plate theory, but ignoring built-in supports, gave better agreement with test results than predicting this load by Baker's theory.

In 1984, Brinker (1984) and Anderson (1984, 1985a, 1985b, 1987) supported the application of the yield line theory as a design method for laterally loaded masonry walls. However, Anderson noted that the yield line theory overestimated the strength of walls with continuity over supports and underestimated the strength of walls with arching restraint.

In 1984, Ma and May (1984) compared a number of test results on the strengths of panels with a proposed finite element technique and with the yield line method. They concluded that in general the design method given in BS 5628: Part 1 overestimated the collapse load of panels particularly when the aspect ratio (ratio of panel length to panel height) was less than 1.0.

In 1988, Candy (1988) used the energy method and compared predictions from 110 test walls with his theory. He found that the predicted failure load was about 74% of the experimental failure load. The scatter of the results by his method was

significantly less than that by the Strip Method. Candy did not, however, establish the theoretical basis for his theory nor were the material properties consistent.

In 1989, Fried (1989) repeated the results of more than forty experiments and the analytical results of the masonry elements and panels in these experiments in his Ph.D thesis. He also produced a summary of the calculation methods for the design and analysis of masonry panels in the UK, Canada, the USA, Australia, Sweden and other countries, since 1932.

Fried pointed out that masonry research had been predominantly experimental rather than theoretical because of the difficulties involved in analysing panels built with two completely different components, which when combined together produced a highly variable composite materials. The purpose of the experiments was to confirm the flexural strength and the first cracking of the masonry structures and the factors which affect their behaviour. The experiments on the full-size panels usually included the experiments on the corresponding masonry specimens/walletes.

Fried also compared the predicted lateral load capacity of panels by the yield line method, the strip method, the principal stress method and the elastic plate method using the same assumed materials in all methods. At the same time he investigated the effects of the aspect ratios, the orthogonal ratio, the boundary conditions on the different methods. His comparisons clearly show the advantages and shortcomings of these methods.

In fact, Fried's work has summarised the experimental and analytical research into laterally loaded masonry panels before 1989. Fried's research clearly identified the

practical application of these analytical techniques, the empirical strip method, the yield line method, the elastic plate theory and the principal stress method, but the application of these methods is not simple and the reasons why these analytical methods are not consistent under some parameters are not clear.

The research at this stage investigated the accuracy of the calculation methods recommended in BS 5628: Part 1 in many aspects and proposed new methods to predict the failure loads of masonry panels. Although these methods are suitable for some cases, the reasons of invalidity in other cases are not clear.

### ***2.5. The Present Period (1990-present)***

After 1990, the research in this field mainly focused on laterally loaded masonry walls with openings. Continuing efforts to accurately predict the failure load of laterally loaded masonry panels were also being advanced by improvements in existing analytical techniques.

In 1991, Lawrence (1991) presented an analytical method using the finite element method which allowed the simulation of the strength of laterally loaded masonry panels with various configurations of door and window openings. The analysis estimated the load at which the first crack formed in a masonry panel under the application of uniformly distributed out-of-plane lateral load. A computer program was developed using the finite element method with a Monte Carlo simulation approach to take account of the random variation in flexural strength of masonry. The influence of self-weight was included. Two failure criteria for the masonry – no interaction between vertical and horizontal moments and a principal moment criterion – were applied and their effects were studied.

Lawrence indicated that the greatest difficulty with analysing walls under lateral loading is coping with the high degree of random variation present in masonry materials. This variability is caused by factors such as natural variation in materials, variation in the manufacturing process, variation in the quality of site workmanship, the difficulty of controlling site-batched mortar, and so on. It is essential to account for this inherent random variation in any theoretical analysis. Lawrence's research clearly directed a main way that pursuing an accurate prediction of masonry panels needed proper modelling of masonry properties for the FEA of the panel. Addressing this issue is the focus of research in this thesis.

In 1993, Chong (1993) continued the research into the behaviour of laterally loaded masonry panels with openings. He carried out a series of experiments on eighteen full-scale masonry panels. Chong applied both yield line theory and FEA in his calculations of failure loads of the masonry panels. His research results demonstrated that the yield line approach, which forms the basis of BS 5628, tends to overestimate the flexural strength of masonry panels as the ratio between height and length of a panel increases (the failure load is overestimated by 29% average for the eighteen masonry panels with different configurations, boundary conditions and material properties). Chong used the smeared cracked material properties obtained from the masonry strength (the biaxial stress failure criterion) in the FEA of the panel. He used a non-linear finite element analysis which gave reasonable agreement with the experimental results of failure loads and to some extent failure patterns of the panels (the failure load is underestimated by 12% average for the eighteen masonry panels with different configurations, boundary conditions and material properties, and using

wallette strengths). He identified that the accuracy of any method for masonry analysis may be in doubt because the fundamental properties of masonry materials are not fully known and more work in relation to lateral loaded masonry walls is required to establish:

- A stress-strain relationship of masonry prior to failure.
- A cracking and failure criterion representing the cracking and ultimate strength of masonry under lateral loading.
- The effect of precompression on the cracking and failure criterion.
- A post failure stress-strain relationship to account for any change of behaviour.
- A cracking model to define direction and propagation of cracks.

Chong's PhD thesis falls short of proposing a suitable analytical method for predicting the first cracking load, the failure patterns and the ultimate load, but rather indicated that global masonry material properties are not applicable to the whole panel and an accurate analysis should consider the changes of elastic modulus with stress levels.

In 1994, Lawrence (1994) carried out an extensive investigation of the out-of-plane load resistance of non-loadbearing clay brick walls. The results of thirty-two full-scale tests on single-leaf panels and a large number of tests on small brickwork specimens in flexure and shear were reported. The support conditions included in the tests were various combinations of simply-supported and built-in edges on three or four sides. Lawrence gave his recommendations for the design of two-way spanning panels without openings based on the comparison with various methods of prediction, and supported the empirical approach of "SAA masonry Code" AS 3700 (1969) as the

best available practical method at that time. He also outlined the needs for further work to develop a biaxial bending failure criterion and to study the behaviour of hollow block panels, walls with openings and cavity walls. Lawrence once again identified the potential for more accurate predictions by an analytical method taking account of random variation.

In 1995, Lawrence (1995) studied the strength of masonry in out-of-plane horizontal flexure, with stress parallel to the bed joints. The experimental results for a large number of masonry beams provided information to understand this important parameter in the design of walls for lateral loading.

In 1996, Lee et al. (1996) introduced a homogenisation technique to investigate the elastic-brittle behaviour of masonry panels subjected to incremental lateral loading. In this technique, tensile cracking was considered to be the only non-linearity parameter. The constitutive model was incorporated in a three-dimensional finite element code. In the homogenisation technique, two stages of homogenisation were used, one for the orthotropic material and the other for smeared cracking of the material. It was shown that the patterns of cracks in masonry panels reasonably agreed with the experimental data. The analytical results were compared with experimental results on the response of a set of laterally loaded rectangular masonry panels with and without openings. It was also considered that the analytical model could be adopted for predicting the physical behaviour of laterally loaded masonry panels of arbitrary geometry and boundary conditions.



In 1998, Lawrence (1998) described the development of a new method of design based on virtual work principles and showed that this approach gives good agreement with test results. This new approach to masonry panel behaviour drew the focus clearly on the torsional behaviour of the bed joints where they overlapped in stretcher-bonded masonry and identified this parameter as the most important parameter in lateral load resistance. Torsional strength can be empirically devised from flexural bond strength as measured by the bond wrench.

In 1998, Duarte (1998) reported investigation into the design of laterally loaded unreinforced brickwork panels with window openings. He compared the ultimate loads predicted by the Yield Line Theory, the Fracture Line Method, the Strip Method and Code BS 5628 with the experimental failure loads of 16 masonry panels with openings. He pointed out that for defined panel conditions the yield line method provides reasonable predictions of the ultimate load carrying capacity of unreinforced brickwork walls with window openings subjected to uniformly distributed load, but that the yield line method in conjunction with the material properties recommended in BS 5628, gives a conservative estimate (by 20% for nine panels whose failure loads are underestimated).

In 1998, Brooks and Baker (1998) presented a new practical method of estimating the modulus of elasticity of clay and calcium brickwork by establishing modulus/strength relationship for mortar and brick units. The method was based on a composite model, adapted to express the modulus of masonry in terms of properties that were generally known to the designer, namely, the strength of the unit, the strength of the mortar and the water absorption of the unit. When compared with the test data of brickwork, this

method can give a more accurate modulus of elasticity of clay and calcium brickwork than can other methods including BS 5628 and Eurocode 6 at that time (the error coefficient being approximately 26% for the proposed method, 38.1% for BS 5628 and 34.0% for Eurocode 6).

In 1999, Mathew et al. (1999) published their research results on predicting failure loads by the hybrid system which combines both case-based reasoning technique and the neural networks (NN) based analysis. The trained NN was able to match the failure load of a masonry panel under lateral pressure and when the wall was subjected to biaxial bending, for instance, masonry cladding panels supported on three or four sides.

The future development of both masonry research and its application in practice was reviewed by de Vekey (1992), Hendry (1996, 1997) and West (1998). The research on masonry placed particular emphasis on the analytical methods developed before 1989 in complex masonry structures or masonry structures under complex loads. Most research results involve the analysis of parameters, such as aspect ratio, flexural strength, orthogonal strength ratio and other factors. After 1990, research further extended to panels with openings (Chong 1993) (Duarte 1998) (Lee et al. 1996) (Lawrence 1994) and variation in masonry material properties (Baker 1982) (Lawrence 1991, 1994), and continued to pursue a more accurate masonry model used in the FEA for masonry (Brooks and Baker 1998) (Chong 1993) (Duarte 1998) (Lee et al. 1996) (Lawrence 1994).

## **2.6. Issues Arising from Review of Previous Research**

### **2.6.1. Facts and Goals**

The above literature reflects the facts:

- The existing analytical techniques have not been reliable and accurate enough to predict both failure load and failure pattern of the panel, because the modelling of masonry properties are still inaccurate, particularly variation in masonry properties.
- The reliable and accurate analytical techniques need to include the variation in masonry properties. So far this variation in masonry properties has not been investigated enough and research in the field has not realised whether or not some factors from structure are closely related to this variation besides random factors.
- Boundary conditions of the panel are the key factor that affects the behaviour of laterally loaded masonry panels, which must be considered in modelling masonry properties.

According to these facts, this research is focused on proposing a more reliable and accurate analytical technique for prediction of both failure load and failure pattern of laterally loaded masonry panels, by quantifying variation in masonry properties and properly modelling the effect of panel boundaries on the overall response of the panel subjected to lateral loading.

### **2.6.2. Issues**

To achieve goals in Section 2.6.1, the following issues are raised from the above review of previous research:

- 1 The FEA predicts the failure load and/or failure pattern for the panels better than other existing methods (Lawrence 1991) (Chong 1993) (Lee et al. 1996). This shows that the FEA technique is suitable for masonry structures because the FEA process can include two different orthotropic strengths and gradually propagate cracking from a zone to other zones within the panel; in other words, the FEA process can reflect the practical properties and behaviour of masonry panels on the basis of reasonably and reliably theoretical fundament. However, due to inaccurate modelling of masonry properties, the FEA still gives some poor results of masonry panels subjected to lateral loads, see Section 8.3. Therefore, a major task of the current research is to focus on proper modelling techniques for masonry structures.
- 2 Except Lawrence's research, the existing methods of predicting the response of laterally loaded masonry panels are based on the assumption of ideal panels, i.e., the masonry panels are considered to be isotropic and all the points within the panel have the same parameters that represent the properties of masonry materials such as flexural rigidity/elastic modulus and strength. Lawrence (1991) inserted random flexural tensile strengths into local zones on the panel and successfully predicted the failure loads and the point of first cracking in non-loadbearing masonry panels under lateral load. However, the consistent correct prediction of both failure loads and failure patterns of masonry panels has not been achieved. From Lawrence's (1991) and Chong's (1993) research results, the existing FEA of masonry panels under lateral loading could be improved by introducing variation in masonry properties into various locations on the panel. This needs to verify whether or not some factors from structure are closely related to this variation besides random factors and the existing experimental data

have included the information about this variation. Naturally, the further research needs to proceed how to model this variation in order to improve the existing analytical techniques for masonry if the existence of the information is verified.

- 3 From West et al's research (1971, 1975), it can be concluded that the boundary effect plays an important role in the behaviour of masonry panels. On the basis of the above conclusions, the research presented in this thesis has focused on the variation in masonry properties and propagating the boundary effect on the variation into various zones within the panel.
- 4 The existing experimental data from laterally loaded full-scale masonry panels are only used to give a comparison with analytical results on lateral load resistance and failure pattern of masonry panels. To date, the information obtained from the comparison of experimental and analytical results has not been quantitatively back-fed into the modelling of masonry properties. In other words, the difference between the experimental and analytical results is, in this thesis, considered to be from the variation in masonry properties. This means that the behaviour of masonry units/walquettes in their experimental environment varies in the structural environment and this variation greatly affects the accuracy of the FEA of masonry panels. To obtain a parameter describing this variation, some experimental data of full-scale masonry panels should be reasonably employed in the parameter. Among the data, the displacements measured at individual points that are distributed at the typical zones of the panel certainly include the factor of the variation in masonry properties. Therefore, a parameter called corrector is proposed in this research to make use of the experimental data of full-scale masonry panels to quantify the variable properties of masonry walquettes in the structural environment.

5 After the parameter quantifying the variation in masonry properties is obtained, it is natural that the new problems are put forward on how to apply the parameters to the FEA of new panels. Generally, there is the similarity of variation in masonry properties at the corresponding zones between panels, because the zones have similar physical, geometrical, loading and boundary conditions. Furthermore, it is needed to know what factors govern the similarity between zones within panels, how to definite this similarity and how to match the similarity between zones within panels. After addressing the above issues, the following task is to verify the validity of the parameter in the FEA techniques, in other words, to verify whether or not this parameter can improve the FEA results of new masonry panels. This research will fully address this issue.

## **3. TECHNIQUES OF FINITE ELEMENT ANALYSIS FOR MASONRY**

### ***3.1. Introduction***

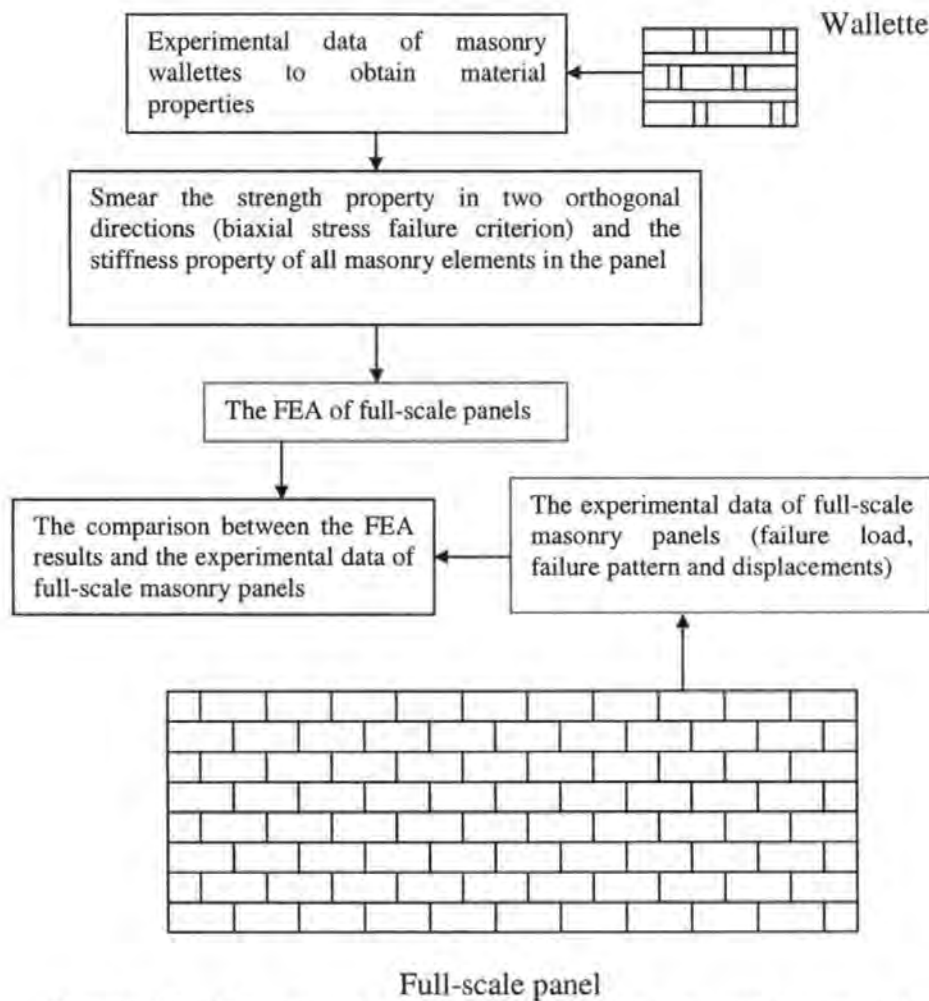
In Section 2.6, it has been mentioned that the FEA techniques for masonry are better than other methods for masonry both in theoretical basis and calculation results. This chapter reviews two different FEA techniques for masonry structures, the biaxial stress failure criterion (Chong 1993) and the homogenous technique (Lee et al. 1996). The main differences between these two techniques are: Chong adopted a four-noded flat shell element and used smeared material properties, and cracking was judged on the basis of stress and strength obtained from wallette experiments. Lee et al. adopted 20-noded solid element and used orthotropic material properties derived from the strain energy of the composite material, and cracking was judged on the basis of stresses and strengths of each of the constituent materials. Both techniques are capable of predicting the failure load and failure pattern of laterally loaded masonry panels for a number of cases.

### ***3.2. The FEA Using Biaxial Stress Failure Criterion***

#### ***3.2.1. Development of the FEA Model***

In this FEA model, Chong (1993) applied a biaxial stress failure criterion technique in which results of laboratory experiments on masonry wallettes were used to establish failure criterion in various directions in masonry panels (see Section 3.2.3 for details). The test results from full-scale masonry panels were compared with the FEA results such as the failure load and failure pattern of the panel. In this analysis, Chong used

globally smeared masonry properties. A diagrammatic process of Chong's analytical technique is given in Figure 3.1

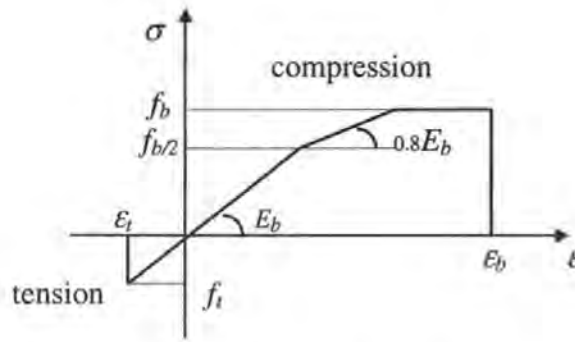


**Figure 3.1** – The procedure of experimental and theoretical analysis using the biaxial stress failure criterion

### 3.2.2. Stress-Strain Models

In Chong's analysis, masonry was modelled (see Figure 3.2) as a tri-linear elastic-plastic material in compression and as a uniaxial material in tension. Linear elastic-brittle behaviour was assumed for bending both parallel and normal to bed joint.





**Figure 3.2** – Uniaxial Stress-Strain Relationship

Within the elastic range, masonry can be considered as either isotropic or anisotropic. However, in Chong's model, masonry was treated as an isotropic material. Other researchers such as Samarasinghe et al (1983) have also used this model. In this model, the non-linearity caused by the constituent materials is insignificant compared with that resulting from progressive cracking. The biaxial stress-strain relationships for isotropic linear elastic materials are given by

$$\begin{Bmatrix} \sigma_x \\ \sigma_y \\ \tau_{xy} \end{Bmatrix} = \frac{E_b}{1-\nu^2} \begin{bmatrix} 1 & \nu & 0 \\ \nu & 1 & 0 \\ 0 & 0 & (1-\nu)/2 \end{bmatrix} \begin{Bmatrix} \epsilon_x \\ \epsilon_y \\ \gamma_{xy} \end{Bmatrix} \quad (3.1)$$

where,  $E_b$  is the elastic modulus of brickwork and  $\nu$  is the Poisson's ratio;  $\sigma_x$  and  $\sigma_y$  are stresses parallel and normal to the bed joint,  $\tau_{xy}$  is the shear stress;  $\epsilon_x$ ,  $\epsilon_y$ , and  $\gamma_{xy}$  are the corresponding strains to  $\sigma_x$ ,  $\sigma_y$  and  $\tau_{xy}$ .

### 3.2.3. Biaxial Stress Failure Criterion

The finite element analysis of masonry panels from zero up to collapse requires:

1. A biaxial failure criterion for the flexural stresses, including the directional properties of masonry;

2. The flexural stresses in terms of the two principal stresses and their orientation to the bed joints;
3. A complete failure criterion which should cover the compression-compression, compression-tension, and tension-tension zones;
4. A relationship between the change of stresses and the change of bed joint orientation (Chong assumed a linear relationship).

Based on the above requirements, Chong proposed Equation (3.2) governing the surface of the failure criterion

$$\frac{\sigma_x^2}{\sigma_{1\alpha}^2} + \frac{\sigma_y^2}{\sigma_{2\alpha}^2} = 1 \quad (3.2)$$

where

$$\sigma_{1\alpha} = \sigma_{10} - (\sigma_{10} - \sigma_{1\pi/2})2\alpha/\pi, \quad \sigma_{2\alpha} = \sigma_{20} - (\sigma_{20} - \sigma_{2\pi/2})2\alpha/\pi$$

$\sigma_x, \sigma_y$  are the failure stresses at a particular angle  $\theta$ ,

and  $\alpha$  is the angle between the direction of the maximum prescribed stress and the bed joints.  $\sigma_{1\alpha}, \sigma_{2\alpha}$  are the maximum prescribed stresses in the directions x and y at the angle  $\alpha$ .

The biaxial stress failure surfaces in the tension-tension, compression-tension, and compression-compression zones are shown in Figure 3.3 (Chong 1993).

### 3.2.4. Modelling of Cracking and Crushing

In general, failure can be divided into either crushing in compression or cracking in tension. Crushing failure leads to the complete disintegration of the material. Masonry is assumed to crush when the deformation level reaches its ultimate capacity. After crushing, the stresses drop abruptly to zero, and the masonry is assumed to completely lose its resistance against further deformation in any direction.

Comparison of the Biaxial Relationship with the Proposed Biaxial Failure Criterion.

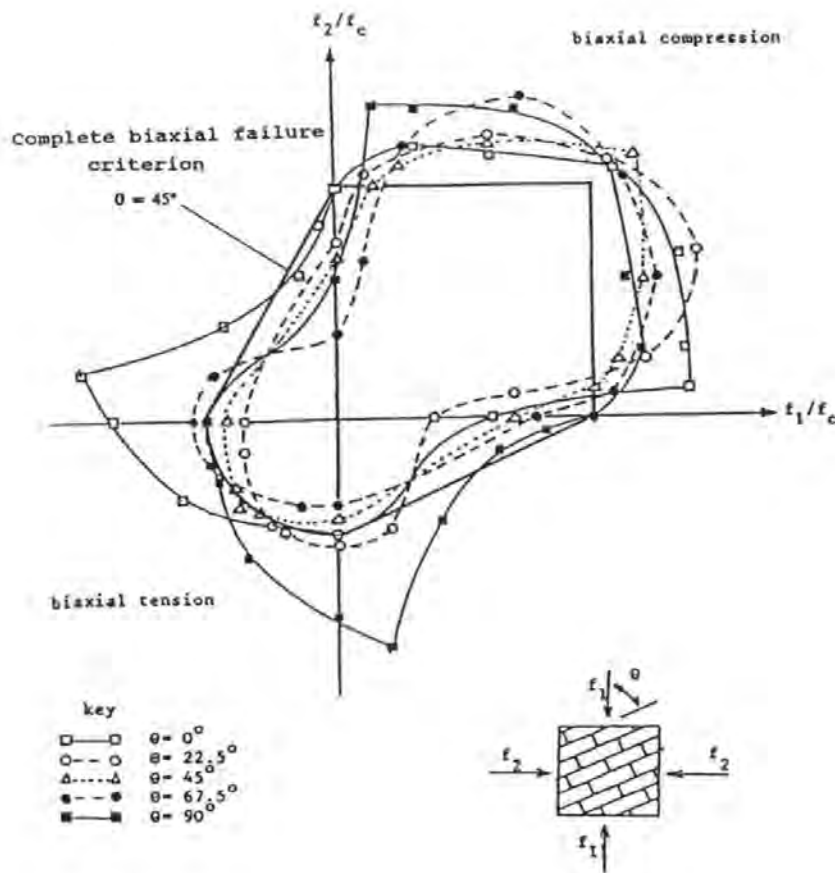


Figure 3.3 – Complete biaxial failure criterion

Cracking is assumed to occur when the tensile stress within an element reaches the limiting tensile value given by the biaxial failure envelope. The direction of the crack is fixed normal to the direction of the principal stress violating the failure direction. After cracking, the masonry abruptly loses its strength normal to the crack direction. However, material parallel to the crack is assumed to carry stress according to the uniaxial conditions prevailing in that direction.

In the tension-compression zone, only tensile failure is assumed to occur initially as the crack forms. Once a crack has formed, the material sustains compressive stress parallel to the direction of the crack according to the uniaxial compressive failure condition.

The onset of tensile failure causes highly anisotropic conditions to develop. After cracking occurs, the material property matrix in the cracked zones is given by Equation (3.3)

$$\begin{Bmatrix} \sigma_n \\ \sigma_p \\ \tau_{np} \end{Bmatrix} = \begin{bmatrix} 0 & 0 & 0 \\ 0 & E_b & 0 \\ 0 & 0 & 0 \end{bmatrix} \begin{Bmatrix} \epsilon_n \\ \epsilon_p \\ \gamma_{np} \end{Bmatrix} \quad (3.3)$$

where,  $\sigma_n$  and  $\epsilon_n$  are the stress and strain normal to the crack direction, and  $\sigma_p$  and  $\epsilon_p$  are the stress and strain parallel to the crack direction.

This equation allows no shear stresses thus this converts the biaxial stress system for uncracked masonry into a uniaxial system after cracking.

### 3.2.5. Masonry Representation

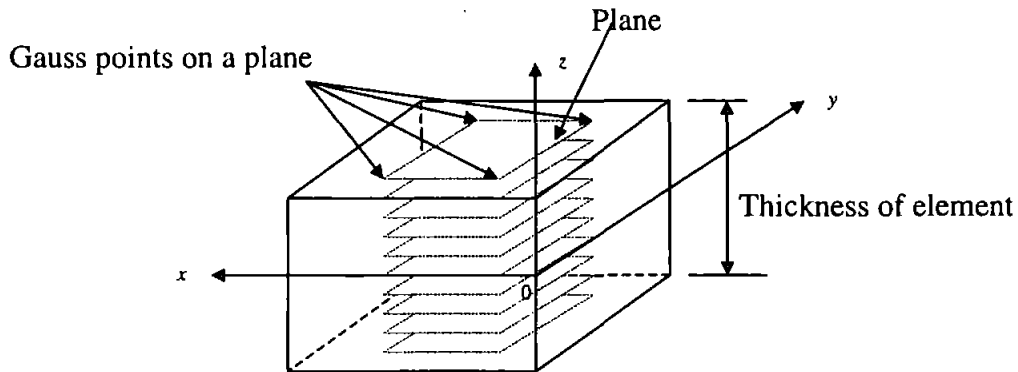
A typical FEA model of masonry panels can adopt a four-noded flat shell element with offset axes (Moffatt and Lim 1976), when masonry is treated as an isotropic material of which properties are modelled based on the data of wallette tests. In this model, each node has six degrees of freedom, three axial displacements  $u$ ,  $v$  and  $w$  in the  $x$ ,  $y$  and  $z$  directions respectively and three rotations  $\theta_x$ ,  $\theta_y$  and  $\theta_z$ .

This form of FEA model permits the stacking of elements into layers with different material properties, and each element having a common reference surface which may be offset from the mid plane of the element.

For the modelling of cavity panels, a slip plane was introduced between the two layers of stacked elements with each layer sharing one common axial displacement  $w$  and two common rotations  $\theta_x$  and  $\theta_y$ . Inplane displacements  $u$  and  $v$  and rotation  $\theta_z$  are not restrained since the wall is free to move in the individual layer of elements. Thus, the degrees of freedom in each node is increased from six to nine, five axial displacement  $u_1, u_2, v_1, v_2, w$  and four rotations  $\theta_x, \theta_y, \theta_{z1}, \theta_{z2}$ , where subscripts 1 and 2 correspond to the two layers (leaves) of elements. In this case, the tie stiffness, joining two leaves, is assumed to have an infinite value (rigid arm).

### 3.2.6. Integration Rules

In plane a  $2 \times 2$  point Gauss-quadrature integration scheme was employed. In addition to sampling the strain on the  $x$ - $y$  plane, it is sampled at ten points to detect non-linear behaviour (cracks) and to determine the variation in the magnitude of stress through the depth of the element (out of plane), as cracks develop along the wall thickness, see Figure 3.4.



**Figure 3.4** – The planes through the depth of element

### 3.2.7. Non-Linear Algorithms

An incremental iterative approach with a constant stiffness matrix was used in the program. Line search techniques are used to reduce the number of iterations required, and hence accelerate convergence.

### 3.2.8. Convergence Criteria

The convergence criteria adopted in this work are based on a residual displacement norm, Equation (3.4) and a residual rotation norm. Equation (3.5)

$$TOD > \sqrt{\frac{\sum (\text{Change in Incremental Displacement})^2}{\sum (\text{Total Displacement})^2}} \quad (3.4)$$

$$TOR > \sqrt{\frac{\sum (\text{Change in Incremental Rotation})^2}{\sum (\text{Total Rotation})^2}} \quad (3.5)$$

where *TOD* and *TOR* are pre-selected convergence tolerance. A value of 0.002 was found to be suitable for both *TOD* and *TOR*. Both criteria have to be satisfied simultaneously before convergence is achieved.

### 3.2.9. Termination of the Analysis

In the non-linear analysis, load is increased in increments and the analysis is terminated when any of the following criteria is satisfied:

- The number of load increments exceeds a maximum specified number.
- Convergence is not achieved after the load increment has been reduced three times, each time the new increment being 1/4 of the previous increment. The load value just before this load increment is defined as the failure load of the panel.
- Convergence is not achieved after 120 iterations.

### 3.3. The FEA Using Homogeneous Technique

#### 3.3.1. Application of Experimental Data

The homogeneous technique (Lee et al. 1996) uses the test data of mortar and brick/block to form the homogenised material properties of masonry elements. The test results from the full-scale masonry panels are used to compare the FEA results with the experimental results. The process of homogeneous technique is summarised in Figure 3.5. All elements within the panel have the same flexural rigidity and tensile strength in the FEA calculation.

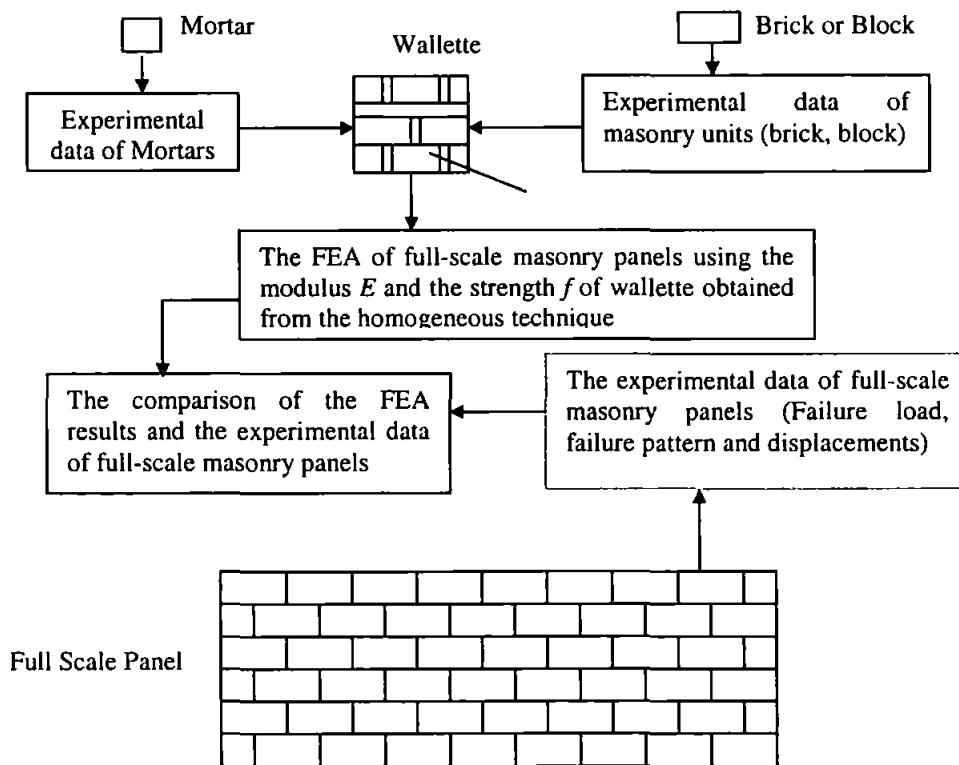


Figure 3.5 - The procedure of experimental and theoretical analysis using homogeneous technique

#### 3.3.2. Homogenisation Technique

The homogenisation technique combines two constituent materials (masonry units and mortar) into a single material. Equivalent (homogenised) material properties of

this combined material, satisfying an equal strain energy principle, were derived. A unique transformation between stresses in the homogenised material and the constituents was derived. The homogenisation technique has two stages as follows.

### 3.3.3. First Stage of Homogenisation-Equivalent Properties of Masonry

This stage assumes that brick and mortar are perfectly bonded and the perpendicular mortar joints are continuous. Let the compliance matrix of the orthotropic equivalent homogenised material be denoted by  $[\bar{C}]$ . The stress-strain relationship of the equivalent homogenised masonry material is represented in incremental form by

$$\bar{\varepsilon} = [\bar{C}] \bar{\sigma} \quad (3.6)$$

where

$$\bar{\sigma} = \left\{ \bar{\sigma}_{xx}, \bar{\sigma}_{yy}, \bar{\sigma}_{zz}, \bar{\tau}_{xy}, \bar{\tau}_{yz}, \bar{\tau}_{zx} \right\}^T \quad (3.7)$$

$$\bar{\varepsilon} = \left\{ \bar{\varepsilon}_{xx}, \bar{\varepsilon}_{yy}, \bar{\varepsilon}_{zz}, \bar{\gamma}_{xy}, \bar{\gamma}_{yz}, \bar{\gamma}_{zx} \right\}^T \quad (3.8)$$

and

$$[\bar{C}] = \begin{bmatrix} \frac{1}{\bar{E}_x} & -\frac{\bar{\nu}_{xy}}{\bar{E}_x} & -\frac{\bar{\nu}_{xz}}{\bar{E}_x} & 0 & 0 & 0 \\ -\frac{\bar{\nu}_{xy}}{\bar{E}_y} & \frac{1}{\bar{E}_y} & -\frac{\bar{\nu}_{yz}}{\bar{E}_y} & 0 & 0 & 0 \\ -\frac{\bar{\nu}_{xz}}{\bar{E}_z} & -\frac{\bar{\nu}_{yz}}{\bar{E}_z} & \frac{1}{\bar{E}_z} & 0 & 0 & 0 \\ 0 & 0 & 0 & \frac{1}{\bar{G}_{xy}} & 0 & 0 \\ 0 & 0 & 0 & 0 & \frac{1}{\bar{G}_{yz}} & 0 \\ 0 & 0 & 0 & 0 & 0 & \frac{1}{\bar{G}_{zx}} \end{bmatrix} \quad (3.9)$$

Using the equivalent strain energy requirement together with equilibrium and kinematic compatibility conditions for the constituents, the exact expression for the nine elements of the compliance matrix  $[\bar{C}]$ , i.e.,  $\bar{E}_x, \bar{E}_y, \bar{E}_z, \bar{\nu}_{xy}, \bar{\nu}_{yz}, \bar{\nu}_{zy}, \bar{G}_{xy}, \bar{G}_{yz}, \bar{G}_{zx}$



in a closed form can be found. These parameters depend on unit size and thickness of mortar joints, elastic properties of units and elastic properties of joints.

The homogenisation procedure outlined above gives the orthotropic properties of masonry in a local co-ordinate system where the axial  $x$  is aligned along the length of the unit, the axial  $y$  along its height and the axial  $z$  through the thickness of the panel. Then the equivalent orthotropic material properties are used to set up the system stiffness matrix in the FEA procedure and, from this, equivalent stresses/strains are calculated. This gives unique relationships between stresses in the equivalent material and the stresses in the masonry constituents,

$$\begin{aligned}\sigma_u &= [S_u] \bar{\sigma} \\ \sigma_{bj} &= [S_{bj}] \bar{\sigma} \\ \sigma_{pj} &= [S_{pj}] \bar{\sigma}\end{aligned}\tag{3.10}$$

where  $[S]$  is a structural matrix and subscripts  $u$ ,  $bj$ ,  $pj$  stand for bricks, bed joints and perpend joints, respectively. Explicit expressions for those structural matrices are given by Lee et al. (1996).

### 3.3.4. Second Stage of Homogenisation-Modelling of Cracking Masonry

Here masonry is modelled as an elastic brittle material with tensile cracking being the only non-linearity considered. Stresses in each constituent material, i.e. brick, bed and perpend mortar joint, are calculated through the structural relationship defined in the previous section and a check for cracking is made based on the maximum principal stress criterion for each constituent material. In other words, it is assumed that cracks

occur in any constituent if the major principal stress  $\sigma_1$  in that constituent equals its tensile strength  $f_t$ , i.e. the failure criterion  $F$  is:

$$F = \sigma_1 - f_t = 0 \quad (3.11)$$

Once cracking occurs in the material, the effect is smeared onto the neighbouring equivalent orthotropic material through the homogeneous technique and equivalent properties of the cracked masonry are developed. Here, a homogenisation (average) procedure based on the work of Pietruszczak and Niu (1993) is adopted for the three-dimensional case and is described below:

Let the stress/strain rate of the equivalent material after cracking (cracked masonry) be represented by

$$\dot{\sigma} = \left\{ \dot{\sigma}_{xx}, \dot{\sigma}_{yy}, \dot{\sigma}_{zz}, \dot{\tau}_{xy}, \dot{\tau}_{yz}, \dot{\tau}_{zx} \right\}^T \quad (3.12)$$

$$\dot{\varepsilon} = \left\{ \dot{\varepsilon}_{xx}, \dot{\varepsilon}_{yy}, \dot{\varepsilon}_{zz}, \dot{\gamma}_{xy}, \dot{\gamma}_{yz}, \dot{\gamma}_{zx} \right\}^T \quad (3.13)$$

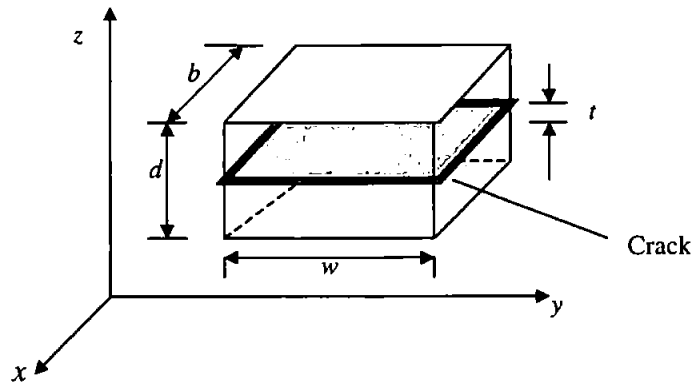
The cracks in masonry are treated as a constituent of masonry. Thus damaged or cracked masonry consists of two constituents – intact masonry and cracks which are assigned properties of a weak material. These stress/strain rates in cracked material can be taken as volume averages of the stress/strain rates in the two constituents of composite material,

$$\dot{\sigma} = \mu_i \dot{\sigma}^i + \mu_j \dot{\sigma}^j \quad \dot{\varepsilon} = \mu_i \dot{\varepsilon}^i + \mu_j \dot{\varepsilon}^j \quad (3.14)$$

where,  $\mu_i$  and  $\mu_j$  represent the volume fraction of the constituent materials and, for simple geometry such as in Figure 3.6, can be defined as

$$\mu_i = 1 - \frac{bwt}{V}; \quad \mu_j = \frac{bwt}{V} \quad (3.15)$$

where  $V = bdw$ . Here subscript  $i$  is used to denote quantities relating to intact material and  $j$  to denote quantities relating to cracks.



**Figure 3.6** - Representation elementary volume including a crack

Assuming perfect bonding at the interface of the crack and surrounding material the equilibrium and kinematic conditions along the interface can be established. It is assumed that the volume occupied by the crack is negligible compared to the volume of the element (which follows from the relatively small width of the crack). The response of cracks can be conveniently described by introducing a velocity discontinuity  $\left\{ \dot{g} \right\}$  (measure of crack width and tangential movements) which is a function of the strain field and the crack width:

$$\left\{ \dot{g} \right\} = \left\{ \dot{g}_y, \dot{g}_x, \dot{g}_z \right\}^T \quad (3.16)$$

Based on the assumption of the negligible crack width and by incorporating the kinematic conditions, strain rate can be written as

$$[\delta] \dot{\epsilon} = [\delta] \dot{\epsilon} + \mu \left\{ \dot{g} \right\} \quad (3.17)$$

where

$$[\delta] = \begin{bmatrix} 0 & 1 & 0 & 0 & 0 & 0 \\ 0 & 0 & 0 & 1 & 0 & 0 \\ 0 & 0 & 0 & 0 & 1 & 0 \end{bmatrix} \quad (3.18)$$

and  $\mu$  is a volume fraction of the crack.

The constitutive relationship for the cracked masonry can be obtained as

$$\dot{\sigma} = [D^{eq}] \dot{\epsilon}, \quad [D^{eq}] = [D][S_i^i], \quad [D_r^{eq}] = [T]^T [D][T] \quad (3.19)$$

Here,  $[S_i^i]$  is structural matrices relating strains between the homogenised cracked material and either of its constituents;  $[D^{eq}]$  is used to take into account the orientation of the crack and the components of the transformation matrix  $[T]$  depend on the normal vector of the plane of the crack.

In the FEA, loads are applied incrementally and within each load increment, this procedure is implemented as follows:

- (1) After stresses in the constituents are determined, occurrence of cracks in each constituent is checked following Equation (3.11). For each point under consideration three checks have to be completed, one for each constituent, i.e. units, bed joints and head joints. It is important to note that tensile strengths of the constituent materials are generally different.
- (2) If cracking is detected the orientation of the crack is calculated together with the velocity discontinuity vector.
- (3) New, homogenised constitutive relationship for the cracked masonry is evaluated using Equation (3.19).
- (4) Out of balance residual stresses are calculated and iteration is performed until equilibrium is achieved.

## **4. INTRODUCTION OF CONCEPT OF STIFFNESS/STRENGTH CORRECTOR**

### ***4.1. Introduction***

The review of the FEA techniques for masonry clearly demonstrated that the models of masonry components were based on results of experimental laboratory experiments on a large number of masonry units/wallettes to determine material properties such as the modulus of elasticity and tensile strength for masonry. However, once these properties are applied to full-scale masonry panels, the results of the FEA do not give reasonable correlation in predicting failure loads and failure patterns of many masonry panels (see the relevant panels calculated in Chapter 8). This indicates that variation in material properties, geometric properties, boundary conditions and many other factors plays an important role in the overall behaviour of masonry panels, which is not reflected by the properties derived from masonry unit/wallette tests. To resolve this problem, this research has focused on the proper modelling of full size masonry panels taking account of variation in material and geometrical properties, variation in quality of site workmanship, and more important the effect of panel boundaries on the behaviour of the panel. This chapter introduces the concept of a “stiffness/strength corrector”, which is used to assign different properties to various zones within a panel. Examples of the calculation of stiffness corrector and its variation in a masonry panel are given in Chapter 5. The application of this corrector has greatly improved the FEA results, which correlate well with experimental laboratory results (see Chapters 7 and 8).

## ***4.2. Significance and Functions of Correctors***

To improve the results of the FEA, it was decided that the inclusion of the variation in masonry properties in individual zones within a panel would be beneficial. Analytical methods developed so far, including the FEA methods, have not modelled variation in masonry properties to predict failure loads and failure patterns of masonry panels. The current research investigates proper modelling of this variation for inclusion in the FEA.

In order to consider the variation in masonry properties within a panel, it was decided to review past experimental data to determine whether this variation in masonry properties could be modelled properly.

From laboratory experiments of masonry panels subjected to lateral loading, three types of measurements are generally recorded: failure loads, failure patterns and displacements at various locations on the panel. The failure load represents the strength of the whole structure and the failure pattern is a phenomenon, that can not be used to quantitatively give any indication about the masonry properties at local zones within the panel. Thus only the measured displacements can to some extent quantitatively describe the variation in the properties of masonry in various locations within the panel, as the measured displacements are related to the individual nodes within the panel. This parameter is therefore used to model the variation in masonry properties by comparing the existing test data from full-scale masonry panels with a corresponding FEA model. Details of introducing a stiffness corrector are discussed in this chapter.

Figure 4.1 shows the basic steps for the introduction of the parameters that describe the variation in masonry properties in a panel. In the figure:

- A new parameter, corrector, is introduced by comparing experimental and analytical displacements of the panel;
- The global flexural rigidity  $D$  or the global tensile strength  $f$  in the existing FEA model is modified, using corrector values related to individual zones within the panel.

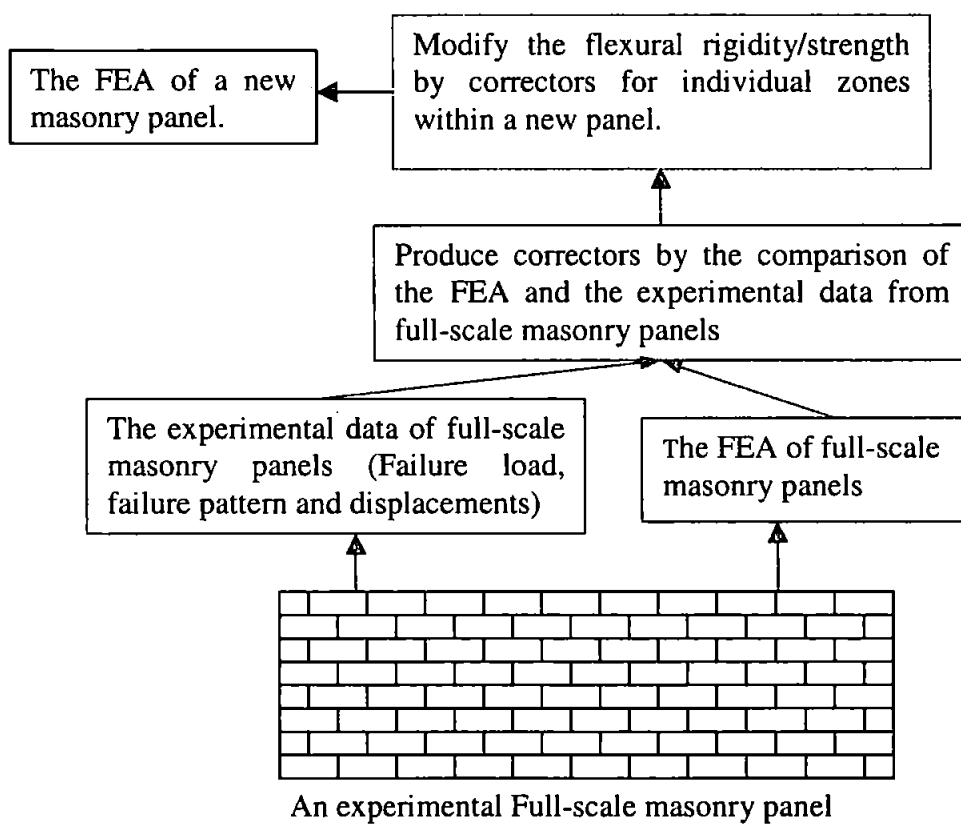


Figure 4.1 – Procedure of producing correctors and their application

### 4.3. Introducing Corrector $\psi_i$

The measured displacements from experiments on masonry panels are affected by many factors such as boundary conditions, aspect ratios, material and geometrical properties, etc. If there were no variation in masonry properties within the experimental masonry panels, the displacement measured from the experiment should

be the same as that calculated by the FEA. Thus the displacement determined by the FEA using globally smeared masonry properties excludes the effect of any variation in masonry properties. Variation in masonry properties is the major reason for differences between the experimental and analytical displacements. In order to model the collective effect of the variation discussed above, and to incorporate this variation into the FEA of masonry model, it is proposed that a corrector should be introduced for each zone within a masonry panel, which globally reflects the various constitutive properties in one parameter.

For the non-linear FEA process (non-linear material) of an experimental panel, the incremental method is used in which the load is applied in increments of  $\{\Delta P\}$  on the structure until the panel fails. In elastic/elastic-plastic analysis, for a load increment  $\{\Delta P\}$ , the displacement increment  $\{\Delta W\}$  of any point within the panel can be calculated by the following equilibrium equation (Ghali and Neville 1997)

$$[K]\{\Delta W\} = \{\Delta P\} \tag{4.1}$$

where  $[K]$ - is the global stiffness matrix

$$[K] = D \begin{bmatrix} \dots & \dots & \dots \\ \dots & \dots & \dots \\ \dots & \dots & \dots \end{bmatrix} \tag{4.2}$$

matrix constant values for a given structure

$\{\Delta W\}$ ---displacement increment vector

$\{\Delta P\}$ ---load increment vector (it is constant vector for a certain load)

$$D = \frac{E_b h^3}{12(1-\nu^2)}, \text{ } D \text{ is the flexural rigidity and } E_b \text{ is the elastic modulus of}$$

brickwork,  $\nu$  is Poisson's ratio. In elastic/elastic-plastic analysis using Equation



(4.1), for a load increment  $\{P\}_j$ , the displacement increment  $\Delta W_i$  of a point  $i$  in the panel, can be written as

$$(\Delta W_i)_j = \frac{C_i^j}{D}$$

where,  $\frac{C_i^j}{D}$  is the displacement increment of  $i$ th point.  $C_i^j$  is the constant for the load increment  $j$ .

Thus, the total displacement of the  $i$ th point for the  $j$ th load increment can also be written as

$$W_i = \sum_j (\Delta W_i)_j = \sum_j \frac{C_i^j}{D} = \frac{1}{D} \sum_j C_i^j \quad (j = 1, 2, \dots) \quad (4.3)$$

In Equation (4.3), the item  $C_i^j$  involves the geometrical structure, mathematical mechanism and load that varies following the increase in the applied load increments, and  $D$  is the global flexural rigidity.

In the FEA, the effect of all variation in masonry properties and the effect of boundary constraints can be collectively modelled by varying the values of  $D$  at different locations on the panel. It is assumed that the differences between the experimental displacement  $W_i^*$  and the FEA displacement  $W_i$  calculated by Equation (4.3) is due to the variation in the values of  $D$  at different zones. A relationship for the experimental displacement  $W_i^*$  at node  $i$  can be written as

$$W_i^* = \sum_j (\Delta W_i^*)_j = \sum_j \frac{C_i^j}{D_i} = \frac{1}{D_i} \sum_j C_i^j \quad (i = 1, 2, \dots) \quad (4.4)$$

Comparing Equation (4.3) with Equation (4.4), the ratio of  $W_i^*$  and  $W_i$ , i.e. the displacement ratio is obtained as

$$R_i = \frac{W_i^*}{W_i} = \frac{D}{D_i'} \quad (4.5)$$

Equation (4.5) can also be written as

$$D_i' = \frac{D}{R_i} = \psi_i D \quad (4.6)$$

Thus, the global flexural rigidity  $D$  is replaced with the modified flexural rigidity  $D_i'$

by applying the factor  $\psi_i = \frac{W_i^*}{W_i}$ .  $\psi_i$  is called stiffness corrector which is derived from

comparing the experimental and analytical results and is different at the different locations on the panel.

Normally, for the FEA analysis, it is easier to introduce the collective variation in the masonry behaviour and the effect of boundary conditions by adjusting values of the modulus of elasticity  $E_b$  at various locations on the panel at elastic and elastic-plastic region in the masonry stress-strain curves (Figures 4.3 and 4.4) as

$$E_i' = \psi_i \times E_b \quad (4.8)$$

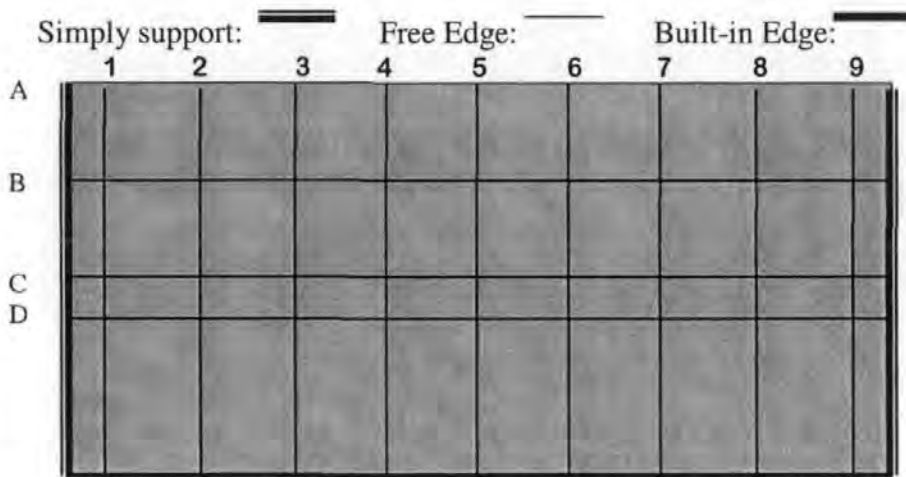
$$\psi_i = \frac{1}{R_i} = \frac{E_{bi}'}{E_b} \quad (4.9)$$

Here,  $\psi_i$  is called stiffness corrector and  $E_{bi}'$  is called the modified modulus. In the following application, the corrector  $\psi_i$  can also be used to assign different tensile strengths, instead of changing  $E$ , at various locations on the panel. For this case  $\psi_i$  would be called strength corrector.

#### **4.4. Characteristics of Stiffness Corrector**

The proposed stiffness correctors need to be investigated to verify whether they reflect the true characteristics of variation in masonry properties related to the collective effect of many factors discussed earlier. For this purpose, a masonry panel

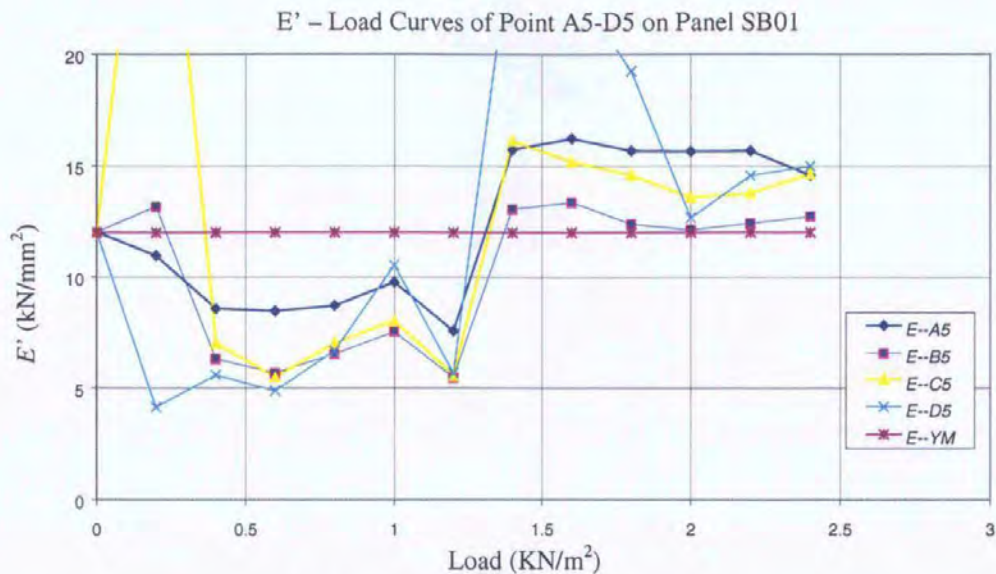
SB01 was selected as the base panel from Chong's experiment (1993). The panel includes three types of boundaries: the free edge at the top, the simple supports at the left and right edges and a built-in support along the bottom edge. On Panel SB01 shown in Figure 4.2 the displacement values were measured at thirty-six typical points (A1-A9, B1-B9, C1-C9 and D1-D9) for increments of lateral load.



**Figure 4.2** – The standard panel SB01

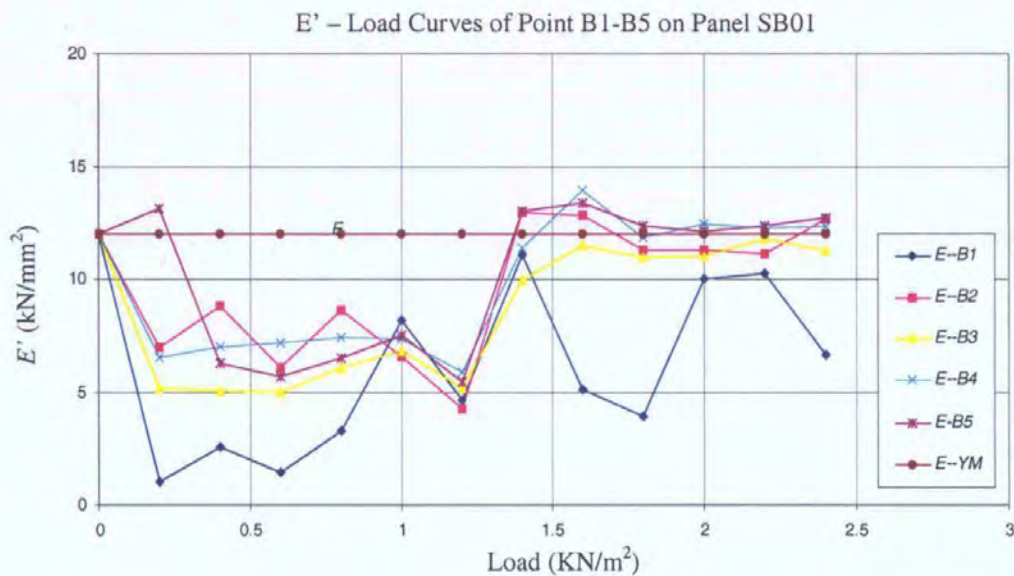
Using the displacement results from Panel SB01, a back substitution process was undertaken using the FEA model to produce modified  $D'$  values for the displacement points on the panel. These values are produced in Figures 4.3 and 4.4 below.

Because  $E_i'$ -Load,  $D_i'$  - Load and  $\psi_i$  -Load curves have similar patterns, this analysis only refers to  $E_i'$  - Load curves. Figures 4.3 and 4.4 show the relationship between modified modulus  $E'$  and load at the local zones on the base panel SB01 which were divided based on the measured points A1-A9, B1-B9, C1-C9 and D1-D9 as shown in Figure 4.2. From these curves, some of the characteristics of the corrector  $\psi_i$  can be described as follows:



(E-YM: Global Young's Modulus  $E$ )

**Figure 4.3** Load – Modified Modulus  $E'$  curves of Points A5-D5 on Panel SB01



(E-YM: Global Young's Modulus  $E$ )

**Figure 4.4** Load – Modified Modulus  $E'$  curves of Points B1-B5 on Panel SB01

(1) Traditionally, the modulus  $E$  (the smeared  $E$  value) is assumed to be constant (straight line with a value of  $12 \text{ kN/mm}^2$  in the above figures) in the FEA of masonry panels. The proposed modified modulus  $E'$ 's are values related to different zones on the panel. It could be implied that correctors reflect the

variation in masonry properties at the local zones within the panel. In other words, this variation is related to the positions of the zones on the panel.

- (2) From Figures 4.3 and 4.4, it would appear that at some zones near the boundaries of the panel, the variation in  $E'$  is quite considerable following the load increment. This indicates that the boundary effect has a critical role on the response of the panel to applied loading.
- (3) Modified modulus  $E'$  values are different under different load values, but when the applied load is greater than  $1.5 \text{ kN/m}^2$ , the  $E'$  values are stable at their individual values. After this load value, any changes in these curves may represent appearance of cracks in the masonry panel.
- (4) It is clear that zones adjacent to different boundaries (free edge, simply supported edge and fixed edge) behave differently.
- (5) The first part of the curves (applied load value of 0 to  $1.5 \text{ kN/m}^2$ ) shows the practical situation of the experimental masonry panel, that is, the panel gradually moved until the wall edges firmly touch the supports. In other words, all the parts of the panel gradually moved into a working-state. The  $E'$  values stabilised after this working state was achieved.

Therefore,  $E_i'$  values (or  $D'_i$  or  $\psi_i$ ) have actually modelled the collective effect of all factors influencing it, such as the anisotropic property of masonry materials, the boundary conditions and geometric properties. In the following chapters, the FEA of lateral loading masonry panels will demonstrate the functions of correctors in improving the predictions of failure patterns and failure loads.

#### **4.5. Summary**

The corrector introduced in this chapter can quantify the variation in masonry properties at the individual zones within the panel. This variation is related to the

collective effect of all factors such as aspect ratios, orthogonal ratio, boundary conditions and geometrical properties. Because the corrector is used to modify the global flexural rigidity of the panel, this is why it is termed the stiffness corrector.

The corrector has two basic characteristics:

1. Local characteristic. Every corrector is closely related to a specific position on the panel.
2. Stable characteristic. After the applied load reaches a level that forces all parts of the panel into a working state, the correctors at individual positions within the panel are in a stable state.

The analysis of variation in masonry properties needs both the theoretical and experimental techniques. The theoretical techniques must be able to describe the local behaviour and material properties of the panel and the FEA techniques properly model this variation. The experimental techniques are needed to satisfy the requirements of the theoretical techniques. Many experiments of full-size masonry panels recorded the displacements at some typical points on the panel. However, these experiments only recorded displacements at a few critical locations on the panel which unfortunately do not reflect the full behaviour of the panel, particularly there are no records of displacements at points near the boundaries.

This chapter described the basis of quantifying values of stiffness correctors at various locations on the panel and reasons for incorporating these into the FEA. The following chapters will seek to apply the corrector to improve the results of the FEA of masonry panels under lateral loads.

## 5. MODELLING SIMILARITY OF ZONES BETWEEN AND WITHIN PANELS

### 5.1. Introduction

Figures 4.3 and 4.4 introduced the concept that the boundary conditions appeared to control the modified value of  $E$  at any part within a masonry panel. There would therefore appear to be a case for investigating whether parts of different masonry panels but with the same adjacent boundaries and the same distances from the boundary will have the same corrector value. This chapter therefore introduces methodologies for calculating stiffness correctors by matching similar zones between a new panel and a base panel. These correctors can then be used for the FEA of the new panel.

In order to apply correctors to improve the results of the FEA of laterally loaded masonry panels, it is necessary to know which correctors on a base panel can be used for the corresponding zones in a new panel. A base panel is one from which stiffness correctors are derived from experimental data. A new panel is one for which the stiffness correctors are derived using the base panel correctors only. This requires that zones can be created for the base panel and the new panel, and the similarity of zones can be matched based on the definition, that similar zones are governed by the similar boundary types and located at the similar positions on the two panels. For the above purpose, the special techniques are proposed to facilitate matching similar zones between a base panel and a new panel. This chapter discusses the concept of zone similarity and details of how a panel is divided into various zones, how similar

zones between a base panel and a new panel are matched and how correctors for various zones within a new panel are selected.

## 5.2. Similarity of Zones

This section investigates what portions within two masonry panels have similar correctors in order to apply the correctors from the base panel to calculate properties for use in the FEA of new panels. Three experimental panels shown in Figures 5.1, 5.2 and 5.4 are selected for the analysis of corrector distribution because the displacements of the three panels were measured at the evenly distributed points on the surface of each panel. These panels also have typical boundaries and sizes. The three panels were built using the same brick and mortar under the similar laboratory environment (Chong 1993). As there were no measured points along the boundaries of these panels except at the top free edge of the panels, the correctors along the boundaries are assumed to be the same as those of the nearest measured points to the specific boundary lines.

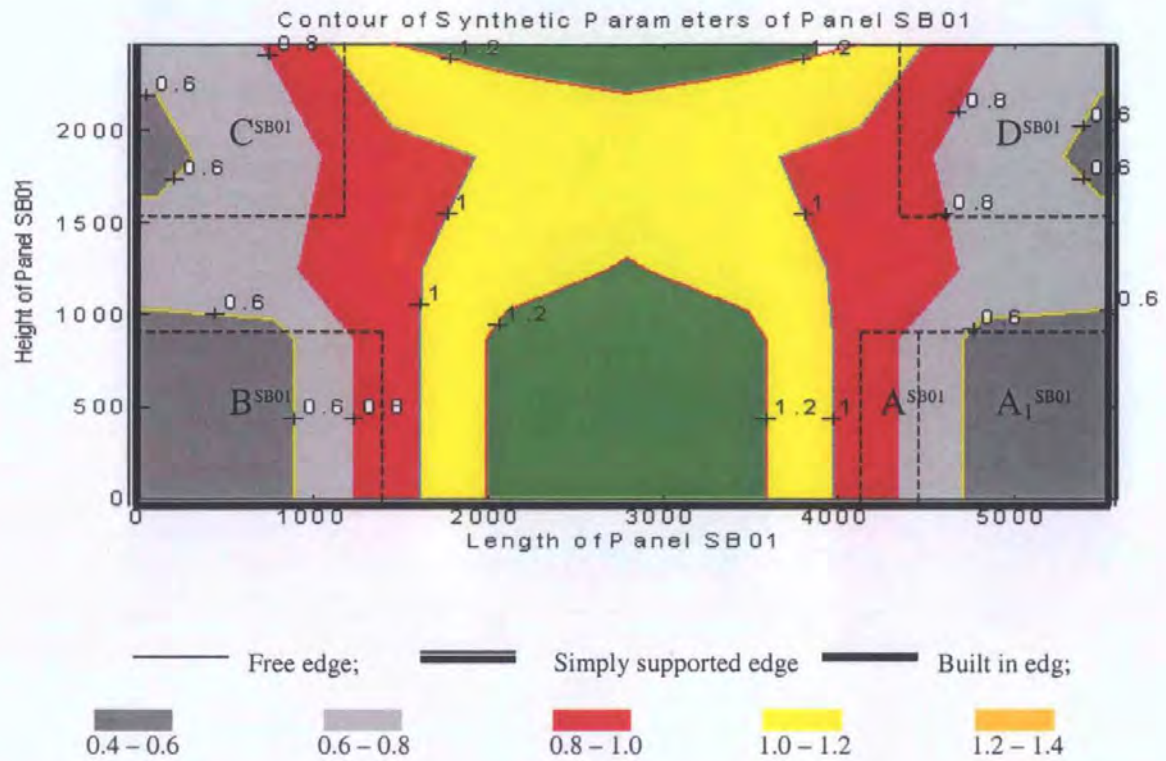
### 5.2.1. Distribution of Correctors on Experimental Panels

Figure 5.1 shows the contour plot of correctors for  $D$  values for Panel SB01, determined from back solution of displacements into the FEA model. The corresponding corrector values are shown in Table 5.1.

**Table 5.1** – The correctors of Panel SB01

$q=2.4\text{kN/m}^2$	Correctors at measured points								
	1	2	3	4	5	6	7	8	9
A	0.637	0.819	1.198	1.262	1.313	1.262	1.198	0.819	0.637
B	0.553	0.706	0.935	1.027	1.059	1.027	0.935	0.706	0.553
C	0.689	0.759	0.957	1.114	1.218	1.114	0.957	0.759	0.689
D	0.530	0.530	0.916	1.268	1.247	1.268	0.916	0.530	0.530





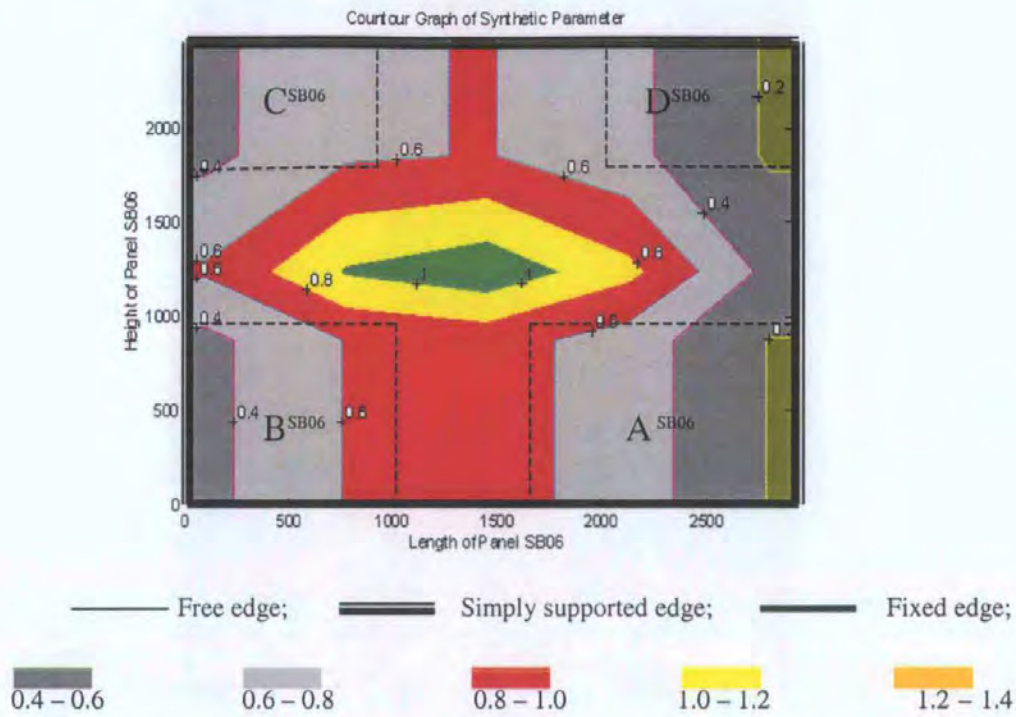
**Figure 5.1** – Contour graph of correctors of Panel SB01

To estimate the correctors for any new panel, the following assumption has been made:

Panel SB01 has been considered to be the base panel. The reason for using this panel as a base panel is that this panel has a general dimension which is typical of a full-scale masonry panel and this panel includes three typical boundary types: simple, free and fixed supports which could represent most realistic situations.

### 5.2.2. Regions with Similar Corrector Distribution

The experimental deflection data for Panel SB06 was used to back solve the FEA model to produce modified  $D'$  values. The correctors for Panel SB06 are shown in Figure 5.2.



**Figure 5.2** – Contour graph of correctors of Panel SB06

By observing and comparing the corrector distributions on the two panels, SB01 and SB06, it is clear that some regions show similar patterns of corrector distribution within/between the two panels. Figures 5.3a and 5.3d are the right-hand bottom corners with different sizes on the base panel SB01 taken out from Figure 5.1. Regions  $A^{SB06}$ ,  $B^{SB06}$ ,  $C^{SB06}$  and  $D^{SB06}$  are taken from Panel SB06. All four regions are shown in Figures 5.3b, 5.3c, 5.3e and 5.3f in which

- Region  $B^{SB06}$  is reversed about its vertical edge;
- Region  $C^{SB06}$  is rotated  $180^\circ$  about its centre;
- Region  $D^{SB06}$  is reversed about its horizontal edge.

For these regions, the following observation can be made:

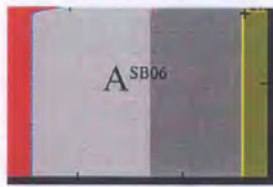
- They are governed by similar boundaries, two simple supports or one simple support and one fixed support;
- Actually, all these regions show similar pattern of corrector distribution;

- Regions  $A^{SB01}$ ,  $A^{SB06}$  and  $B^{SB06}$  have similar sizes. Regions  $A_1^{SB01}$ ,  $C^{SB06}$  and  $D^{SB06}$  have similar sizes.



Region  $A^{SB01}$  on Panel SB01

(a)



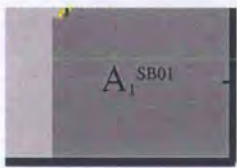
Region  $A^{SB06}$  on Panel SB06

(b)



Region  $B^{SB06}$  on Panel SB06

(c)



Region  $A_1^{SB01}$  on Panel SB01

(d)



Region  $D^{SB06}$  on Panel SB06

(e)



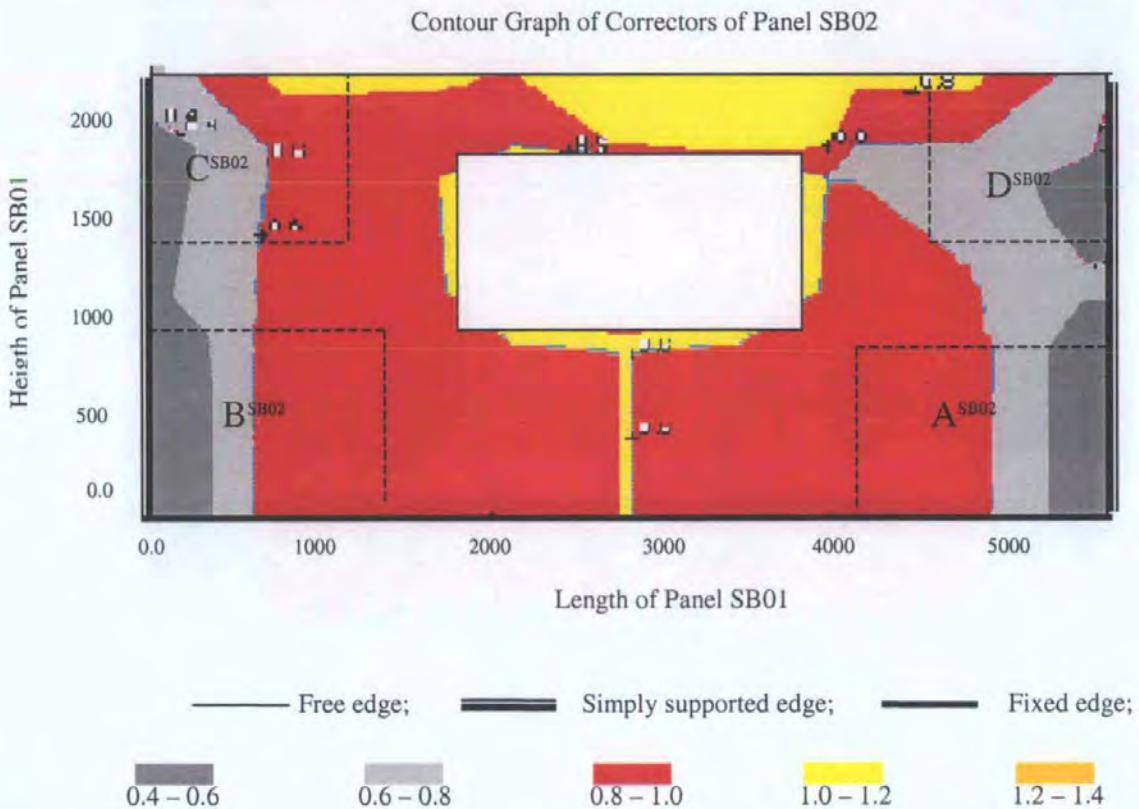
Region  $C^{SB06}$  on Panel SB06

(f)

**Figure 5.3** – Comparison of similar regions between Panels SB01 and SB06

The base panel used in this investigation to establish values of zone corrector does not have all combinations of boundary conditions. It is therefore necessary to estimate values of zone correctors adjacent to boundaries which do not correspond to the base panel to their similar boundaries. From the contour plots in Figures 5.3e and 5.3f, it is clear that Regions  $C^{SB06}$  and  $D^{SB06}$ , surrounded by simply supported boundaries and with similar corrector patterns, do not have the exact boundary types on the base panel which can match the boundary types surrounding these two regions on Panel SB06. However, Region  $A_1^{SB01}$  (Figure 5.3d), surrounded by a built-in boundary and a simple support, has the similar corrector pattern with Regions  $C^{SB06}$  and  $D^{SB06}$ . Thus for Regions  $C^{SB06}$  and  $D^{SB06}$  on the panel SB06, Region  $A_1^{SB01}$  on the base panel can be considered to be their similar region.

The same observation on Panels SB01 and SB02 has been made as follows. Figure 5.4 shows the contour plot for correctors of Panel SB02 with an opening. Except for the existence of an opening, Panel SB02 is identical to Panel SB01 in its boundaries, material and sizes. The correctors within the opening area of the panel are considered to be zero.



**Figure 5.4** – Contour graph of correctors of Panel SB02 with opening

Firstly, the four regions  $A^{SB02}$ ,  $B^{SB02}$ ,  $C^{SB02}$  and  $D^{SB02}$  at the four corners of Panel SB02 are defined. These four regions are then compared with the corresponding regions  $A^{SB01}$ ,  $B^{SB01}$ ,  $C^{SB01}$  and  $D^{SB01}$  at the four corners of Panel SB01, the same observation which is described in comparison of Panel SB06 with Panel SB01 can be made.

The above comparisons provide the evidence that there are similar regions with similar corrector distribution, which are governed by similar boundary types. The same correctors lie in the corresponding local zones, the parts with the same colour within similar regions. These zones with the same correctors are called similar zones. Similar zones mainly relate to the panel boundaries, positions and sizes of the zone.

In the following section, rules are developed for matching zone similarities and the applicability of the rules and the process of matching zone similarities are discussed.

### ***5.3. Modelling Similarity of Zones between Two Panels***

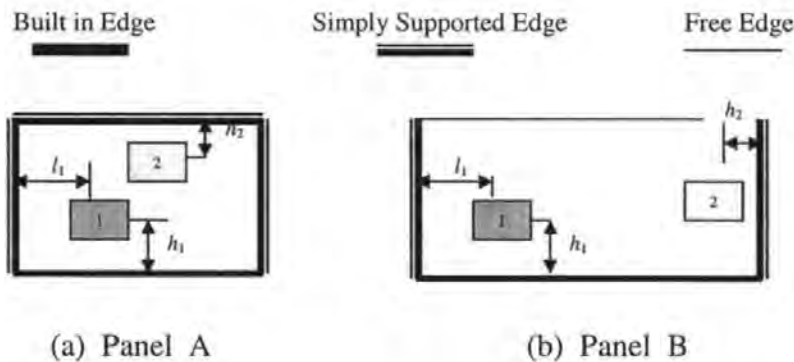
As stated in Chapter 4, correctors are derived from comparing experimental and theoretical displacement relationship. Correctors, among other factors, mainly depend on the four factors: geometrical properties, boundary conditions, material properties and intensity of applied loading. Therefore the methodology for matching similar zones between two panels must include all the above factors. Among these factors, the boundary constraints have a significant effect on the magnitude of correctors. The sizes of individual zones have also been included in the rules for determining correctors.

#### **5.3.1. Boundary Conditions**

In this study, the position of a zone within the panel and the types of the panel boundaries near the zone are considered to be the major factors influencing the behaviour of zones within the panel. In other words, the distance from a zone within the panel to an edge with specific boundary condition is the basis of similarity of two zones in two panels separately.

For instance, Zone 1 within Panel A in Figure 5.5a has the distances,  $l_1$  and  $h_1$ , to the two closest supports, the left simple support and the bottom built-in support of the panel. Zone 1 within Panel B in Figure 5.5b also has the distances,  $l_1$  and  $h_1$ , to two closest supports, the left simply support and the bottom built-in support of the panel. Thus Zone 1 in Panel A and Zone 1 in Panel B can be considered similar and the same corrector can be assigned to these two zones.

Zone 2 in Panel A in Figure 5.5a lies near the vertical symmetrical line of the panel. Its shortest distance to the simply supported edge at the top of the panel is  $h_2$ . According to the position of Zone 2 in Panel A and the boundary types of the panel, its similar zone, Zone 2 in Panel B in Figure 5.5b, is located at the middle of a simply supported edge which in this case is at the right-hand edge of Panel B, and the distance to the simply support must also be  $h_2$ . Therefore, Zone 2 in Panel A and Zone 2 in Panel B are similar zones and the same corrector can be assigned to both zones.



**Figure 5.5** – Similar zones between Panels A and B

### 5.3.2. Material Properties

When values of correctors are assigned from the base panel to the new panel, two panels must be made of the similar material. In fact the corrector is a normalised dimensionless parameter, which reflects the collective effect of variation in masonry

properties and boundary conditions into a single adjustment at the individual zones in the base panel. This dimensionless parameter reflects the general variation characteristics of panels built using similar masonry material. Thus the values of correctors from the base panel can be assigned to similar zones in the new panel with the same material properties.

### 5.3.3. Load

From Figures 4.3 and 4.4, it is clear that the value of each corrector settles to a stable value after the applied load reaches a specific level. In other words, the load value has little effect on the corrector after all the parts of the panel enter their working-state. Therefore load factor is not included in the similarity rules.

## 5.4. Rules for Matching Similar Zones

In Section 5.2, the types of boundaries and the position of zone with respect to these boundaries were prepared as the basis of similarity between zones in two panels. Based on this assumption, the rules for matching zone similarities can be defined as:

Firstly, for a zone within a new panel, its distances to two boundaries nearest to the zone are calculated by

$$\delta_i^{b-x} = \min[ x_i^{b-left}, (L - x_i^{b-left})^{b-right} ] \quad (5.2)$$

$$\delta_i^{b-y} = \min[ y_i^{b-bottom}, (H - y_i^{b-bottom})^{b-top} ] \quad (5.3)$$

where

$L, H$  are the length and the height of the panel;

$x_i$  and  $y_i$  are the co-ordinates of the centre of the  $i$ th zone;

$\delta_i^{b-x}$ : minimum distance from a vertical boundary;

$\delta_i^{b-y}$ : minimum distance from a horizontal boundary;

$b$ : boundary type, s for simply supported edge, f for free edge and b for built in edge;

$b_{left}$ : the boundary on the left edge of the zone;

$b\_right$  : the boundary on the right edge of the zone;

$b\_bottom$  : the boundary to the bottom edge of the zone;

$b\_top$  : the boundary to the top edge of the zone.

After an edge boundary condition of a new panel matches with an edge boundary condition of a base panel, the following two cases need to be considered:

*Case 1.* If the length of the edge of the new panel is longer than the length of the corresponding edge of the base panel, this edge length of the new panel is divided into the same number of divisions as the base panel edge. The sizes of each division should be proportional to those of the base panel.

*Case 2.* If the length of the edge of the new panel is smaller than the length of the corresponding edge of the base panel, the new panel is divided into zones whose sizes are equal to those of the corresponding zones they superimpose on the base panel. The zones on the new panel have the same sizes as the corresponding zones on the base panel.

Finally,  $\delta_i^{b-x}$  and  $\delta_i^{b-y}$  are used to locate similar zones within the base panel. For example, in Figure 5.5 Panels A and B are the new panel and the base panel respectively.

For Zone 1 within the new panel A:  $\delta_{1new}^{b-x} = l_1$ ,  $\delta_{1new}^{b-y} = h_1$ ;

For Zone 1 within the base panel B:  $\delta_{1base}^{b-x} = l_1$ ,  $\delta_{1base}^{b-y} = h_1$ ;

$$\delta_{1new}^{b-x} = \delta_{1base}^{b-x} = l_1; \delta_{1new}^{b-y} = \delta_{1base}^{b-y} = h_1.$$

Therefore, Zone 1 within Panel B is similar to Zone 1 within Panel A, as they have the same distances from the similar boundaries.



For Zone 2 within the new panel A:  $\delta_{1new}^{b-x} = 0.5H_{base}$  (see the following explanation on  $0.5H_{base}$ ),  $\delta_{1new}^{b-y} = h_2$ ;

$H_{base}$  is the height of the base panel B. Because the top boundary of the new panel A matches the left/right boundary of the base panel B and the length of the new panel A is larger than the height of the base panel B, the length of the new panel A is in proportion changed into the height of the base panel A when calculating  $\delta_{1new}^{b-x}$ .

For Zone 2 within the base panel B:  $\delta_{1base}^{b-x} = h_2$ ,  $\delta_{1base}^{b-y} = 0.5 H_{base}$ ;

$$\delta_{1new}^{b-x} = \delta_{1base}^{b-y} = 0.5H_{base}, \quad \delta_{1new}^{b-y} = \delta_{1base}^{b-x} = h_2.$$

Therefore, Zone 2 within Panel A is similar to Zone 2 within Panel B.

Finally, the corrector for the zone in the new panel is selected from its similar zone in the base panel.

### **5.5. Procedure for Applying Rules for Matching Similar Zones**

According to the rules for matching similar zones, a procedure can be applied to establish similarity of zones and determine values of correctors at different zones within the new panel. For the experimental panel SB01, used as the base panel, its correctors are obtained by comparing the displacements at various locations from the experiment with those obtained from the FEA calculation of the panel, as described in Chapter 4. A procedure is used to identify similar zones between the base panel and the new panel. Once similar zones between two panels are located, appropriate correctors for the new panel are selected for use in the FEA of the new panel. This procedure is described below:

- Take a zone in the new panel and locate the co-ordinates  $x_i$  and  $y_i$  at the central point of the zone as the position of the zone;

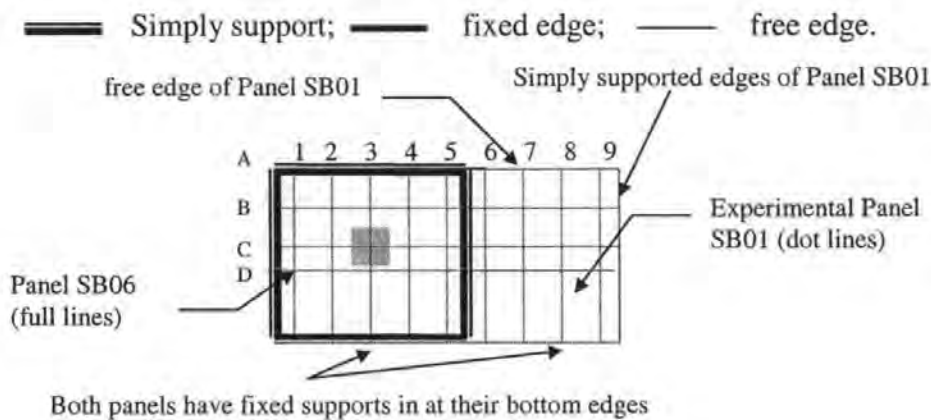
- Calculate  $\delta_i^{b-x}$  and  $\delta_i^{b-y}$  considering the types of panel boundaries;
- $\delta_i^{b-x}$  and  $\delta_i^{b-y}$  are used to locate the position of the similar zone on the base panel. If the edge of the new panel, from which  $\delta_i^{b-x}$  and  $\delta_i^{b-y}$  are calculated, is smaller than the corresponding edge of the base panel, values of  $\delta_i^{b-x}$  and  $\delta_i^{b-y}$  are directly used to identify similar zones on the base panel. If, however, the length of the edge on the new panel, from which  $\delta_i^{b-x}$  and  $\delta_i^{b-y}$  are calculated, is larger than the length of the corresponding edge of the base panel,  $\delta_i^{b-x}$  and  $\delta_i^{b-y}$  are proportionally enlarged to locate the similar zone on the base panel. If  $\delta_i^{b-x}$  and  $\delta_i^{b-y}$  correspond to the same boundary type on the base panel, the larger one should correspond to a similar boundary type of which the orientation is normal to the orientation of the boundary type which the smaller one corresponds to, in order to enable to locate a similar zone on the base panel.
- Select the corrector values from the similar zones on the base panel for the zones on the new panel.

In Figure 5.6, Panel SB06 is superimposed on the base panel SB01. The corresponding similar zone at centre of the panel SB06 (solid line), for instance, is located as follows:

1. The left simple support and the bottom built-in support are nearest to the central zone of Panel SB06;
2. The base panel SB01 also has a left simple support and the bottom fixed support;
3. Superimpose Panel SB06 over the base panel SB01 by placing their left-hand bottom corners at the same position.

4. The central zone of Panel SB06 matches with the zone C3 in the base panel SB01. Thus the zone C3 in the base panel is considered to be a similar zone to the central zone in the panel SB06.

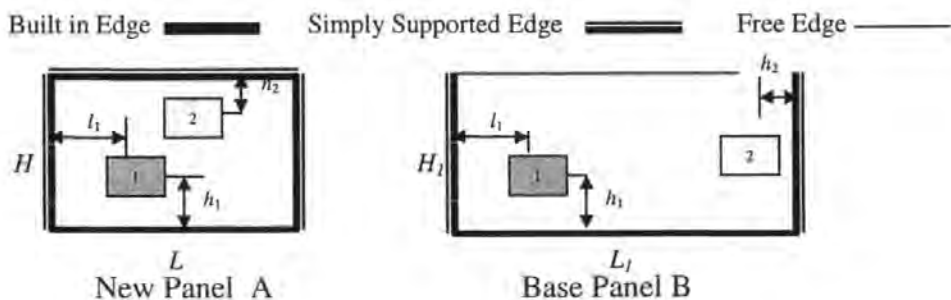
When analysing the panel SB06 using the FEA, the correctors of the zone C3 in the base panel SB01 can be used for the central zone of Panel SB06.



**Figure 5.6** – Manually matching similar zones using a geometrical method

For example, for Zone 1 on the new panel A shown in Figure 5.7:

- Locate the co-ordinates of Zone 1 on the new panel A :  $x_1 = l_1$  and  $y_1 = h_1$ ;
- Calculate:  $\delta_{1new}^{y-x} = l_1$ ,  $\delta_{1new}^{b-y} = h_1$ ;
- Locate the similar zone on the base panel A:  $\delta_{1base}^{b-x} = \delta_{1new}^{b-x} = l_1$ ;  $\delta_{1base}^{b-y} = \delta_{1new}^{b-y} = h_1$ , see Zone 1 on the base panel B.



**Figure 5.7** – Matching similar zones using an analytical method

For Zone 2 on the new panel A shown in Figure 5.7:

- Locate the co-ordinates of Zone 2 on Panel A :  $x_2 = 0.5L$  ( $L$  is the length of the new panel A) and  $y_2 = H-h_2$  ( $H$  is the height of the new panel A);
- Calculate:  $\delta_{2new}^{s-x} = 0.5L$ ,  $\delta_{2new}^{s-y} = h_2$ ;
- Locate the similar zone on the base panel A: Because both  $\delta_{2new}^{s-x}$  and  $\delta_{2new}^{s-y}$  correspond to the same boundary type, simply support, but  $\delta_{2new}^{s-x} = 0.5L > \delta_{2new}^{s-y} = h_2$ ,  $\delta_{2new}^{s-y}$  is firstly used to locate the similar zone on the base panel A,  $\delta_{2base}^{s-x} = \delta_{2new}^{s-y} = h_2$ . As the length of the top edge corresponding to  $\delta_{2new}^{s-y}$  is larger than the length of the corresponding edge (the right vertical edge) of the base panel,  $\delta_{2new}^{s-x}$  is proportionably used to locate the similar zone on the base panel A,  $\delta_{2base}^{b-y} = \frac{\delta_{2new}^{s-x} H_1}{L} = 0.5H_1$ , see Zone 2 on the base panel B shown in Figure 5.7;
- Finally, the corrector for the zone in the new panel is selected from its similar zone in the base panel.

## 5.6. Summary

The definition of zone similarity is based on the two findings:

1. The corrector distribution on some regions within panels presents similar patterns.
2. Similar regions are governed by similar closest adjacent boundary conditions.

Thus, in similar regions, zones with the same corrector values are located at similar positions and also governed by similar boundary conditions.

According to the conclusions above, a method was proposed to match similar zones between a new panel and a base panel. Every zone within the base panel is located based on the measured point whose ratio between the experimental and the FEA displacements is defined as corrector. This means that the sizes of the divided zones within the base panel have been fixed. Because similar zones are required to have similar sizes or proportional sizes according to the dimensions between the base panel and the new panel, the sizes of divided zones within a new panel must take the sizes of zones within the base panel as reference.

However the method proposed for selecting correctors is not easy to use. Therefore, in the following chapter methodologies for automatically identifying similar zones between two panels and estimating correctors for various zones within a new panel.

## **6. APPLICATION OF CELLULAR AUTOMATA IN MODELLING SIMILAR ZONES WITHIN PANELS**

### ***6.1. Introduction***

The concept of a corrector established in Chapter 4 has quantified the variation in masonry properties, based on the comparison of displacement values measured in the laboratory with those calculated by the FEA. After a comprehensive investigation, it became clear that the main factor governing individual corrector values is the panel boundary conditions. In Chapter 5 the basic criteria for estimating corrector values at locations on the panel were developed in order to modify properties of various zones within a panel. These criteria were based on the modelling of zone similarity between a base panel and a new panel. Based on the criteria a method was developed to identify similar zones within two panels, but this method is not easy to operate as the accuracy of mapping the division of zones within the base panel and the new panel requires a deeper understanding of the influence of different types of boundaries on local zones. It also requires a consideration of the relevant sizes and positions of the zones within the base panel and the new panel. Therefore, there is a need for developing a comprehensive automatic technique to divide the zones on the new panel having different boundary conditions and sizes, match the similar zones in the new panel with those in the base panel and select appropriate correctors for the FEA of the new panel.

This chapter proposes an automatic method using Cellular Automata (CA) (see Section 6.2.1) to accomplish this task. Cellular automata are selected to implement this process as it smoothly propagates the effect of boundaries on the individual zones

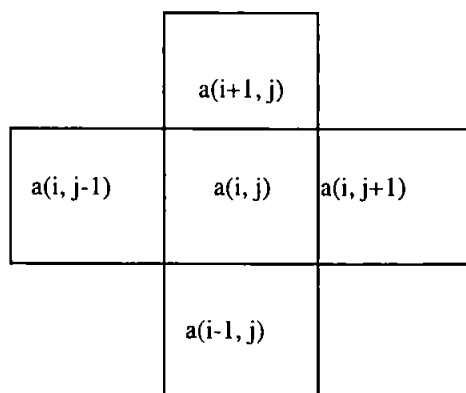
within the panel using a transition function of a predefined boundary parameter. The value that every zone obtains in this transition function is described as the “state value” related to the positions of individual zones which are affected by their neighbourhood zones. This state value is different from any physical responses calculated by the FEA. In other words, the effect of boundaries in the FEA is reflected in the actual physical response of the panel to the applied loading such as displacement, stress, strain etc, but the boundary effect expressed in the CA is purely a numerical value (scalar quantity) which can be related to the extent that the boundaries of a panel can affect a zone within the panel.

Cellular Automata are implemented to firstly propagate the effect of panel boundaries to individual zones within the base panel to determine state values of different zones. The same process is applied to a new panel having different boundary conditions and/or sizes from the base panel. The similarity rules are then used to identify similar zones within the new panel to those within the base panel. Finally a computer programme has been developed to translate the state values on the new panel into actual corrector values, based on the correctors of similar zones in the base panel. These corrector values can then be used directly in the FEA of the new panel. The research included an extensive study to examine what parameter values best describe particular boundary types and what transition coefficients are appropriate in the CA application, to improve standard FEA results.

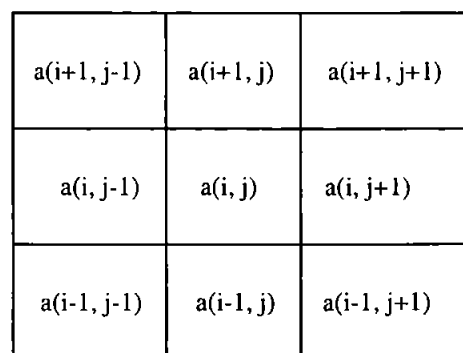
## 6.2. Modelling Boundary Effect Using Cellular Automata

### 6.2.1. Cellular Automata Model

Referring to Soschinske's statement (1997), cellular automata (CA) are described as discrete "space-time models that can be used to model any system in the universe (Rietman and Edward 1989)". "They are dynamical systems with discrete values in space and time state used for solving biological, physical and mathematical problems" (Eissler et. al 1992). Whichever definition is used it is clear that CA can be used to model a wide variety of physical phenomena (Halpern May 1989). CA consists of cells in a lattice network (Rietman and Edward 1989). The cells may be a one-dimensional, two-dimensional (including 2-D hexagonal), or three-dimensional (including cubic) array, with each cell capable of existing in one or more states (e.g., 0 to 6 for a hexagonal system). The "neighbourhood", are defined as number of cells adjacent to the cell under consideration, which will influence the behaviour of this cell state. Figure 6.1a and b show the examples of two 2-D neighbourhood cell models developed by von Neumann and Moore (Soschinske 1997) (Goles et al. 1990) respectively. The von Neumann cell  $a(i, j)$  is affected by four neighbourhood cells, while the Moore cell is affected by eight adjacent cell.



(a) von Neumann neighbourhood



(b) Moore neighbourhood

**Figure 6.1** – Cellular Automata Neighbourhoods of von Neumann and Moore



The change in a state from time  $t$  to time  $t+1$  is governed by some “local rules” (Rietman and Edward 1989) or “transition rules” (Goles et al. 1990). For a CA model, neighbourhood structure and transition rules need to be the same for all sites. Rules need not be fixed; a random input could be used to introduce stochastic rule (Rietman and Edward 1989). Updating the cells for a CA network must be done in a “synchronous” or parallel mode (Goles et al. 1990). Rucker and Rudy (1989) summarised the properties of a CA as follows:

- Parallel: an individual cell is updated independent of other cells;
- Locality: new cell state values depend on their old cell state values, and state values of their neighbourhood cells;
- Homogeneity: same rules are applied to all cells.

Halpern (1989) formalized the cellular automata transition model in the case of the von Neumann neighbourhood as:

$$a_{i,j}^{(t+1)} = \psi(a_{i,j}^{(t)}, a_{i,j+1}^{(t)}, a_{i+1,j}^{(t)}, a_{i,j-1}^{(t)}, a_{i-1,j}^{(t)}) \quad (6.1)$$

where

$a$  = lattice site value

$i, j = x, y$  lattice co-ordinates

$t$  = time interval

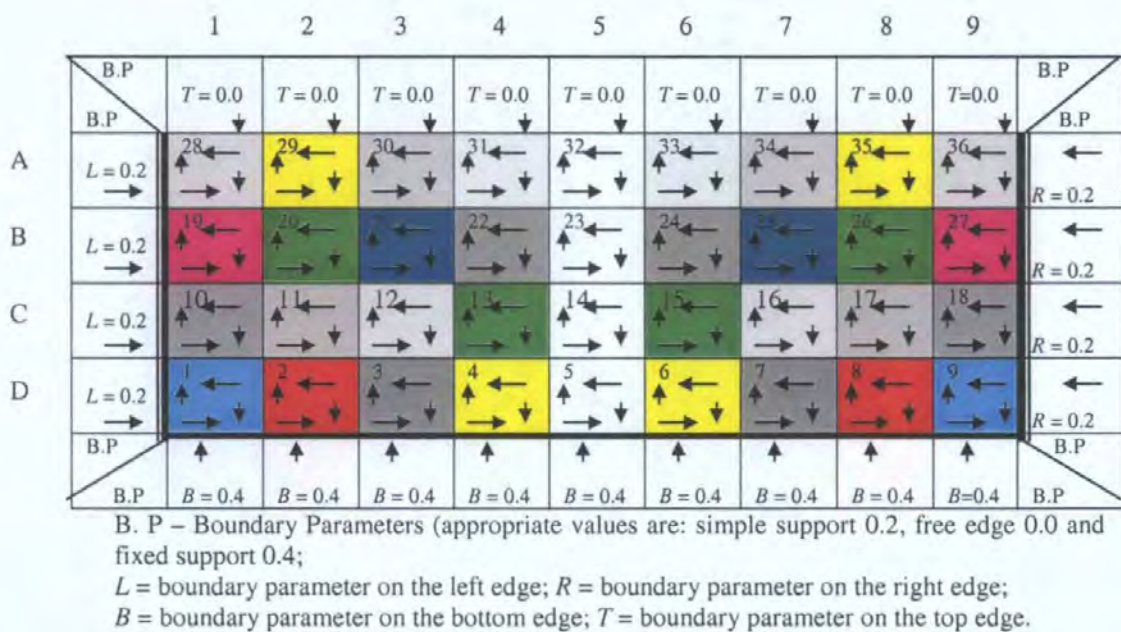
$\psi$  = function related to iteration rule

### 6.2.2. Modelling Boundary Effect by Cellular Automata

The results in Chapter 5 indicate that a panel can be divided into many zones for which the similarity of zones are closely related to the panel boundary conditions and the positions of the zone relative to the boundaries of the panel. When compared with the properties, parallel, locality and homogeneity of the CA, the characteristics of

zone similarity can be suitably described by the space properties of CA. To describe this CA model, the following assumptions are made:

- (1) Panel SB01 is used as a base panel. This panel is divided into thirty-six zones based on the positions of experimentally measured points on the panel (see Figure 6.2 for details, the zones with same colour are symmetrical);
- (2) The following parameters are used for each boundary condition, 0.2 for simple support, 0.0 for free support and 0.4 for fixed support. Justification for these values is given in Section 6.5.2.



**Figure 6.2** – Panel is modelled as a CA system.

Figure 6.2 shows how the base panel SB01 is modelled as a CA system using the CA:

- Each zone represents a cell of the CA system. The boundaries with specified values for different types (0.0, 0.2 or 0.4) are described as initial values of transition functions. These initial values or boundary effects are then propagated into individual cells by the transition functions.

- The position of each cell in the CA system corresponds to the position of a zone within the panel. The position of a zone is described by the co-ordinates of the central point of the zone
- The state value of each cell (zone) is affected by the state values of its neighbourhoods.

Thus, in order to describe the influence of different boundaries at four supported edges of the panel, a von Neumann model is sufficient because the panel is as a two-dimension panel in this CA application. The transition functions of CA, which propagate the effect of individual boundaries on individual zones within the panel, can be shown as:

$$\begin{aligned}
 L_{ij} &= L_{i,j-1} + \eta(1 - L_{i,j-1}) \\
 R_{ij} &= R_{i,j+1} + \eta(1 - R_{i,j+1}) \\
 B_{ij} &= B_{i-1,j} + \eta(1 - B_{i-1,j}) \\
 T_{ij} &= T_{i+1,j} + \eta(1 - T_{i+1,j})
 \end{aligned}
 \tag{6.2}$$

where

$\eta$  = coefficient of transition

$L$  --- state value of zone changes from the left boundary effect

$R$  --- state value of zone changes from the right boundary effect

$B$  --- state value of zone changes from the bottom boundary effect

$T$  --- state value of zone changes from the top boundary effect

and the local rule for the calculation of the state value  $S_{i,j}$  of the individual zones within the panel are described as:

$$S_{i,j} = \frac{(L_{i,j} + R_{i,j} + B_{i,j} + T_{i,j})}{4}
 \tag{6.3}$$

The value of the state value,  $S_{i,j}$ , is the average effect from neighbourhood cells. The transition functions represented in Equation (6.2) produces numerical series to reflect

the effect of boundaries on individual zones within the panel. Equation (6.3) sums up the effect of all four boundaries at the four edges of the panel on a zone  $a(i, j)$  within the panel. It should be noted that the CA model used here is not time-dependent and the original state value of each cell is zero.

The properties of parallel, locality and homogeneity of CA are sufficient in the proposed CA model for the boundary effect on zones within the panel:

- For the property of parallel, the state values of individual cells can be updated independent of other cells/zones, see Equation (6.3).
- For the property of locality, the new cell/zone state value depends on state values of its neighbouring cells/zones, see Equation (6.2).
- For the property of homogeneity, the same rules can be applied to each cell/zone within the panel (the CA net work). The governing rules, used in this CA model, are described in Equations (6.2) and (6.3).

However, Equations (6.2) and (6.3) are not enough to completely describe the similarity of zones. In other words, if two zones have the same state value calculated by Equations (6.2) and (6.3), these two zones do not necessarily have the same corrector. For example, for a panel which is the same as Panel SB01 shown in Figure 6.2 except for its right built-in edge, the state values of the individual zones are calculated using Equations (6.2) and (6.3) and the result of the CA is summarised in Table 6.1. In Table 6.1, Zones D2 and A5 (or D3 and B7 or B3 and C9) have the same state value, but they are not similar zones because Zone D2 lies close to a fixed edge and Zone A5 is adjacent to a free edge. Therefore, it is necessary to establish a set of new rules to identify similar zones having the same corrector values on two panels.

**Table 6.1** State values from Equations (6.2) and (6.3)

		1	2	3	4	5	6	7	8	9	
		0	0	0	0	0	0	0	0	0	
A	0.2	0.558	0.585	0.605	0.62	0.624	0.625	0.62	0.609	0.592	0.4
B	0.2	0.583	0.61	0.629	0.64	0.649	0.649	0.644	0.634	0.616	0.4
C	0.2	0.596	0.623	0.642	0.65	0.661	0.662	0.657	0.646	0.629	0.4
D	0.2	0.597	0.624	0.644	0.66	0.663	0.664	0.659	0.648	0.631	0.4
		0.4	0.4	0.4	0.4	0.4	0.4	0.4	0.4	0.4	

### 6.2.3. Application of CA to Determine Correctors

It can be seen from Table 6.1 above that the CA applied to any panel with consideration of comparison of state value of each zone only will not give good correlation between similar zones. Therefore, the following sections will try to propose the rules which can produce satisfying results of matching similar zones.

Section 6.3 below shows a rule for matching similar zones with consideration of state values of each zone and its four neighbourhoods. Section 6.4 below shows how orientations of zones in a new panel need to be undertaken in order that like boundaries coincide. Section 6.4 also involves the same process for rotating regions on a new panel in order that like boundaries coincide and are therefore correctly modelled. Section 6.5 shows how the values for the boundary parameters and the transition coefficient have been derived.

### 6.3. Rules of Matching Zone Similarity

As mentioned in the previous sections, comparing state values of individual zones calculated by the CA only is not enough to fully define similarity between zones, as this gives misleading results as shown in Table 6.1 (Zones D2 and A5, D3 and B7, B3 and C9). In order to be able to use the state values of individual zones to match the similarity between zones, it is necessary to simultaneously consider the state values of a zone along with the state values of its four neighbourhoods/zones. According to the

above analysis, the rules for matching similarity between zones using the CA state values are developed in the following sections.

### 6.3.1. Pre-Conditions

- (1) The FEA of the new panel and the base panel uses the same FEA technique;
- (2) The new panel and the base panel have the same material properties;
- (3) The new panel and the base panel are subjected to uniformly distributed lateral load only.

### 6.3.2. Development of Rules for Matching Similar Zones

To accurately match similar zones between panels using CA, it is necessary to compare each individual zone of a new panel along with its four neighbouring zones with every zone on the base panel along with its four neighbouring zones using the state values of these zones on both panels. This is necessary as the four neighbourhoods, as shown in Equation (6.2), determine the state value of a zone. Thus the following relationship is derived to evaluate a comparison error:

$$E_{i,j \rightarrow new}^{k,l \rightarrow base} = \underset{m=1, n=1}{MIN}^{M, N} (|S_{i,j}^{new} - S_{m,n}^{base}| + |S_{i,j-1}^{new} - S_{m,n-1}^{base}| + |S_{i,j+1}^{new} - S_{m,n+1}^{base}| + |S_{i-1,j}^{new} - S_{m-1,n}^{base}| + |S_{i+1,j}^{new} - S_{m+1,n}^{base}|) \quad (6.4)$$

where

$E_{i,j \rightarrow new}^{k,l \rightarrow base}$  --- the minimum error of  $M \times N$  errors in Equation (6.4)

$\underset{m=1, n=1}{MIN}^{M, N}$  --- calculate  $M \times N$  errors and then select the minimum one

$M, N$  --- the number of row and the number of column for divided zones within the base panel corresponding to the measured points of the base panel in its experiment

*base* --- items related to the base panel

*new* --- items related to the new panel

$S$  --- state value of zone in the panel

$(k, l \rightarrow base)$  and  $(i, j \rightarrow new)$  mean that Zone  $(k, l)$  on the base panel is matched to be similar zone with Zone  $(i, j)$  on the new panel.

Once the minimum error value for a zone in the new panel, based on comparisons with every zone in the base panel, is determined using Equation (6.4), the zone on the base panel is defined as the similar zone to the zone on the new panel. The value of the corrector in the base panel for the zone with minimum error is then used for the zone on the new panel for the FEA process.

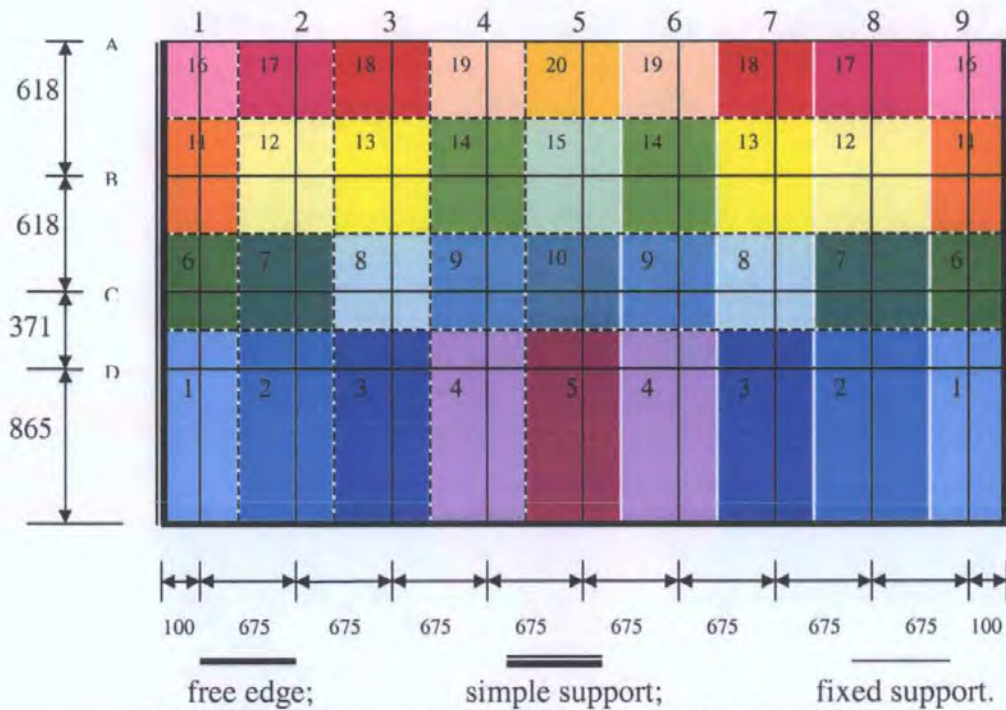
## **6.4. Analysis of Equations for Matching Similar Zones**

### **6.4.1. Effect of Neighbourhood Orientation in Developing Rules for Matching Similar Zones**

In order to assess whether Equation (6.4) is sufficient to accurately match similar zones between two panels, an important check would be to investigate whether this equation can perfectly match zones on both sides of the line of symmetry.

To check the validity of this equation, it was decided to test this equation on the base panel SB01 as existing information on this panel was available. Panel SB01 (Figure 6.3) was divided into 36 zones based on the experimental measured points A1 – A9, B1 – B9, C1 – C9 and D1 – D9. Considering the symmetry of the panel along the vertical central line, there are only 20 different zones on the panel. In this investigation, two zones on the panel (Zone D2 on the left side and Zone C9 on the right side) are selected to check the validity of Equation (6.4). To find a zone similar to Zone D2, the equation should first locate the zone D2 itself and it should also find a

similar zone on the other symmetrical half of the panel which is Zone D8. Similarly, for Zone C9, it should be able to locate Zone C9 and C1.



Note: The Measure Points are A1~A9, B1~B9, C1~C9 and D1~D9.  
**Figure 6.3** - Divided zones of Panel SB01 around every measure points

By inspection, Zone D2 must match Zone D8 and Zone C9 must match Zone C1. The CA was used to establish state values for all zones in the panel. Table 6.2 shows the results of the CA for state values for these zones given in Equations (6.2) and (6.3) which were used for this calculation. Equation (6.4) was then applied to calculate the errors between Zones D2 and C9 along with their four neighbourhood zones with every other zone and their corresponding four neighbourhoods on the panel. The results of the analysis are summarised in Table 6.3 for Zone D2 and Table 6.5 for Zone C9 separately.

From Table 6.3 it is clear that the minimum error for matching Zone D2 using Equation (6.4) is Zone D2 itself with the error value of 0.0 and Zone D8 is with the



error value of 0.085. Based on the proposed rules, the error for Zone D8 should also 0.0. This indicates that Equation (6.4) has not perfectly calculated the error for Zone D8. This rule needs to be improved. The result of matching errors in Table 6.5 for Zone C9 using Equation (6.4) shows that this rule was only able to match Zone C9 to itself with the error value of 0.0; however, it fails to match this zone to its symmetrical Zone C1 (the error value = 0.8289). Therefore, it can be concluded that Equation (6.4) is effective in matching some zones, but fails to find all similar zones within the panel.

**Table 6.2** – State values of Panel SB01 calculated using Equation (6.3)

State Values		1	2	3	4	5	6	7	8	9	
		0	0	0	0	0	0	0	0	0	
A	0.2	0.5517	0.577	0.5942	0.6042	0.6075	0.6042	0.5942	0.577	0.5517	0.2
B	0.2	0.5764	0.6016	0.6189	0.6289	0.6321	0.6289	0.6189	0.6016	0.5764	0.2
C	0.2	0.5892	0.6144	0.6317	0.6417	0.6449	0.6417	0.6317	0.6144	0.5892	0.2
D	0.2	0.5908	0.616	0.6333	0.6433	0.6465	0.6433	0.6333	0.616	0.5908	0.2
		0.4	0.4	0.4	0.4	0.4	0.4	0.4	0.4	0.4	

**Table 6.3** - Errors of Zone D2 to all other zones calculated using Equation (6.4)

SB02	1	2	3	4	5	6	7	8	9
A	1.0745	0.6803	0.752	1.2062	1.3278	1.1993	0.752	0.6872	1.0745
B	0.8413	0.6059	1.0839	1.8016	2.2591	1.8016	1.0839	0.6059	0.8414
C	0.8676	0.6193	1.1389	2.0001	2.477	2.0001	1.1389	0.6193	0.8676
D	0.4332	0	0.1445	0.6852	0.6878	0.6002	0.0939	0.085	0.4838



**Figure 6.4** - State values of Zones D2 and D8 as well as their neighborhood zones

**Table 6.4** – State values of Panel SB01 calculated using Equation (6.3)

State Values		1	2	3	4	5	6	7	8	9	
		0	0	0	0	0	0	0	0	0	
A	0.2	0.5517	0.577	0.5942	0.6042	0.6075	0.6042	0.5942	0.577	0.5517	0.2
B	0.2	0.5764	0.6016	0.6189	0.6289	0.6321	0.6289	0.6189	0.6016	0.5764	0.2
C	0.2	0.5892	0.6144	0.6317	0.6417	0.6449	0.6417	0.6317	0.6144	0.5892	0.2
D	0.2	0.5908	0.616	0.6333	0.6433	0.6465	0.6433	0.6333	0.616	0.5908	0.2
		0.4	0.4	0.4	0.4	0.4	0.4	0.4	0.4	0.4	

**Table 6.5** - Errors of Zone C9 to all other zones calculated using Equation (6.4).

SB01	1	2	3	4	5	6	7	8	9
A	1.4196	1.0563	1.0512	1.0572	1.0505	1.0307	0.9968	0.9713	0.6656
B	0.8551	0.4938	0.5301	0.555	0.5715	0.555	0.5045	0.4176	0.0518
C	0.8289	0.5328	0.5692	0.6196	0.6362	0.6196	0.5692	0.4822	0
D	1.0356	0.7127	0.735	0.7755	0.7888	0.7755	0.735	0.6653	0.2068



**Figure 6.5** - State values of Zones C1 and C9 as well as their neighborhood zones

To improve the results of using Equation (6.4) it is necessary to include the orientation of the neighbourhood zones according to their actual positions from the boundaries of the panel. To explain this point better, Figures 6.4a and 6.4b show state values of Zones D2 and its identical symmetrical zone D8 along with their four neighbourhoods. Similarly, Figures 6.5a and 6.5b show state values of Zones C9 and its identical symmetrical zone C1 along with their four neighbourhoods. From Figure 6.4 (or Figure 6.5), it is clear that the state value of the zone on the right of Zone D2 (or Zone C9) is the same as that of the zone on the left of Zone D8 (or Zone C1). Therefore, in order to calculate the minimum error using Equation (6.4) the order of zones on the left and right hand sides of Zone D8 must be reversed.

Further investigation of this issue reveals that eight different orientations for the four neighbourhood zones of each zone must be considered to locate a perfect match. Details of this investigation are described in the following Section 6.6.

#### 6.4.2. Division of Regions and Method for Matching Their Similarity

The above analysis shows that to improve the results for Equation (6.4) three extra conditions should also be considered:

1. Properly divide both the base panel and the new panel into several regions according to their boundary conditions. This is needed to be done either manually or automatically.
2. Match a region of the new panel with a region of the base panel based on the similarity of their boundary condition, taking into account the orientation of each zone along with its four neighbourhoods.
3. The terms in Equation (6.4) must be arranged according to the orientation of neighbouring zones based on their distances from panel boundaries.

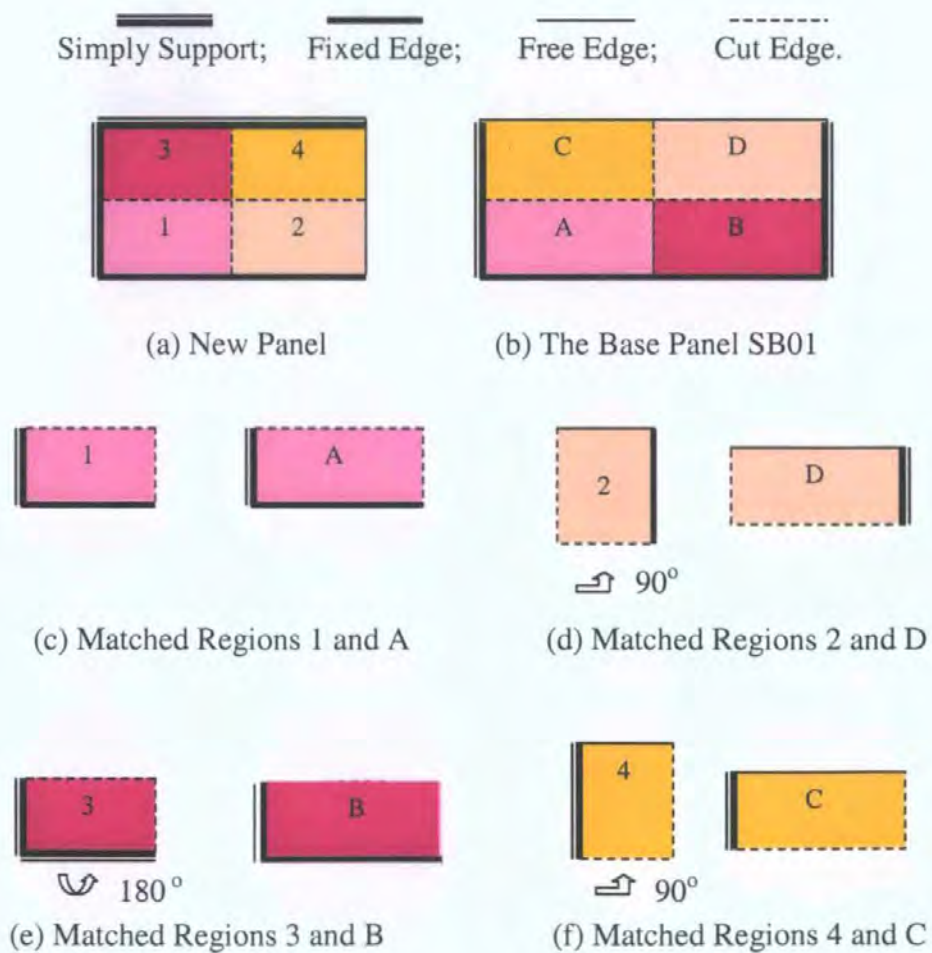
Based on these three pre-conditions, the method for dividing regions within panels without or with openings is introduced in the following section.

#### **6.4.2.1. Solid Panels**

Under these conditions, both a new solid panel and a solid base panel are separately divided into four regions by a horizontal and a vertical line crossing the centre of the panel. Then the four regions in the new panel are matched with their similar regions in the base panel. For instance, for a new panel and the base panel SB01, their divided regions are shown in Figures. 6.6a and 6.6b. The positions of all regions in the base panel are fixed. Regions in the new panel can be moved or rotated to perfectly match with their similar regions in the base panel.

For example, Region 1 on the new panel (Figure 6.6 (a)), is surrounded by the same boundary types (i.e., a simply supported edge, a fixed edge and the other two cut continuous edges) as the base panel. This region is similar to Region A on the base panel SB01. Region 1 does not need to be rotated to match with Region A, see Figure 6.6c.

For Region 2 in the new panel, there are no regions with the same boundaries in the base panel to match this region directly. But Region 2 in the new panel can be considered as the similar region to Region D or Region C on the base panel if the simply supported edge is considered to have approximately similar characteristic with fixed edge according to the analysis in Chapter 5. Region 2 needs to be rotated by  $90^\circ$  counterclockwise about its centre to bring its free edge in the same orientation as the free edge on the base panel and its fixed edge to the simply supported edge of the base panel, see Figure 6.6d. This means the neighbourhoods of zones within Region 2 also needs to be rotated by  $90^\circ$  counterclockwise to perfectly use Equation (6.4) to match similar zones between Region 2 and Region D.



**Figure 6.6** – Example of matching similar regions

Similar operations are performed in Regions 3 and 4 in the new panel to match with their similar Regions B and C in the base panel SB01, see Figure 6.6e and 6.6f.

To demonstrate the effectiveness of this improvement, Zones D2 and C9 of Panel SB01 as discussed in Section 6.4.1 are examined again to verify the robustness of Equation (6.4). Because the region A including Zone D2 is similar with Zone B including Zone D8, the positions of two regions are arranged as shown in Tables 6.6 and 6.7 which include the state values of zones in and around Regions A and B calculated by Equations (6.2) and (6.3).

**Table 6.6** – State values of zones in and around Region A calculated using Equation (6.3)

5	4	3	2	1		
0.6321	0.6289	0.6189	0.6016	0.5764	0.2	B
0.6449	0.6417	0.6317	0.6144	0.5892	0.2	C
0.6465	0.6433	0.6333	0.616	0.5908	0.2	D
	0.4	0.4	0.4	0.4		

**Table 6.7** – State values of zones in and around Region B calculated using Equation (6.3)

4	5	6	7	8	9		
0.6289	0.6321	0.6289	0.6189	0.6016	0.5764	0.2	B
0.6417	0.6449	0.6417	0.6317	0.6144	0.5892	0.2	C
0.6433	0.6465	0.6433	0.6333	0.616	0.5908	0.2	D
0.4	0.4	0.4	0.4	0.4	0.4		

**Note:** Region A and Region B are placed in accordance with boundaries.

Table 6.8 shows the errors calculated by Equation (6.4) based on Tables 6.6 and 6.7 (separately by arranging Region A to itself and Region A to Region B). By introducing this modification, Equation (6.4) is able to find the perfect match error value of 0.0 for both Zones D2 and D8. Therefore, Equation (6.4) is able to produce an accurate result of matching similar zones by dividing the panel into regions and rearranging the orientations of divided regions according to the similarity of boundaries.

**Table 6.8** – Errors of Zone D2 to all Zones in Region A and Region B using Equation (6.4)

Region A to Itself					Region A to Region B				
	1	2	3	4	5	6	7	8	9
C	0.6653	0.23365	0.2854	0.3358	0.3524	0.3358	0.2854	0.2336	0.6653
D	0.45855	0	0.0697	0.1102	0.1235	0.1102	0.0697	0	0.4585

Similarly, Zone C9 matches itself and another similar zone C1 by applying Equation (6.4) in the similar regions A and B, see Table 6.9.

**Table 6.9** – Errors of Zone C9 to all Zones in Region A and Region B using Equation (6.4)

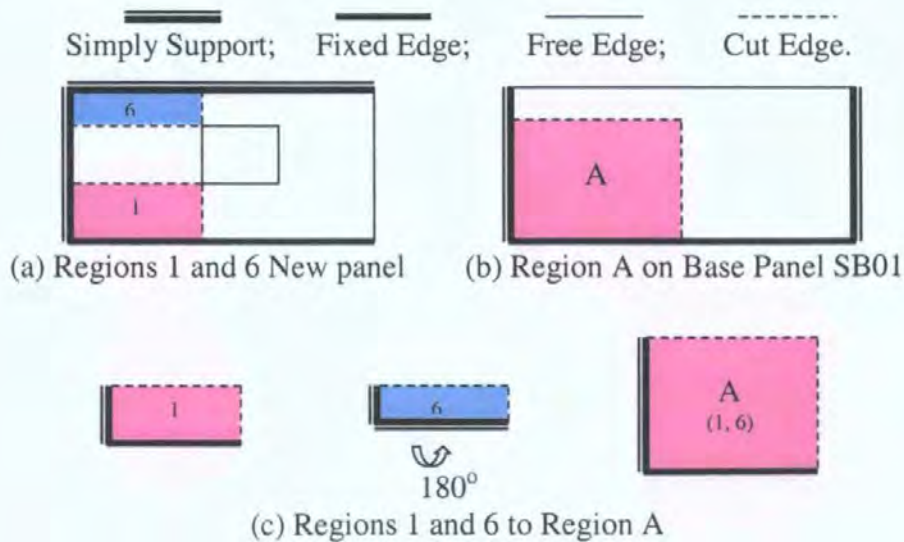
Region A to Itself					Region A to Region B				
	1	2	3	4	5	6	7	8	9
C	0	0.48224	0.5692	0.6196	0.6362	0.6196	0.5692	0.4822	0
D	0.20676	0.6653	0.735	0.7755	0.7888	0.7755	0.735	0.6653	0.2068

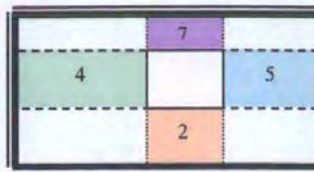
### 6.4.2.2. Panels with Openings

For new panels with openings, division of their regions can be arranged around the opening in the panel, for instance, a new panel shown in Figure 6.7 can be divided into eight regions to use Equation (6.4) for matching zone similarity.

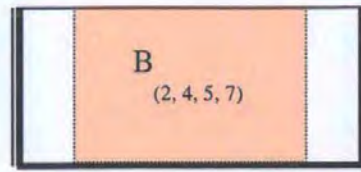


**Figure 6.7** – The division of regions of a new panels with opening

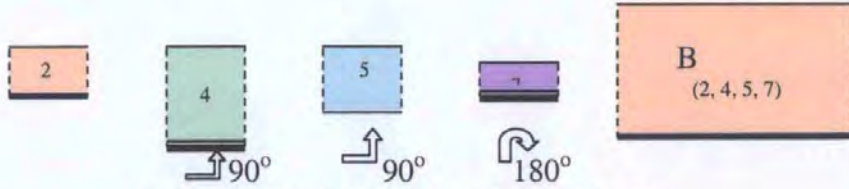




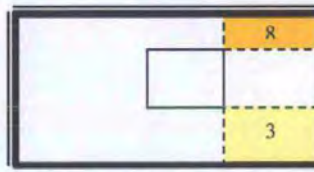
(d) Regions 2,4,5,7 on the new panel



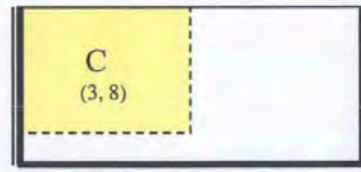
(e) Region B on Base Panel SB01



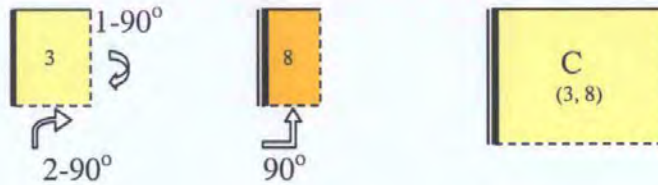
(f) Regions 2, 4, 5 and 7 match Region B



(g) Regions 3 and 8 on the new panel



(h) Region C on Base Panel SB01



(i) Regions 3 and 8 to Region C

**Figure 6.8** – Similar regions between the panel with opening and the solid base panel SB01

Once again the solid panel SB01 is used as the base panel. Three regions on the solid base panel SB01 are selected as the base regions to be matched to various regions on the new panel with opening shown in Figures 6.8b, 6.8e and 6.8h. As described in Section 6.4.2.1, the similar regions between the new panel with an opening and the solid base panel SB01 are matched as shown in Figure 6.8c, 6.8f and 6.8i.

Table 6.10 shows the state values of the new panel with opening as shown in Figure 6.7. The state values in the cells within the opening zones are set 0.0. Zone B8 in

Region 5 and Zone A1 in Region 6 are selected to find their similar zones within the base panel SB01.

For Region 5 on the new panel, its closest similar region would be Region B on the base panel, based on the boundary similarities, see Table 6.11. For the more accurate application of Equation (6.4), Region 5 was rotated counterclockwise by 90° and Region B is fixed. The result of the analysis is shown in Table 6.12. Using Equation (6.4) considering the orientations of similar regions, it was determined that Zone B8 on the new panel and Zone A2 on the base panel SB01 are two similar zones, see Table 6.12. On the basis of rules applied for similar zones discussed in Section 5.4, this result is valid. If Equation (6.4) is applied to match a zone on the new panel to a similar zone on the base panel without consideration of its orientation, the result given in Table 6.13 will be obtained. From Table 6.13, it can be seen that Zone B8 on the new panel matches with Zones B2 and B9 on the base panel. However, Zone A2 on the base panel should match Zone B8 on the new panel. Therefore the results in Table 6.13 are misleading.

**Table 6.10** – State values of the new panel with opening.

		1	2	3	4	5	6	7	8	
		0.2	0.2	0.2	0.2	0.2	0.2	0.2	0.2	
A	0.2	<b>0.5766</b>	<b>0.5981</b>	0.4721	0.4762	0.6106	0.5981	0.5766	0.545	0
B	0.2	0.4752	0.4672	0	0	0.4928	0.5072	0.5072	<b>0.4928</b>	0
C	0.2	0.4816	0.4736	0	0	0.4992	0.5136	0.5136	0.4992	0
D	0.2	0.5961	0.6177	0.5121	0.5162	0.6301	0.6177	0.5961	0.5645	0
		0.4	0.4	0.4	0.4	0.4	0.4	0.4	0.4	

Region 6 (similar to Region A)    Region 5 (similar to Region B)

Region B (similar to Region 5)

**Table 6.11** – State values of Panel SB01

		1	2	3	4	5	6	7	8	9	
		0	0	0	0	0	0	0	0	0	
A	0.2	0.5517	<b>0.577</b>	0.5942	0.6042	0.6075	0.6042	0.5942	<b>0.577</b>	0.5517	0.2
B	0.2	0.5764	0.6016	0.6189	0.6289	0.6321	0.6289	0.6189	0.6016	0.5764	0.2
C	0.2	0.5892	0.6144	0.6317	0.6417	0.6449	0.6417	0.6317	0.6144	0.5892	0.2
D	0.2	0.5908	0.616	0.6333	0.6433	0.6465	0.6433	0.6333	0.616	0.5908	0.2
		0.4	0.4	0.4	0.4	0.4	0.4	0.4	0.4	0.4	



**Table 6.12** – Errors of Zone B8 in the new panel to all zones in Region B in the base panel SB01 using Equation (6.4) with considering orientation of region

	2	3	4	5	6	7	8
A	<b>0.2804</b>	0.3501	0.3906	0.4038	0.3906	0.3501	<b>0.2804</b>
B	0.9441	1.031	1.0815	1.098	1.0815	1.031	0.9441
C	1.0087	1.0957	1.1461	1.1627	1.1461	1.0957	1.0087
D	1.0247	1.0944	1.1349	1.1482	1.1349	1.0944	1.0247

**Table 6.13** – Errors of Zone B8 in the new panel to all zones in the base panel SB01 using Equation (6.4) without considering orientation of region

	1	2	3	4	5	6	7	8	9
A	1.5653	1.3704	1.4401	1.4806	1.4938	1.4806	1.4401	1.3704	0.9509
B	1.0891	<b>0.9441</b>	1.031	1.0815	1.098	1.0815	1.031	0.9441	<b>0.4747</b>
C	1.1409	1.0087	1.0957	1.1461	1.1627	1.1461	1.0957	1.0087	0.5265
D	1.1646	1.0087	1.0784	1.1189	1.1322	1.1189	1.0784	1.0087	0.5502

Similarly, for Region 6 on the new panel, its similar region A on the base panel is matched based on boundary similarity, see Table 6.14. Region B is also rotated counter-clockwise by  $90^\circ$  and Region A is fixed. The result is shown in Table 6.15. Zone A1 on the new panel matches Zone B1 on the base panel SB01. Verified by rules for similar zones discussed in Section 5.4, this result is also valid. If without consideration of orientations of two similar regions, the result obtained by Equation (6.4) that Zone A1 on the new panel is similar to Zone A1 on the base panel, is also misleading, see Table 6.16.

**Table 6.14** - State values of Panel SB01

	1	2	3	4	5	6	7	8	9		
	0	0	0	0	0	0	0	0	0		
A	0.2	0.5517	0.577	0.5942	0.6042	0.6075	0.6042	0.5942	0.577	0.5517	0.2
B	0.2	<b>0.5764</b>	0.6016	0.6189	0.6289	0.6321	0.6289	0.6189	0.6016	0.5764	0.2
C	0.2	0.5892	0.6144	0.6317	0.6417	0.6449	0.6417	0.6317	0.6144	0.5892	0.2
D	0.2	0.5908	0.616	0.6333	0.6433	0.6465	0.6433	0.6333	0.616	0.5908	0.2
	0.4	0.4	0.4	0.4	0.4	0.4	0.4	0.4	0.4	0.4	

Region A (similar to Region 6)

**Table 6.15** – Errors of Zone A1 in the new panel to all zones in Region A in the base panel SB01 using Equation (6.4) with considering orientation of zone

	1	2	3	4	5
B	<b>0.1731</b>	0.9553	1.0159	1.0658	1.089
C	0.1736	0.9777	1.0727	1.1304	1.1537
D	0.364	0.8046	0.8743	0.9147	0.928

**Table 6.16** – Errors of Zone A1 in the new panel to all zones in the base panel SB01 using Equation (6.4) without considering orientation of region

	1	2	3	4	5	6	7	8	9
A	<b>0.3472</b>	0.6825	0.7443	0.7848	0.7981	0.7926	0.7866	0.7675	1.1012
B	0.4694	0.9384	1.0253	1.0758	1.0923	1.0758	1.0253	0.9819	1.2657
C	0.5208	1.003	1.0899	1.1404	1.1569	1.1404	1.0899	1.021	1.317
D	0.4964	0.955	1.0247	1.0651	1.0784	1.0651	1.0247	0.9697	1.2927

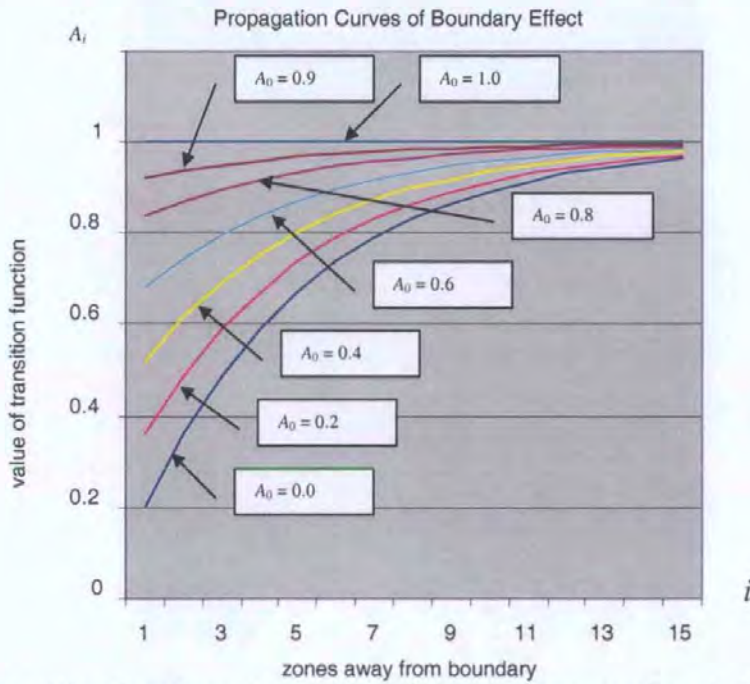
## **6.5. Investigation into Values of Boundary Parameter and Transition Coefficient**

### **6.5.1. Characteristics of Transition Function Related to Boundary Parameters and Transition Coefficient**

In Section 6.4, it was discovered that the validity of Equation (6.4) is related to the orientation of two similar regions. In this section, the magnitudes of both boundary parameter and the transition coefficient  $\eta$  are investigated which can affect the results of Equation (6.4). Because both boundary parameter and the transition coefficient  $\eta$  are directly included in Equation (6.2), the study is focused on the effect of them on Equation (6.2).

Boundary parameters are the initial values of Equation (6.2) and the equation propagates them into all zones within the panel. The initial value for  $A_o$  is between 0.0 and 1.0. Figure 6.9 shows the effect of various initial values on the transition function (Equation (6.2)). From the figure, the smaller initial values, the more obvious the difference ( $A_{i+1} - A_i$ ) of transition function values between two adjacent zones. When using Equation (6.3) to calculate state values of zones on the panel, the large difference ( $A_{i+1} - A_i$ ) means the obvious difference between the state values  $S_i$  and  $S_{i+1}$  of two adjacent zones  $i$  and  $i+1$ . Because the function that is used in Equation (6.4) to match similar zones depends on the differences between relevant state values, the

more obvious are these differences, the better are the results of Equation (6.4). Therefore, the selection of values of boundary parameters should be as small as possible.

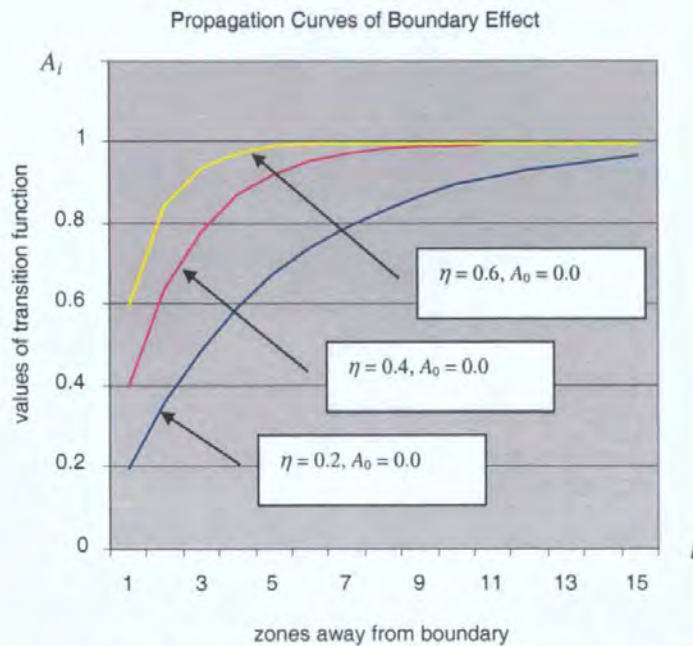


Transition function:  $A_{i+1} = A_i + \eta(1 - A_i)$ ; Zone number  $i = 1, 2, \dots$ ;  
 $A_0$ : boundary parameter;  $A_1, A_2, \dots$ : State values at zones/cells;  
 $\eta$ : transition coefficient, here let  $\eta = 0.2$

**Figure 6.9** - Investigation into initial values describing boundary types

While considering as small values of boundary parameters in Equation (6.2), another important factor is the difference  $(A_i|_{A_0=\text{value of boundary type 1}} - A_i|_{A_0=\text{value of boundary type 2}})$  between two transition function curves for two different boundary types. In other words, if the distances from a zone to two boundaries of different types are the same, the difference between two values for this zone, calculated by Equation (6.2) using the initial values describing these two boundary types, should be as great as possible. Thus Equation (6.3) can distinguish state values and Equation (6.4) can match similar zones effectively. To establish initial values for different boundaries, a parametric study was conducted and the results of this parametric study are presented in Section 6.5.2.

Figure 6.10 shows the effect of the transition coefficient  $\eta$  on the propagation of Equation (6.2). It shows that small values of the transition coefficient  $\eta$  can make the difference  $(A_{i+1} - A_i)$  of two adjacent zones away from the boundary greater than can the large values of transition coefficient  $\eta$ . However, this does not mean that the lower is the value of transition coefficient  $\eta$  the better is the result of the transition function, because if the value of transition coefficient  $\eta$  gradually closes to zero, the curve of transition function gradually closes to a horizontal straight line. This will make the difference  $(A_{i+1} - A_i)$  reduced so that it results in Equation (6.4) producing inaccurate results of matching similar zones. Therefore, it was decided to use a transition coefficient value of 0.2 in Equation (6.2) for the following calculation, because the transition function curve obtained by this value of transition coefficient  $\eta$  is located at a proper position, see Figure 6.10.



Transition function:  $A_{i+1} = A_i + \eta(1 - A_i)$ ; Zone number  $i = 1, 2, \dots$ ;  
 $A_0$ : boundary parameter;  $A_1, A_2, \dots$  : State values at zones/cells.

**Figure 6.10** – Investigation into transition coefficient

### **6.5.2. Parametric Study for Matching Similar Zones Using Different Initial Boundary Parameter Values**

This section presents the results of a parametric study to investigate the effect of initial boundary parameter values on establishing zone similarities using Equation (6.4). In this study, the solid panel SB01 was used as a base panel and two other solid panels with different sizes and boundaries were used to find their similar zones in the base panel.

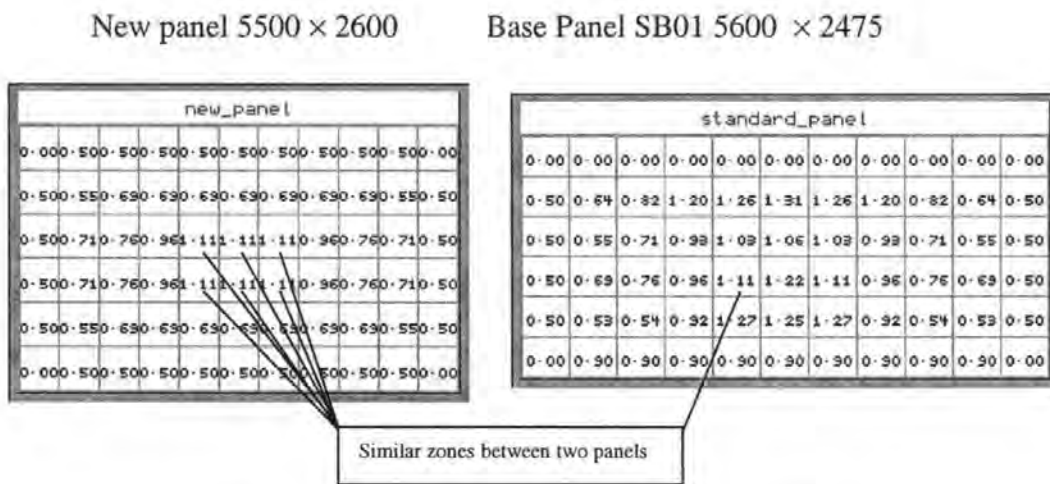
The new panel in Figure 6.11a is simply supported along its four edges. The smaller new panel in Figure 6.12a is simply supported at its left vertical and top edges, built in its bottom edge and free at its right vertical edge. The base panel SB01 is simply supported at its two vertical edges, built in its bottom edge and free at its top edge.

Both the base panel and two new panels are divided into zones, as shown in Figures 6.11 and 6.12. The division of zones of the base panel is based on the positions of measured points in the experiment. The measured points are represented as the centre of each zone. The zones of the new panels were divided based on the sizes of the zones of the base panel.

Figures 6.11a to c and 6.12a to c show the result of CA models on the two new panels and the base panel SB01. Values in the cells adjacent to four boundaries are used to set initial values for the cellular automata calculation. As it was described in Chapter 4, the corrector values for each zone in the base panel was determined by comparing the FEA results with the experimental results using Equation (4.5) and (4.9), as shown

in Figure 6.11. Values of correctors for all zones in the new panel were determined by Equation (6.4).

Figure 6.11a shows the similar zones and corresponding corrector values obtained by CA method using Equation (6.4). The following initial values of boundary parameters were used: free edge = 0.0, simply supported edge = 0.5, built in edge = 0.9. The transition coefficient  $\eta$  for all studies was 0.2. The zone with a corrector of 1.11 in the base panel corresponds to the six different zones in the new panel. Because the two panels have similar sizes, this matching result is not considered to be very accurate, see Figure 6.11a.



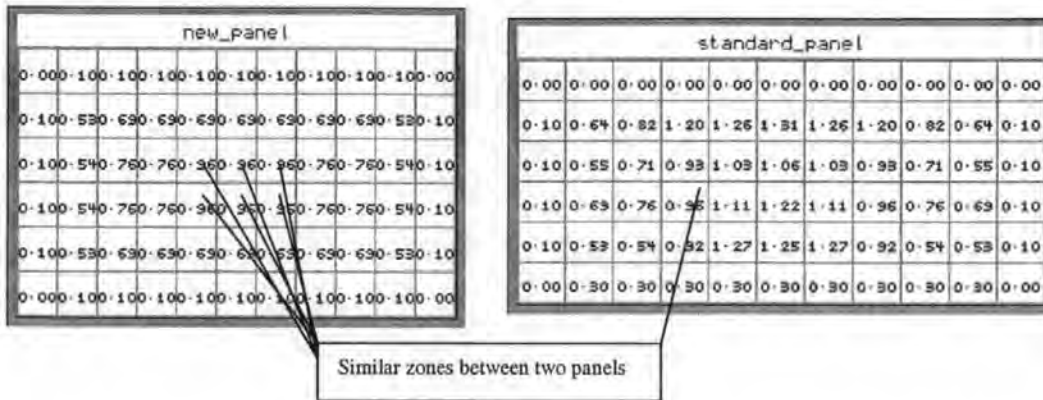
free edge = 0.0,    simply supported edge = 0.5,    built in edge = 0.9

**Figure 6.11a** – Investigation into proper boundary parameters

For the next case, the initial values of boundary parameters were modified as: free edge = 0.0, simply supported edge = 0.1, built in edge = 0.3. The result of this analysis is presented in Figure 6.11b.

New panel 5500 × 2600

Base Panel SB01 5600 × 2475

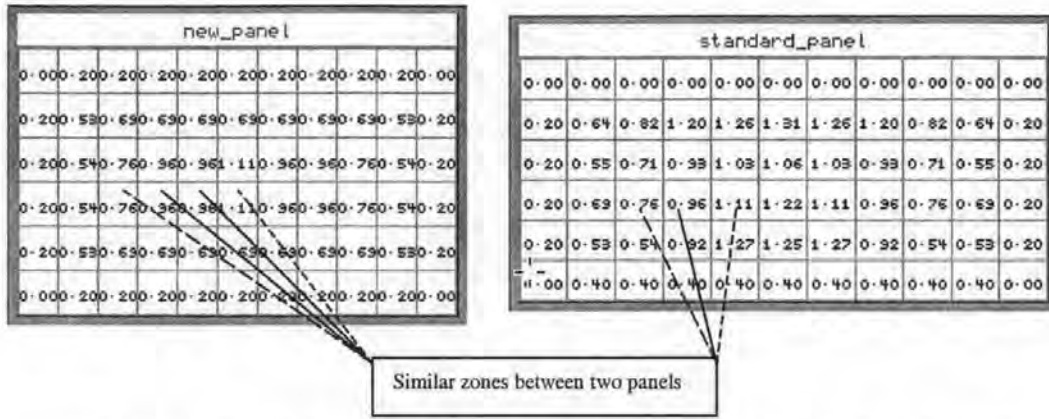


free edge = 0.0, simply supported edge = 0.1, built in edge = 0.3

**Figure 6.11b** – Investigation into proper boundary parameters

Figure 6.11b shows that the zone with corrector of 1.11 within the base panel does not correspond to any zone within the new panel. Values of correctors for the six zones in the new panel, as shown in Figure 6.11a, was changed from 1.11 to the 0.96. This value of 0.96 is in a different location on the base panel which matches with these six zones in the new panel. This indicates that changing initial values for boundary parameters changes the result of matching similar zones, because the state values of the neighbourhood cells are changed following the changes in the initial values of boundary parameters.

In order to pursue a better result of matching similar zones using the CA, another set of boundary parameter values were selected as: free edge = 0.0, simply supported edge = 0.2, built in edge = 0.4. In Figure 6.11c, three zones with corrector values of 1.11, 0.96 and 0.76, within the base panel, separately match three different zones within the new panel. Comparing this result with the results in Figures 6.11a and 6.11b, the rules of matching similar zones are more accurate with these new values. This shows that the best result was obtained when this set of the initial boundary parameter values were used for Equation (6.4).

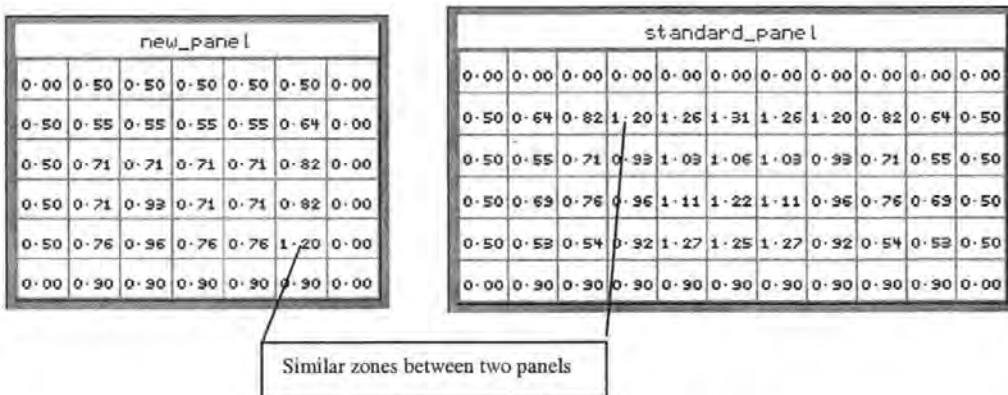


free edge = 0.0, simply supported edge = 0.2, built in edge = 0.4

**Figure 6.11c** – Investigation into proper boundary parameters

In order further to investigate the validity of these boundary parameter values, a parametric study is conducted using another panel with different size and boundary conditions. Similarly to the above study, the initial values of boundary parameters were firstly set as: free edge = 0.0, simply supported edge = 0.5, built in edge = 0.9.

Figure 6.12a shows the zone with corrector value of 1.20 within the base panel. This zone matches with a zone at the right-hand bottom corner in the new panel. According to the rule of zone similarity, the right-hand bottom zone of the new panel should be similar to the second left-hand top zone of the base panel. Therefore, this matching result is not accurate for these boundary parameter values.

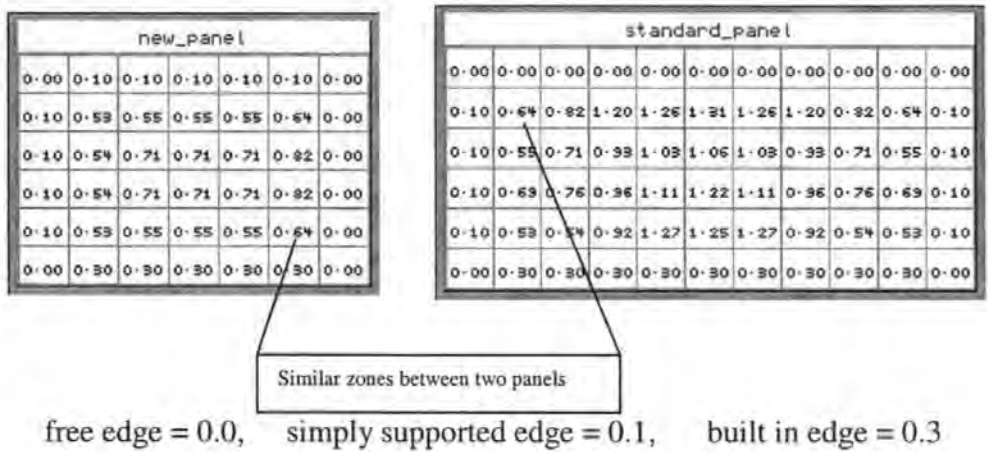


free edge = 0.0, simply supported edge = 0.5, built in edge = 0.9

**Figure 6.12a** – Investigation into proper boundary parameters

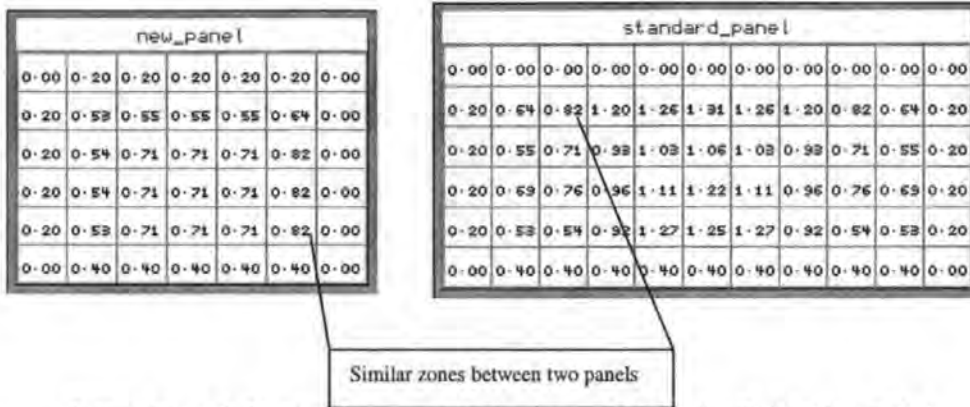


In Figure 6.12b, these values of boundary parameters were used: free edge = 0.0, simply supported edge = 0.1, built in edge = 0.3, This set of boundary parameter values makes the right-hand bottom zone within the new panel match the left-hand top zone within the base panel. When compared with Figure 6.12a, the matched zone within the base panel in Figure 6.12a has the simple support at its left side and the matched zone within the base panel in Figure 6.12b connects with the right side of its left zone. The simple support can not restrain the rotation of the side connected with the constraint (a moment does not exist there), but two zones connected to each other can limit the rotation at their common side (a moment exists there). Therefore the matching result in Figure 6.12a is better than that in Figure 6.12b.



**Figure 6.12b** – Investigation into proper boundary parameters

Because in the last example the best matching result was achieved under these boundary parameter values free edge = 0.0, simply supported edge = 0.2, built in edge = 0.4, the same parameter values are used in this case to test whether they can produce an ideal result of matching similar zones. Figure 6.12c shows the result using this set of parameter values. The matched zone within the base panel is just to the second left-hand top zone of the panel. Once again, the best result was achieved using these values of boundary parameters.



free edge = 0.0, simply supported edge = 0.2, built in edge = 0.4

**Figure 6.12c** – Investigation into proper boundary parameters

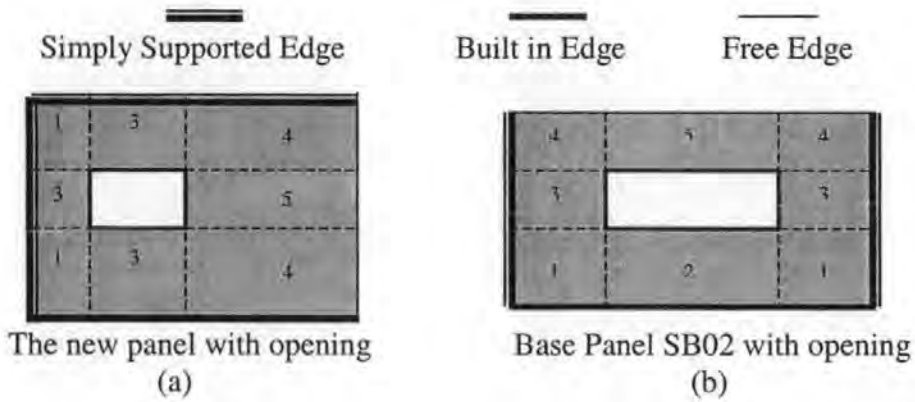
Figures 6.11 and 6.12 confirm that reasonable initial values for boundary parameters used in Equation (6.4), 0.0 for free edge, 0.2 for simply supported edge and 0.4 for built in edge, produce matching rules which more efficiently differentiate the boundary effect and more accurately match similar zones between two panels.

### 6.5.3. CA Matching Similar Zones of Panels with Openings Using Panel SB02 as the Base Panel

Because Panel SB02 with opening (see Figure 6.13b) (as the standard panel in Chong's experiments (1993) has the same typical size, boundary types and opening, it was used as the base panel in this research. Except with an opening (2260mm×1125mm), Panel SB02 is the same as the base panel SB01 in size, material property and boundary condition. The following examples further verify the validity of the initial boundary parameter values concluded in Section 6.5.1 in the calculation of matching similarity. Both the new panels and the base panel are panels with an opening.

Panel SB02 was divided into the five regions with different boundaries and the new panel with an opening was also divided into several similar regions as shown in

Figure 6.13b. By inspection using the method in Section 6.4.2, similar regions can be made. Figures 6.13a and 6.13b show regions on the new panel which match regions with similar boundaries on the base panel SB02. With consideration on the orientations of similar regions, the CA matching Equation (6.4) was then used to identify similar zones within the similar regions between the two panels.



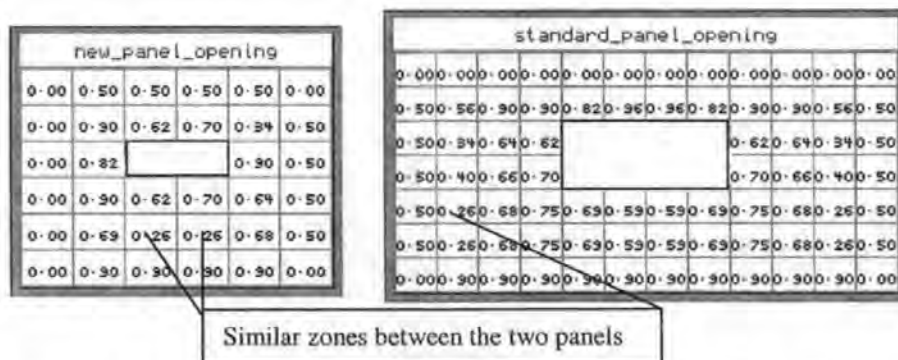
**Figure 6.13** – Similar zones between the base Panel SB02 and a new panel

The new panel with opening in Figure 6.13a is simply supported at its left and top edges, built-in at its bottom edge and free at its right edge. The new panel sizes are 2700mm×2400mm and an opening size 1000mm×600mm. The base panel is Panel SB02 (Chong 1993).

Once again a parametric study was conducted using the same range of boundary parameters as in Section 6.5.2. The result of the parametric study is shown in Figures 6.14a, 6.14b and 6.14c. From comparison of the three cases, once again the same conclusion as that in Section 6.5.2 can be drawn.

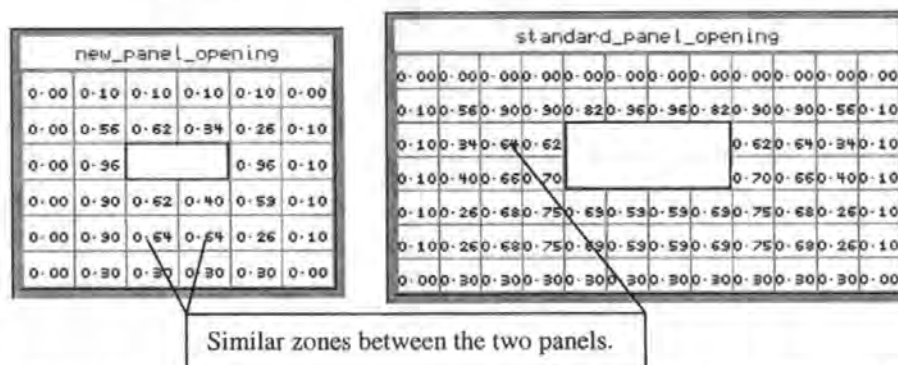
For instance, the two zones in the middle of the bottom edge for the new panel are matched with the two separate similar zones within the base panel under the

parameters, free edge = 0.0, simply supported edge = 0.2 and built-in edge = 0.4, see Figure 6.14c. Under the other two sets of boundary parameters, the results are not accurate, see Figures 6.14a and 6.14b. This once again proves that the boundary parameters under Figure 6.14c reasonably locate similar zones within two panels.



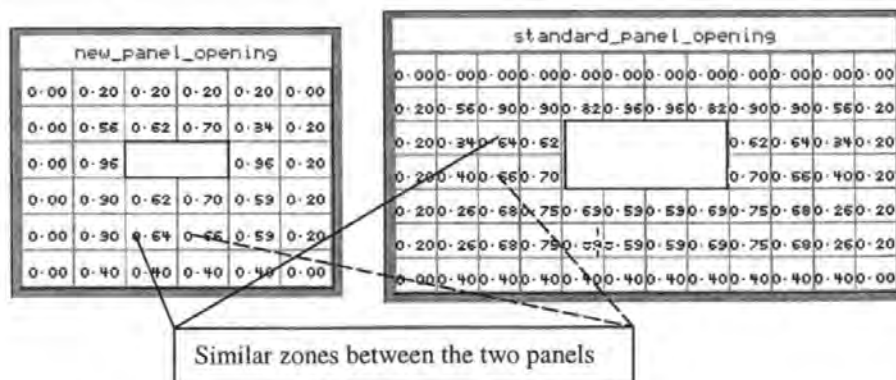
free edge = 0.0, simply supported edge = 0.5 and built-in edge = 0.9

**Figure 6.14a** – Investigation into proper boundary parameters



free edge = 0.0, simply supported edge = 0.1 and built-in edge = 0.3

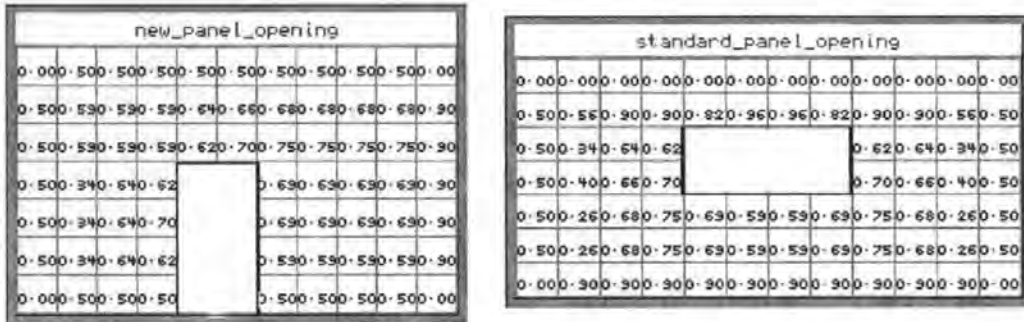
**Figure 6.14b** – Investigation into proper boundary parameters



free edge = 0.0, simply supported edge = 0.2 and built-in edge = 0.4

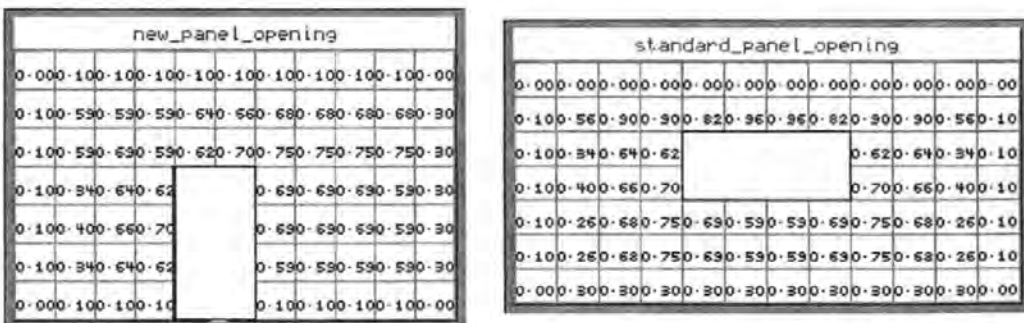
**Figure 6.14c** – Investigation into proper boundary parameters

Figures 6.15a to c show the result of another parametric study on another new panel. The new panel with opening in Figure 6.15a was simply supported at its left, bottom and top edges and built-in at its right edge. The new panel has the size 5400mm×3000mm, the co-ordinates of the central of the opening is (2400mm, 1000mm) and the opening size 1000mm×2000mm. The base panel was Panel SB02. The sizes of the two panels are slightly different and their opening configurations are obviously different. The result of this study once again shows that the boundary parameters: free edge = 0.0, simply supported edge = 0.2 and built-in edge = 0.4 give results similar to other cases.



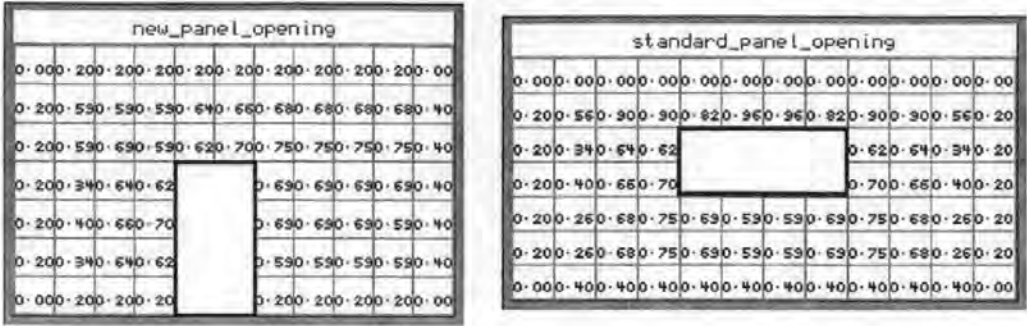
free edge = 0.0, simply supported edge = 0.5 and built-in edge = 0.9

Figure 6.15a – Investigation into proper boundary parameters



free edge = 0.0, simply supported edge = 0.1 and built-in edge = 0.3

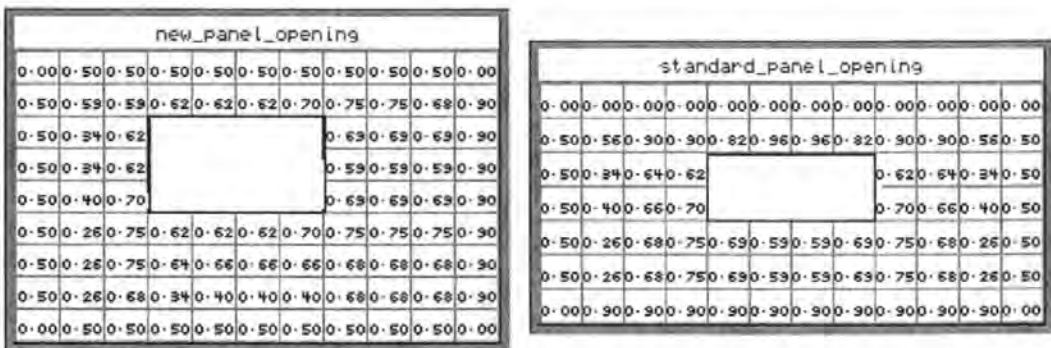
Figure 6.15b – Investigation into proper boundary parameters



free edge = 0.0, simply supported edge = 0.2 and built-in edge = 0.4

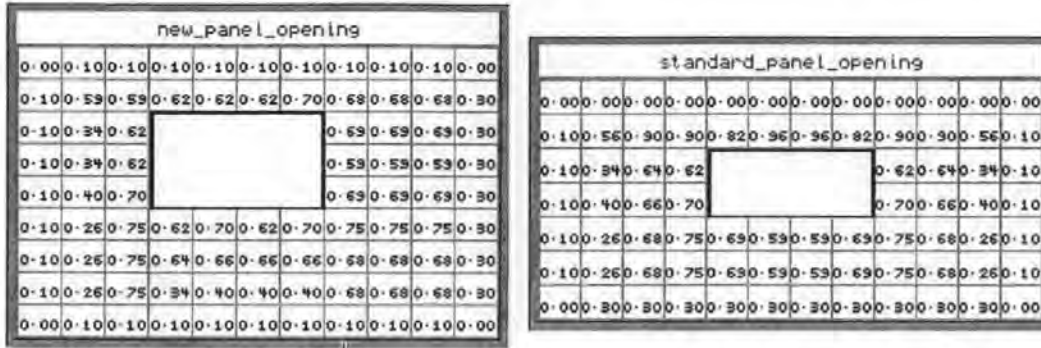
**Figure 6.15c** – Investigation into proper boundary parameters

Finally, a new panel with larger size than the base panel SB02 was used in this parametric study for boundary types. The new panel with an opening in Figure 6.16 has the same boundaries as the panel in Figure 6.15, but the size of the large panel is 5400mm×3200mm, the co-ordinates of the central point of the opening (2400mm, 2000mm) and the opening size 2000mm×1600mm. The sizes of the new panel and the base panel as well as their opening configurations are different. The result of this study once again shows that the boundary parameters: free edge = 0.0, simply supported edge = 0.2 and built-in edge = 0.4, give results similar to other cases.



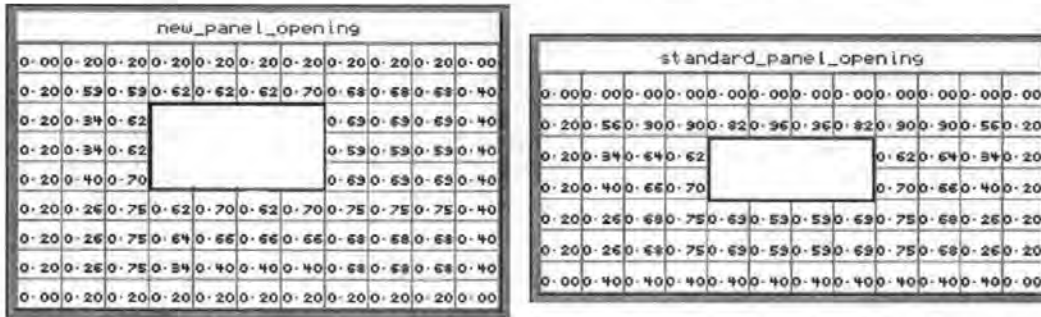
free edge = 0.0, simply supported edge = 0.5 and built-in edge = 0.9

**Figure 6.16a** – Investigation into proper boundary parameters



free edge = 0.0, simply supported edge = 0.1 and built-in edge = 0.3

Figure 6.16b – Investigation into proper boundary parameters



free edge = 0.0, simply supported edge = 0.2 and built-in edge = 0.4

Figure 6.16c – Investigation into proper boundary parameters

The results of parametric studies on the three new panels with openings verify that boundary parameter values: free edge = 0.0, simply supported edge = 0.2, built-in edge = 0.4 and transition coefficient = 0.2 can efficiently identify matching zones more accurately than the other two cases. These parameter values were adopted for the CA method in this research.

### 6.6. Further Improvement of Matching Similarity Method

The following section proposes an improved methodology using Equation (6.4) in which the manual process of dividing the panel into several regions can be totally avoided and the CA method can directly match similar zones within panels, and directly estimate corrector values for each zone within a panel.

In Section 6.4, it was concluded that for proper matching of similar zones the orientation of the four neighbouring zones was essential. Repeated matching of zones with their individual four neighbourhood zones from two different orientations reduces the errors in Equation (6.4). This criterion can be used to replace the process of matching similar regions within two panels. Details of this process are shown in Figures 6.17 to 6.24.

In Figure 6.17, for a zone (i, j) and its four neighbourhood zones (i, j-1), (i, j+1), (i-1, j) and (i+1, j) within the new panel, there are eight different orientations that can be used to match every zone (m, n) and its neighbourhoods (m, n-1), (m, n+1), (m-1, n) and (m+1, n) within the base panel. The eight errors from  $E_{k1,l1}^1$  to  $E_{k8,l8}^8$  of state values under the eight cases are separately calculated by Equations (6.5) to (6.12). In other words, Equation (6.4) can be repeatedly applied to calculate the errors for eight different orientations separately in order to match a zone in the new panel with a zone within the base panel.

$$E_{k1,l1}^1 = \underset{m=1, n=1}{\overset{M, N}{\text{MIN}}} \left( \left| S_{i,j}^{new} - S_{m,n}^{sta} \right| + \left| S_{i,j-1}^{new} - S_{m,n-1}^{sta} \right| + \left| S_{i,j+1}^{new} - S_{m,n+1}^{sta} \right| + \left| S_{i-1,j}^{new} - S_{m-1,n}^{sta} \right| + \left| S_{i+1,j}^{new} - S_{m+1,n}^{sta} \right| \right) \quad (6.5)$$

Here,

M – the row number of zones within the base panel.

N - the column number of zones within the base panel.

(k1, l1) – the similar zone within the base panel with Zone (i, j) within the new panel under Case 1.

Other items are the same as those in Equation (6.4).



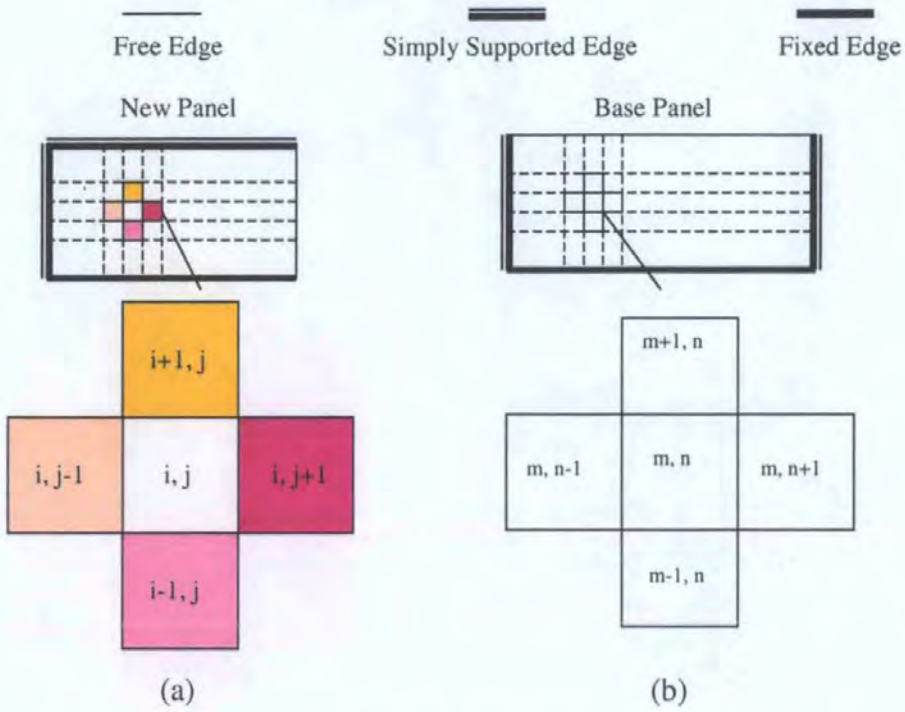


Figure 6.17 - Case 1: Orientation of the new panel to the base panel

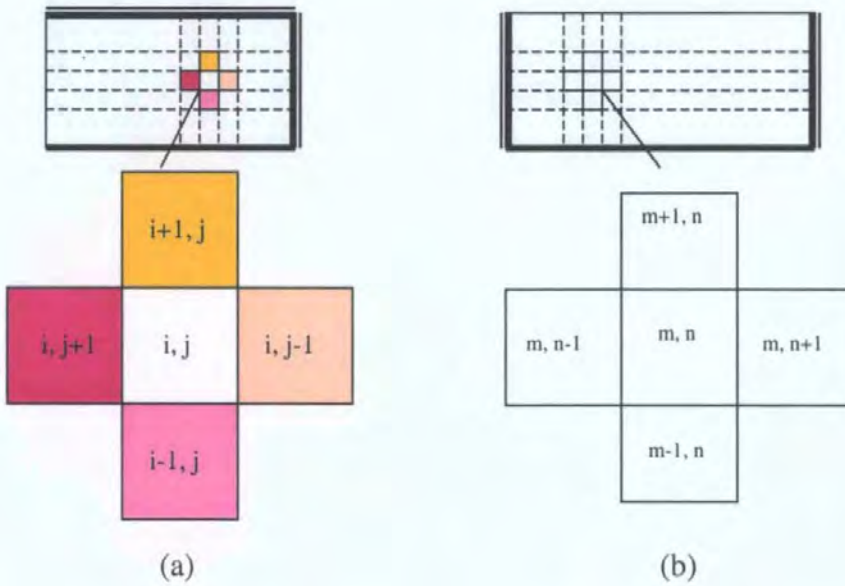


Figure 6.18 - Case 2: Orientation of the new panel to the base panel

$$E_{k2,12}^2 = \underset{m=1, n=1}{\overset{M, N}{\text{MIN}}} (|S_{i,j}^{new} - S_{m,n}^{sta}| + |S_{i,j+1}^{new} - S_{m,n-1}^{sta}| + |S_{i,j-1}^{new} - S_{m,n+1}^{sta}| + |S_{i-1,j}^{new} - S_{m-1,n}^{sta}| + |S_{i+1,j}^{new} - S_{m+1,n}^{sta}|) \quad (6.6)$$

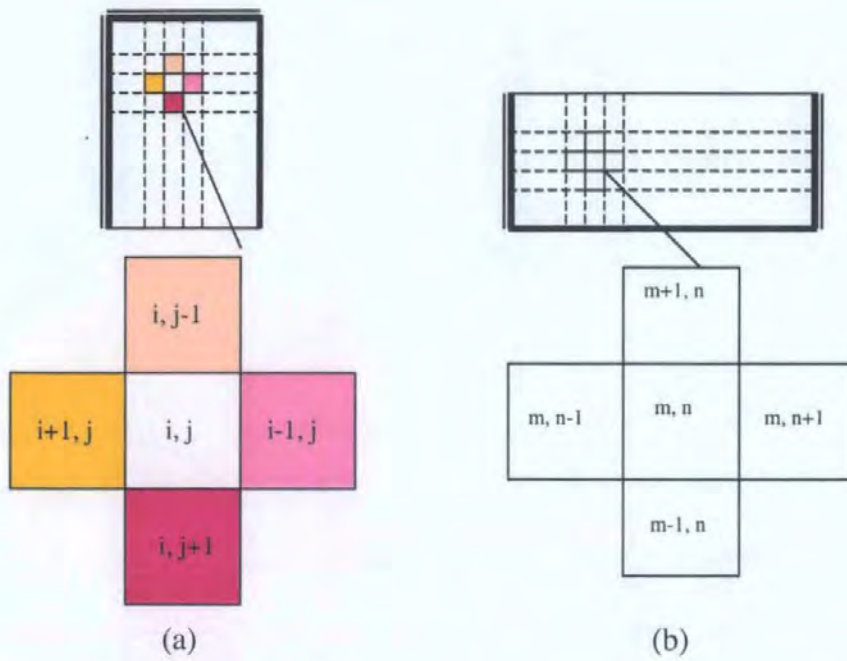


Figure 6.19 - Case 3: Orientation of the new panel to the base panel

$$E_{k3,l3}^3 = \underset{m=1, n=1}{\overset{M, N}{\text{MIN}}} ( |S_{i,j}^{new} - S_{m,n}^{sta}| + |S_{i+1,j}^{new} - S_{m,n-1}^{sta}| + |S_{i-1,j}^{new} - S_{m,n+1}^{sta}| + |S_{i,j+1}^{new} - S_{m-1,n}^{sta}| + |S_{i,j-1}^{new} - S_{m+1,n}^{sta}| ) \quad (6.7)$$

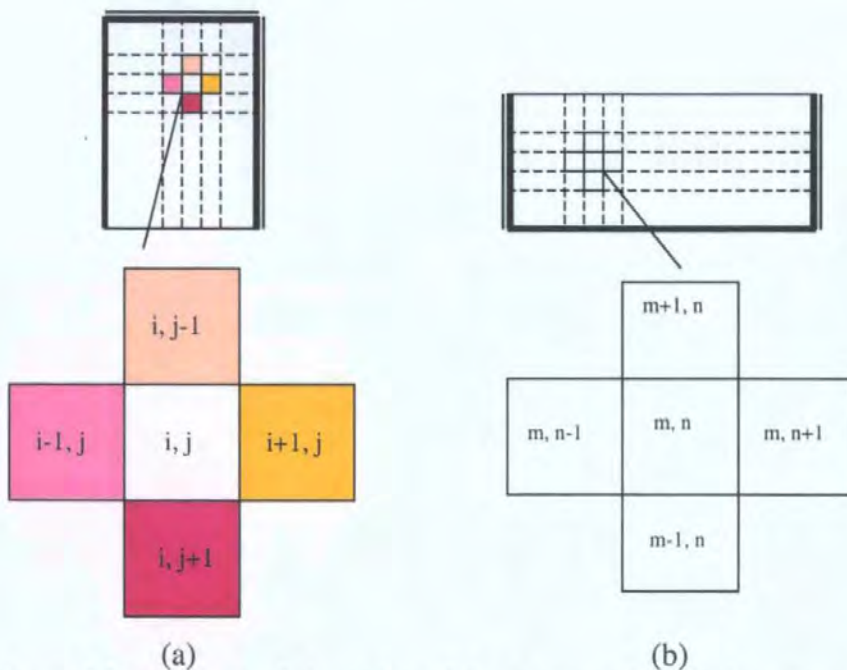


Figure 6.20 - Case 4: Orientation of the new panel to the base panel

$$E_{k4,j4}^4 = \underset{m=1,n=1}{\text{MIN}}^{M,N} (|S_{i,j}^{\text{new}} - S_{m,n}^{\text{sta}}| + |S_{i-1,j}^{\text{new}} - S_{m,n-1}^{\text{sta}}| + |S_{i+1,j}^{\text{new}} - S_{m,n+1}^{\text{sta}}| + |S_{i,j+1}^{\text{new}} - S_{m-1,n}^{\text{sta}}| + |S_{i,j-1}^{\text{new}} - S_{m+1,n}^{\text{sta}}|) \quad (6.8)$$

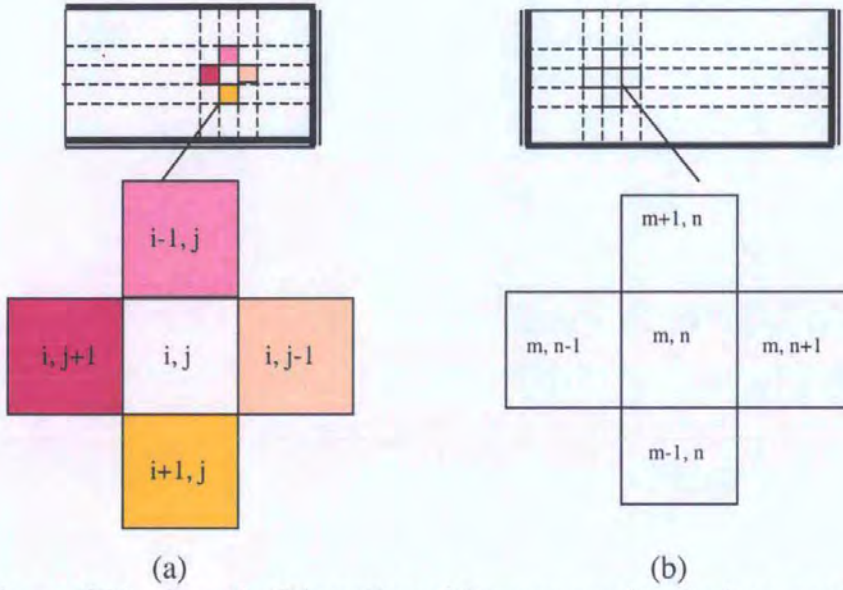


Figure 6.21 - Case 5: Orientation of the new panel to the base panel

$$E_{k5,l5}^5 = \underset{m=1,n=1}{\text{MIN}}^{M,N} (|S_{i,j}^{\text{new}} - S_{m,n}^{\text{sta}}| + |S_{i,j+1}^{\text{new}} - S_{m,n-1}^{\text{sta}}| + |S_{i,j-1}^{\text{new}} - S_{m,n+1}^{\text{sta}}| + |S_{i+1,j}^{\text{new}} - S_{m-1,n}^{\text{sta}}| + |S_{i-1,j}^{\text{new}} - S_{m+1,n}^{\text{sta}}|) \quad (6.9)$$

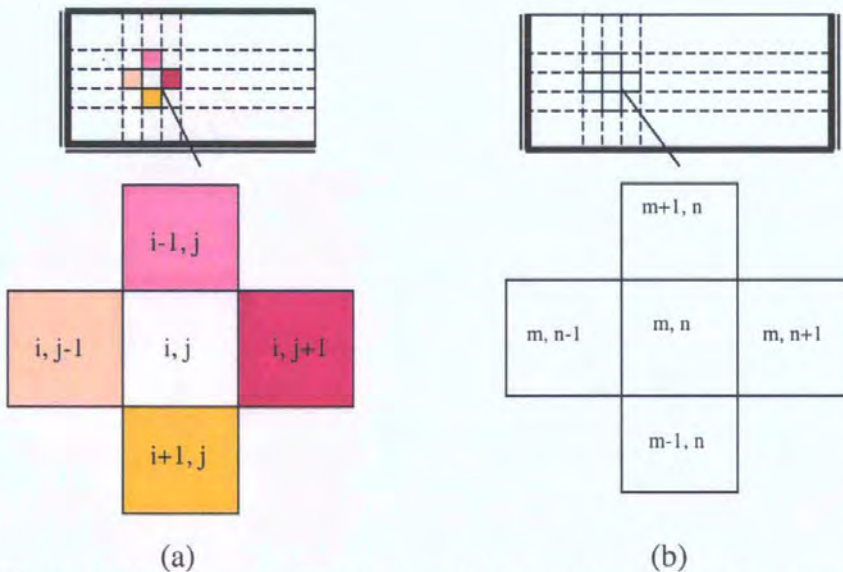


Figure 6.22 - Case 6: Orientation of the new panel to the base panel

$$E_{k6,l6}^6 = \underset{m=1,n=1}{\overset{M,N}{\text{MIN}}} ( |S_{i,j}^{new} - S_{m,n}^{sta}| + |S_{i,j-1}^{new} - S_{m,n-1}^{sta}| + |S_{i,j+1}^{new} - S_{m,n+1}^{sta}| + |S_{i-1,j}^{new} - S_{m-1,n}^{sta}| + |S_{i+1,j}^{new} - S_{m+1,n}^{sta}| ) \quad (6.10)$$

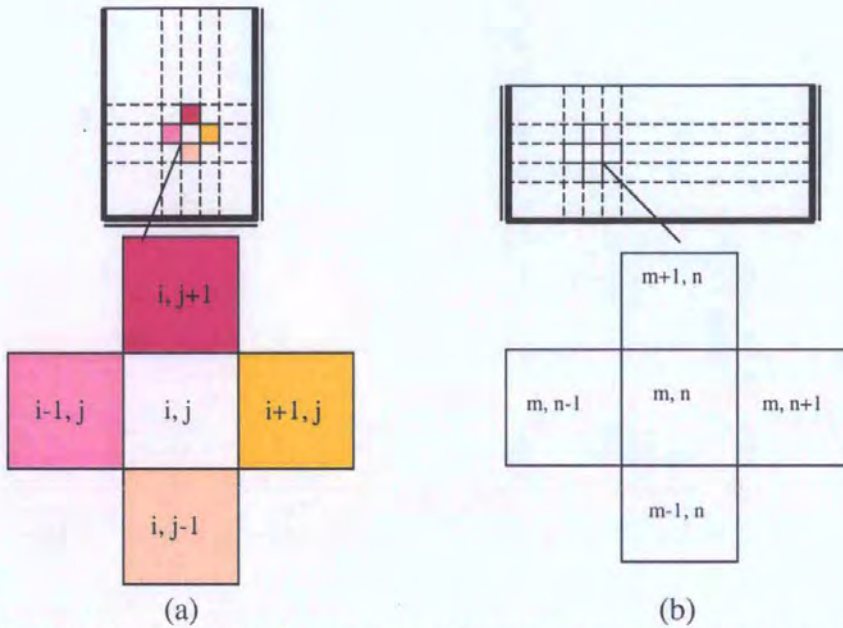


Figure 6.23 - Case 7: Orientation of the new panel to the base panel

$$E_{k7,l7}^7 = \underset{m=1,n=1}{\overset{M,N}{\text{MIN}}} ( |S_{i,j}^{new} - S_{m,n}^{sta}| + |S_{i-1,j}^{new} - S_{m,n-1}^{sta}| + |S_{i+1,j}^{new} - S_{m,n+1}^{sta}| + |S_{i,j-1}^{new} - S_{m-1,n}^{sta}| + |S_{i,j+1}^{new} - S_{m+1,n}^{sta}| ) \quad (6.11)$$

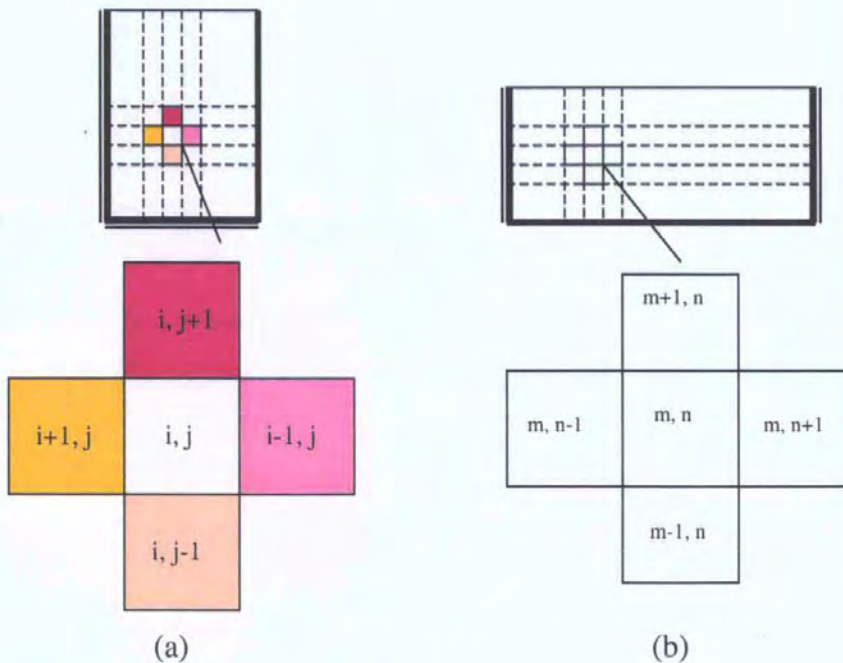


Figure 6.24 - Case 8: Orientation of the new panel to the base panel

$$E_{k8,l8}^8 = \underset{m=1,n=1}{\overset{M,N}{\text{MIN}}} (|S_{i,j}^{new} - S_{m,n}^{sta}| + |S_{i+1,j}^{new} - S_{m,n-1}^{sta}| + |S_{i-1,j}^{new} - S_{m,n+1}^{sta}| + |S_{i,j-1}^{new} - S_{m-1,n}^{sta}| + |S_{i,j+1}^{new} - S_{m+1,n}^{sta}|) \quad (6.12)$$

Once the eight errors for a zone in the new panel are calculated, the minimum error among these eight errors,  $E_{k1,l1}^1, E_{k2,l2}^2, \dots, E_{k8,l8}^8$ , is calculated by

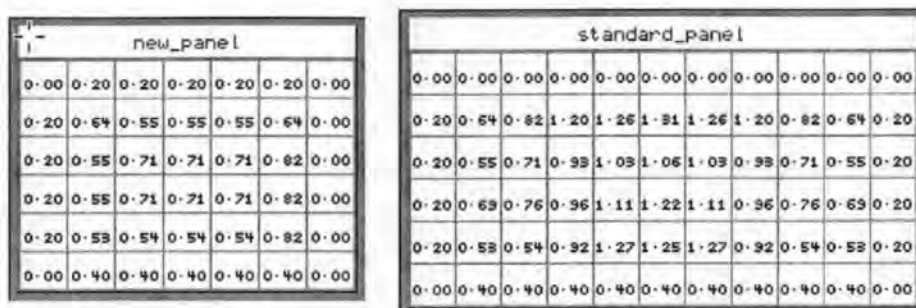
$$E_{k,l} = \underset{p=1}{\overset{8}{\text{MIN}}}(E_{kp,lp}^p) \quad (6.13)$$

Thus the zone  $(i, j)$  in the new panel is similar with the zone  $(k, l)$  in the base panel, which corresponds to this minimum error.

Figures 6.25 and 6.26 show the examples of applying Equations (6.5) to (6.13). The two solid panels the same as those in Figure 6.11 and Figure 6.12, discussed in Section 6.5, have been used. The solid panel SB01 has been used as the base panel. The parameter values used in CA are based on the initial values of boundary parameters, developed in Section 6.5 (0.0 for 1st free edge, 0.2 for 2nd simply supported edge and 0.4 for 3rd built-in edge and 0.2 for transition coefficient). The matching results are the same as those using Equation (6.4), described in Section 6.5.

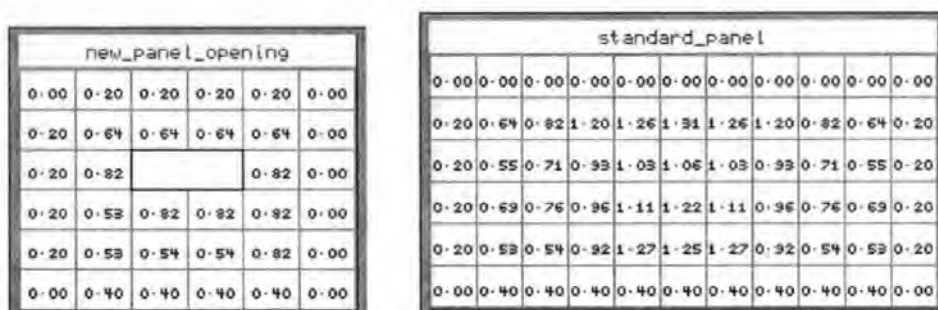
new_panel												standard_panel											
0.00	0.20	0.20	0.20	0.20	0.20	0.20	0.20	0.20	0.20	0.20	0.00	0.00	0.00	0.00	0.00	0.00	0.00	0.00	0.00	0.00	0.00	0.00	
0.20	0.53	0.63	0.63	0.63	0.63	0.63	0.63	0.63	0.63	0.53	0.20	0.20	0.64	0.82	1.20	1.26	1.31	1.26	1.20	0.82	0.64	0.20	
0.20	0.63	0.76	1.03	0.96	1.11	0.96	1.03	0.76	0.63	0.20	0.20	0.20	0.55	0.71	0.93	1.03	1.06	1.03	0.93	0.71	0.55	0.20	
0.20	0.63	0.76	1.03	0.96	1.11	0.96	1.03	0.76	0.63	0.20	0.20	0.20	0.63	0.76	0.96	1.11	1.22	1.11	0.96	0.76	0.63	0.20	
0.20	0.53	0.63	0.63	0.63	0.63	0.63	0.63	0.63	0.53	0.20	0.20	0.20	0.53	0.54	0.92	1.27	1.25	1.27	0.92	0.54	0.53	0.20	
0.00	0.20	0.20	0.20	0.20	0.20	0.20	0.20	0.20	0.20	0.00	0.00	0.00	0.40	0.40	0.40	0.40	0.40	0.40	0.40	0.40	0.40	0.00	

Figure 6.25 – Matching similar zones using Equations (6.5) – (6.13)

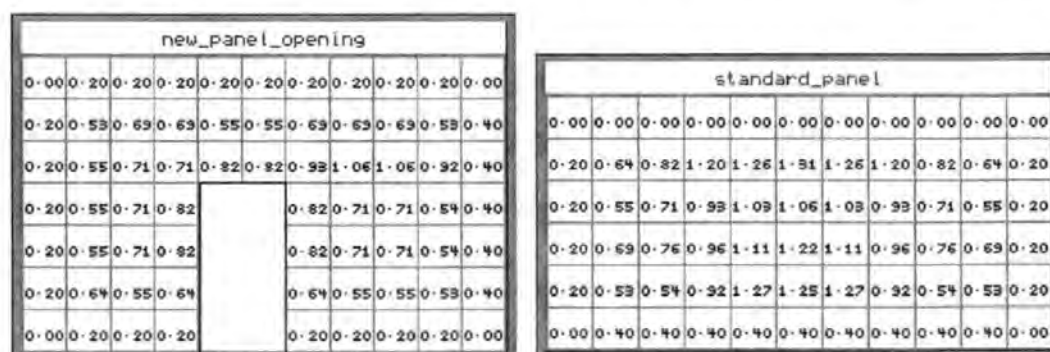


**Figure 6.26** – Matching similar zones using Equations (6.5) – (6.13)

Figures 6.27 and 6.28 show examples of applying Equations (6.5) to (6.13) on two new panels with an opening, the same panels analysed in Section 6.5 (Figure 6.14 and 6.15). Once again the solid panel SB01 has been used as the base panel. The result of CA for matching similar zones shows the validity of Equations (6.5) to (6.13) which are capable of matching similar zones on panels with and without openings using the solid panel SB01 as the base panel.



**Figure 6.27** – Matching similar zones using Equations (6.5) –(6.13)



**Figure 6.28** – Matching similar zones using Equations (6.5) –(6.13)

## 6.7. Summary

The above analysis shows that the CA is a powerful tool for matching similar zones within panels with various sizes, boundary conditions, openings etc. The study also demonstrated the significance of boundary parameter values in the result of the CA method in matching similar zones between panels. In order to make a clearer understanding of the CA technique for matching similar zones, the basic procedure is summarised as follows:

1. The geometrical sizes of the new panel and the base panel are input.
2. The boundary parameter values are input as initial values of CA transition function (Equation (6.2)) for the new panel and the base panel.
3. The new panel is divided into zones based on the zones of the base panel. The division of zones in the base panel is based on the positions of measurement points on the panel from experimentation.
4. The state factors of individual zones of both the new panel and the base panel were calculated using Equations (6.2) and (6.3). It has been proved that the boundary parameter values, as the initial values of the transition Equation (6.2), 0.2 for 0.0 for free edge, simply supported edge, 0.4 for fixed edge and 0.2 for the transition coefficient, were suitable for application of derived matching rules (Equations (6.5) to (6.13)).
5. Similar zones between the new panel and the base panel are matched using Equations (6.5) to (6.13) and then the correctors from the similar zone on the base panel were put into the corresponding zones in the new panel.

After obtaining correctors of individual zones within the new panel from the base panel, the FEA model of the new panel can use the correctors to modify the global flexural rigidity or global strength in the corresponding zones. The improvements

achieved in the FEA of laterally loaded masonry panels using correctors is presented in Chapter 7.



## 7. EFFECT OF CORRECTORS ON DISPLACEMENT PREDICTED USING CORRECTORS

### 7.1. Introduction

Correctors and methodologies for matching similar zones between the new panel and the base panel were fully discussed in previous chapters. These parameters were used to properly model variation in masonry properties and boundary conditions to improve the FEA results of laterally loaded masonry panels. Thus the validity of both correctors and the rules for matching similarity of zones is verified by the FEA of the typical experimental masonry panels in this chapter.

The existing FEA techniques using smeared masonry properties for laterally loaded masonry panels have not included variation in the flexural rigidity or strength variation related to individual zones within the panel. The effect of boundary conditions of the panel, which was found to be one of the most important parameters, has not been properly modelled in the variation of flexural rigidity of masonry panel, in the traditional FEA techniques. In the past, great efforts were focused on making accurate models of masonry wallettes in order to establish values for some of masonry design parameters. Traditionally, in FEA, a smeared value of flexural rigidity [ $D$ ] and/or tensile strength  $f$ , have been used in the analysis. The smeared material properties of masonry components (brick, mortar) or smearing cracking of the material, or in general, the constituent relationships were not discretized individually and they were represented as the equivalent orthotropic properties, for the FEA of masonry panels. Using a globally smeared flexural rigidity and strength in the existing FEA techniques does not guarantee an accurate prediction of failure loads and failure

patterns of masonry panels. The research presented in this thesis has introduced a new methodology, as discussed in Chapter 6, which uses correctors to properly model variation in flexural rigidity at various zones within the panel. This methodology has been shown to considerably improve the FEA results.

In this chapter, results of the implementation of this new approach are tested by comparing results of panel laboratory experiments with the results predicted by the FEA. In the FEA model, appropriate values of correctors related to individual zones within the panel are used to modify the flexural rigidity of the panel at these locations. To validate the results of the FEA obtained by the proposed approach, these results are compared with the experimental results and results obtained from traditional FEA using globally smeared masonry properties.

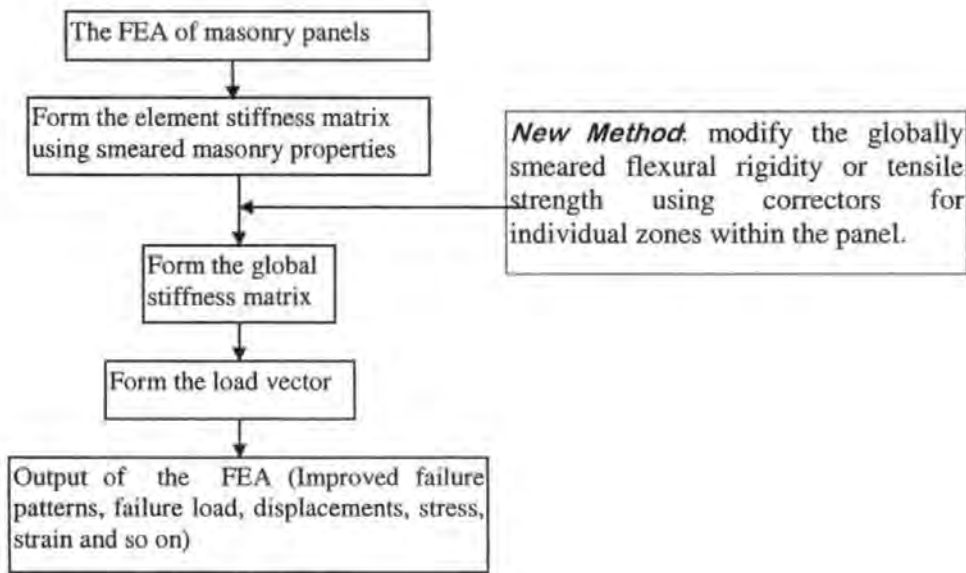
This chapter will examine the accuracy of displacement values calculated by incorporating correctors in the FEA modelling. The examination of failure load and failure pattern will be discussed in Chapter 8.

## ***7.2. Methods for Improving the FEA of Masonry Panels***

The correctors introduced in Chapter 4 and the methods for matching similar zones in Chapter 6 were used to improve the existing FEA techniques for laterally loaded masonry panels. This technique applies correctors to modify global flexural rigidity or tensile strength at individual zones within the panel. The basic procedure is described in Figure 7.1.

Thus in the FEA shown in Figure 7.1, the flexural rigidity or the tensile strength are modified using correctors at various zones to replace the globally smeared flexural

rigidity or tensile strength. In other words, the elements within every zone form their local stiffness matrix using the corrector in that zone to modify masonry properties at the zone. It needs to be stressed again that the division of zones and the corresponding correctors are based on actual results obtained from laboratory experiment of masonry panels, not by introducing a random division and random noise to various zones as used by some researchers (Lawrence 1991).



**Figure 7.1** - Procedure of the FEA using correctors

### **7.3. Improved Panel Displacement Using Correctors**

There are many factors that can improve the displacement, failure load and failure pattern of the masonry panel calculated using the FEA. For the application of correctors in the FEA of the panel, these factors may include: the method of dividing the panel into zones, suitability of techniques for matching similar zones and the accuracy of experimental results of the panel from which correctors are derived. In this chapter, factors affecting the FEA displacement of the panel are investigated. The investigation into the failure load and failure pattern of the panel will be carried out in Chapter 8.

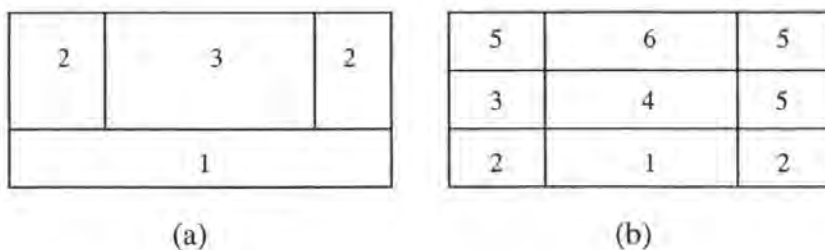
The correctors used in investigating the displacement response of the panel are based on the experimental result of Panel SB01. The corresponding corrector data is shown in Appendix A.

For comparison purposes, the following processes were used:

- Firstly, the panel was analysed using globally smeared  $D$ .
- The panel was divided into three, six zones (see Figure 7.2) and twenty zones (see Figure 6.3), and the values of modified  $D'$  at the corresponding zones were established and the panel was re-analysed.
- Load-displacement curves using the FEA result along with the experimental result were plotted for comparison purposes. The results of this investigation are summarised in Figures 7.3 to 7.7.

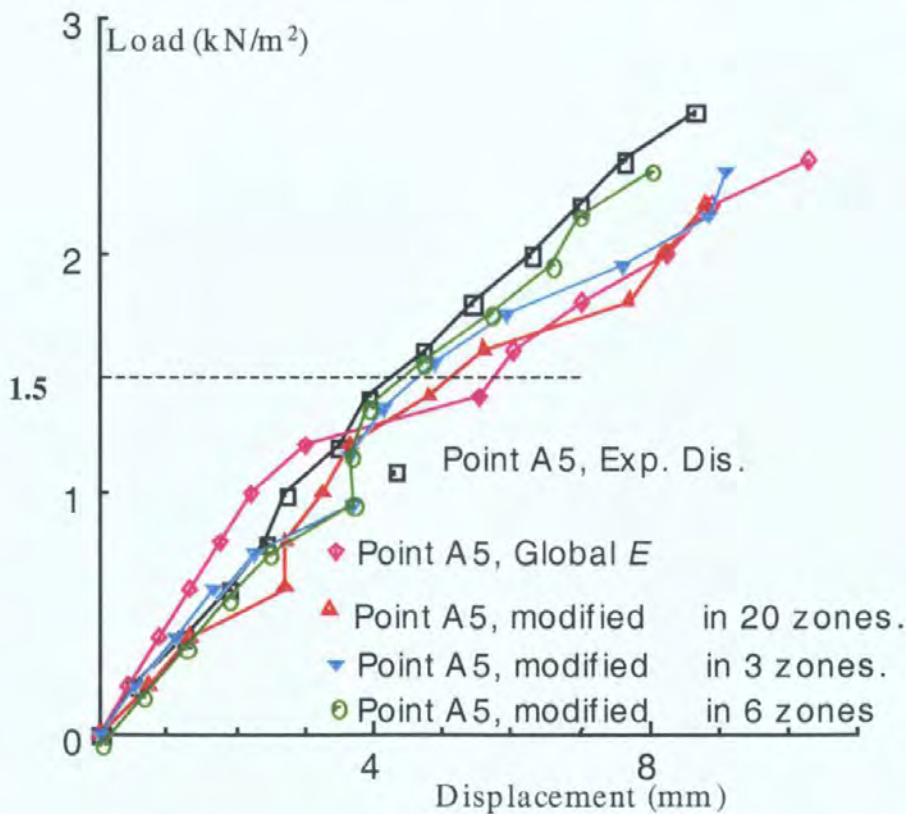
The following points were considered in this comparison:

- (1) Effect of introducing  $D'$ ;
- (2) Effect of increasing number of zones;
- (3) Sensitivity of location of the zone within the panel with respect to its distance from the panel boundaries.



**Figure 7.2** - The two cases of zone division of Panel SB01

Figures 7.3 to 7.7 show the results of the FEA using correctors. It is clear that the greater the number of the divided zones, the closer are the predicted displacements of the points such as Points B3, B4 and B5 to their experimental results. These figures also show that in the range of normal working load of  $1.5\text{kN/m}^2$ , the application of correctors makes the predicted displacements much closer to the experimental results. For the displacements of the points such as Points A5 and C5, they can be closer to the experimental result, when the panel is divided into fewer zones and the load value was larger than  $1.5\text{kN/m}^2$ . The above analysis indicates that, although the application of the corrector can improve the prediction of displacement of many measured points on the panel, a scheme for the zone division of the panel can not improve the prediction of displacement of all measured points on the panel. Fortunately, the prediction of displacement of all the important points measured in the experiment are closer to their experimental values because of the application of correctors.



**Figure 7.3** - The displacement – load curves of Point A5 within Panel SB01.

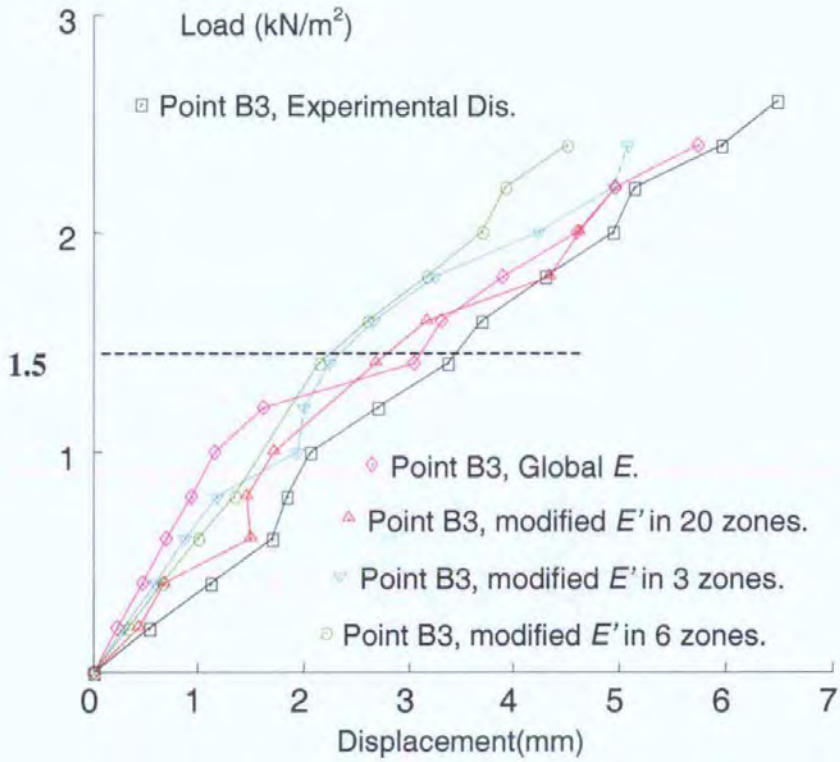


Figure 7.4 - The displacement – load curves of Point B3 within Panel SB01

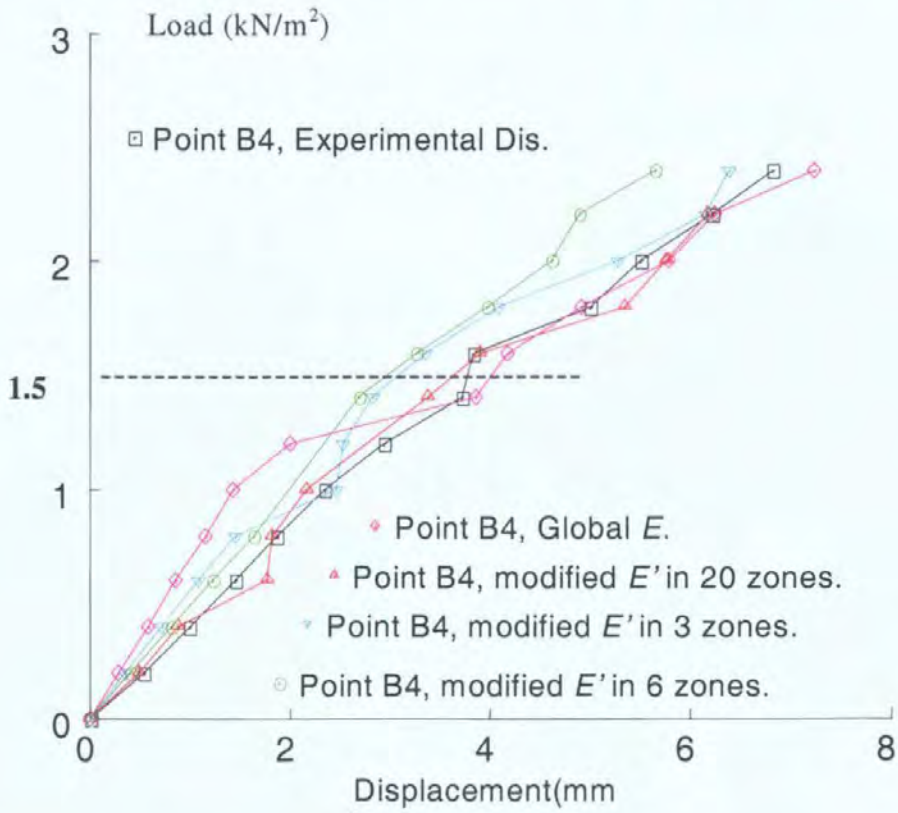


Figure 7.5 - The displacement – load curves of Point B4 within Panel SB01

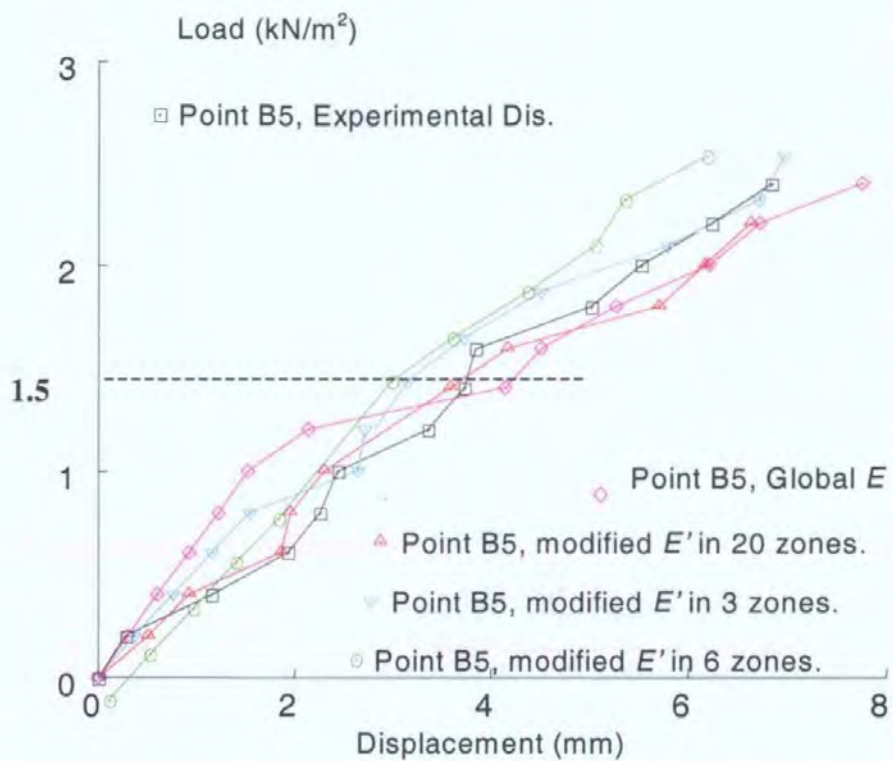


Figure 7.6 - The displacement – load curves of Point B5 within Panel SB01

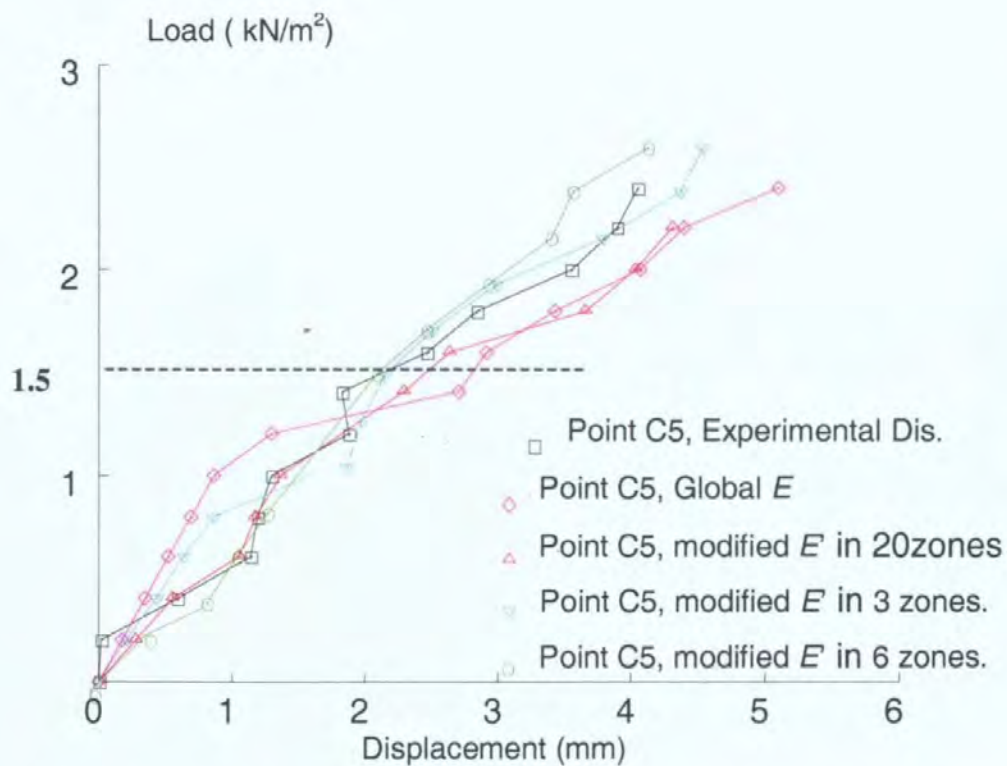
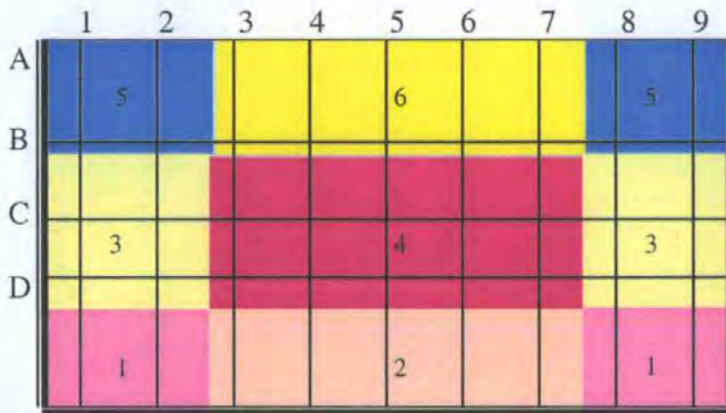


Figure 7.7 - The displacement – load curves of Point C5 within Panel SB01

However this conclusion might not fit the application of correctors in other panels, because here the analysed panel SB01 and its derived correctors were used in the FEA for the displacement calculation. One reason for dividing the panel into more zones is that there are more experimental results to compare with.

**7.4. Investigation into Effect of Introducing Noise at Local Regions within the Panel**

In this section the effect of random noise at different regions on the displacement response of the panel is investigated. Once again Panel SB01 is used in this analysis. To introduce noise into local regions, the value of Elastic Modulus  $E$  was randomly changed at specific regions and the panel was analysed using the FEA. For this investigation, Panel SB01 was divided into six regions as shown in Figure 7.8.



**Figure 7.8 – Divided regions of Panel SB01**

The noise was introduced by randomly adjusting the value of  $E$  in a particular region. The effect of this noise on panel displacement was investigated. The results of introducing noise at locations A5 and B3 (two typical points) on the panel are plotted in Figures 7.9 and 7.10. In both figures,

$$x\text{-Axis represents modulus ratio} = \frac{\text{modified modulus } E' \text{ at a region}}{\text{global modulus } E}$$



$$y\text{-Axis represents displacement ratio} = \frac{\text{displacement of Point } j \text{ under } E}{\text{displacement of Point } j \text{ under global modulus } E}$$

#### 7.4.1. Changes in Displacement Pattern Due to Introducing Noise

By separately introducing noise at Regions 1, 2, 3 and 4, the displacement changes at Points A5 and B3 for a lateral load of  $1\text{ kN/m}^2$  are shown in Figures 7.9 and 7.10. It was observed that the displacement of the panel was less sensitive to  $E$  change in the local regions than to the change of the global  $E$  value on the whole panel. The displacement of the panel is more sensitive to changes in the value of  $E$  at the local Regions 1, 2 and 3 adjacent to the boundaries than to changes in the value of  $E$  at Region 4 away from the boundaries. Once again it proves that boundaries have a critical effect on the overall behaviour of the panel.

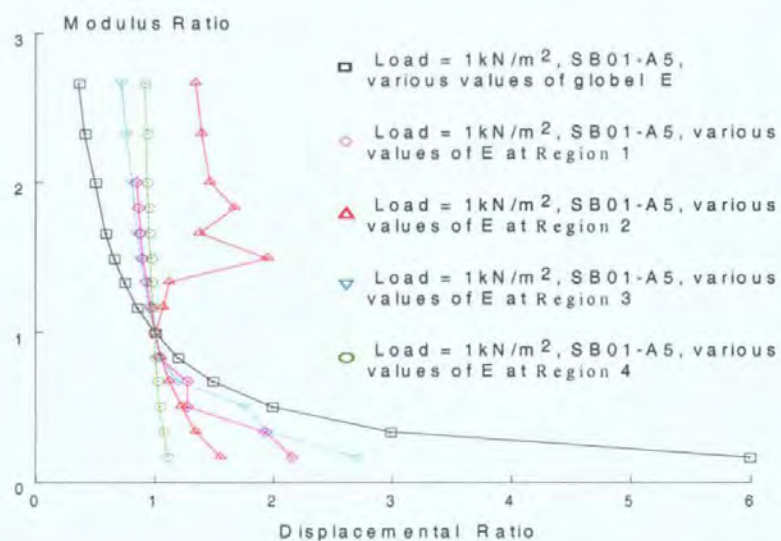


Figure 7.9 – Displacement ratio- $E$  ratio curves of Point A5 on Panel SB01

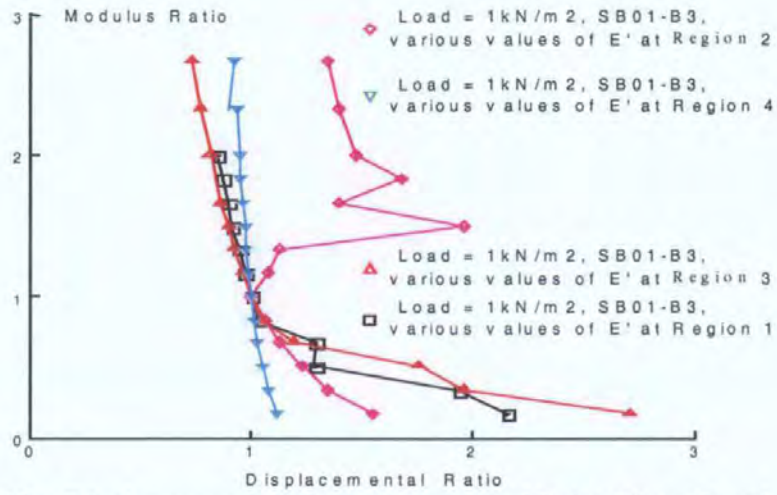
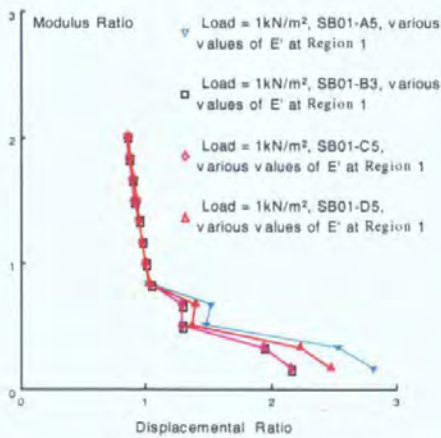


Figure 7.10 – Displacement ratio- $E$  ratio curves of Point B3 on Panel SB01

The effect of noise at Regions 1, 2, 3 and 4 on the displacements of Points A5, B3, C5 and D5 on the panel is shown in Figures 7.11 to 7.14. From these figures, it is clear that the displacements at these points on the panel follow a similar pattern. The displacement of the panel is more sensitive to parametric variation in regions adjacent to the panel boundaries, especially Region 2 near the fixed boundary at the bottom support. The  $E$  values at the central Region 4 have little effect on the displacement response of the panel.



Displacement ratio- $E$  ratio curves of Points A5, C5, D5 and B3 on Panel SB01 to  $E$  noise at Regions 1 and 3.

Figure 7.11

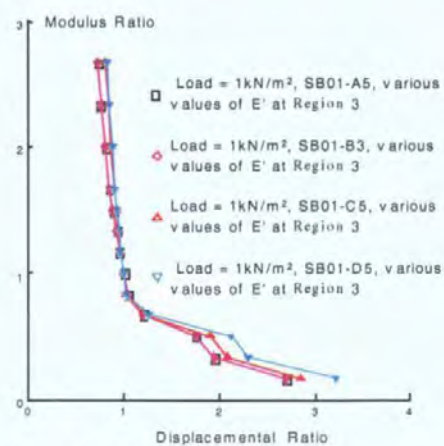
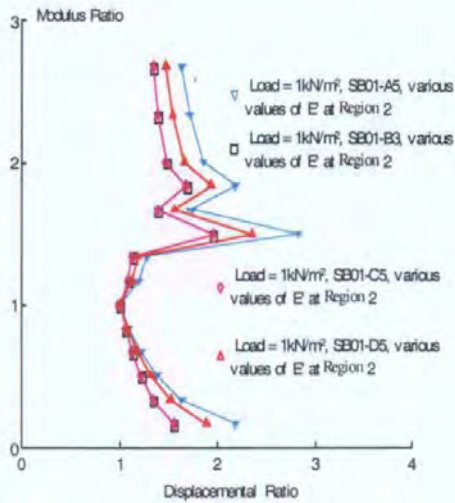


Figure 7.12



Displacement ratio- $E$  ratio curves of Points A5, C5, D5 and B3 on Panel SB01 to  $E$  noise at Regions 2 and 4.

Figure 7.13

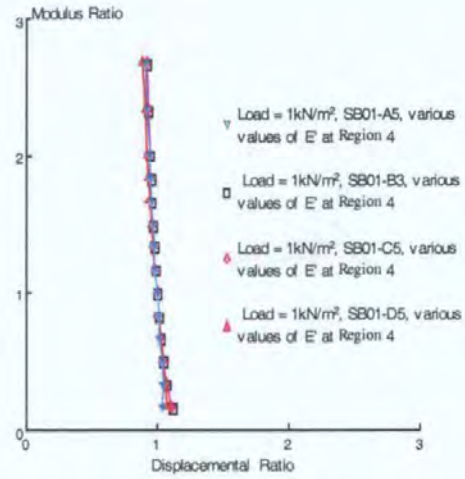


Figure 7.14

### 7.4.2. Effect of Region Size

The effect of region sizes on the displacement of the panel is shown in Figures 7.16 and 7.17, when  $E$  noise is introduced into the region. Panel SB01 divided into different region sizes is shown in Figure 7.15.

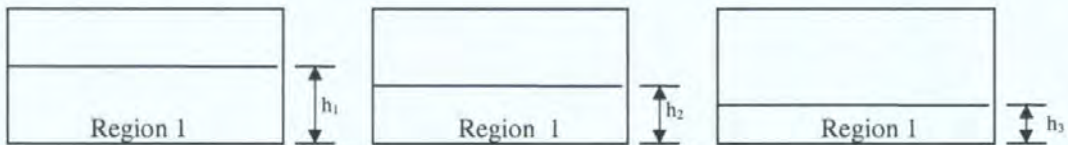
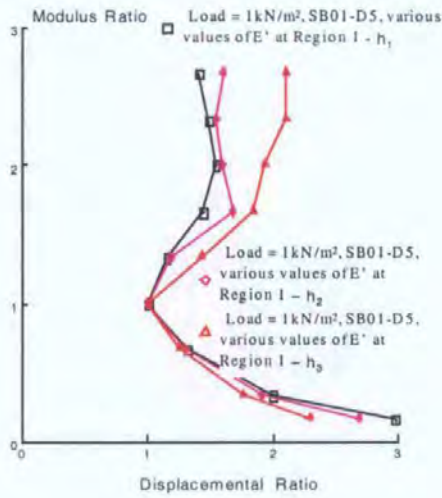


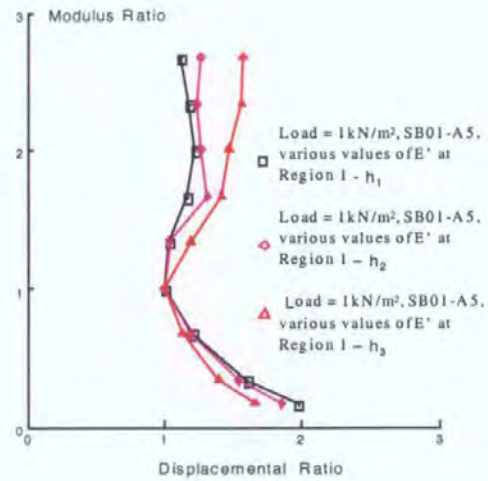
Figure 7.15 – Sizes of the region near the bottom support of the panel

Figures 7.16 and 7.17 show that the sizes of regions change the effect of noise on the displacement of the panel. For the region shown in Figure 7.15, the effect of noise in the region on the displacement response of the panel was reduced following the enlargement of the region size. This indicates that variation in properties of a narrow region adjacent to the bottom boundary greatly affect the panel behaviour.



Displacement ratio- $E$  ratio curves of Points D5 and A5 on Panel SB01 to  $E$  noise and three different region sizes.

**Figure 7.16**



**Figure 7.17**

### 7.4.3. Analytical Summary

It can be concluded that the effect of changing flexural rigidity on the displacements of the panel was related to the position of the region in which the noise was introduced and it was affected by the size of the region. The displacement of the panel was sensitive to noise which was introduced into regions adjacent to boundaries, especially adjacent to that region near the bottom support (built-in support). Changing noise at the central region of the panel has little effect on the displacement of the panel. This indicates that the behaviour of the panel under laterally loading was seriously affected by boundaries.

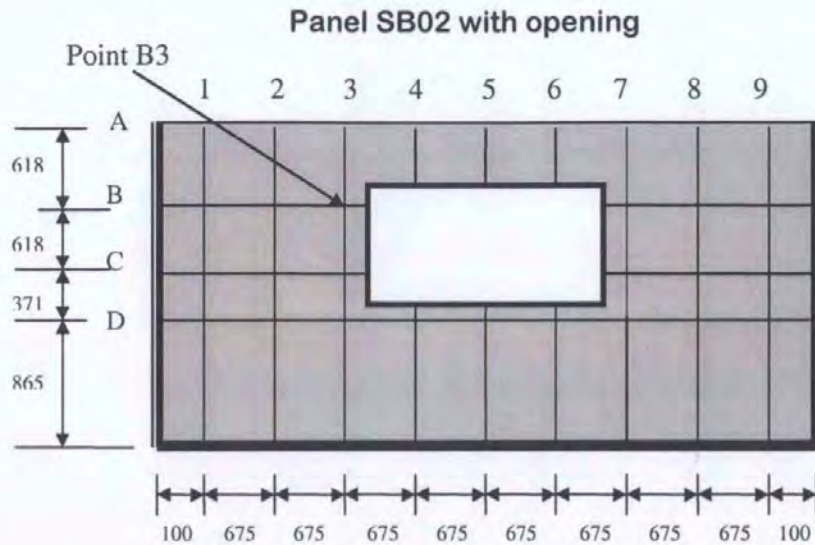
### 7.5. Comparison of Experimental and Analytical Displacements on Panels with and without openings

In this section, correctors on the base panel were applied to similar zones on the new panel to modify the displacements obtained from the FEA under globally smeared material properties. These modified displacements were then compared with the

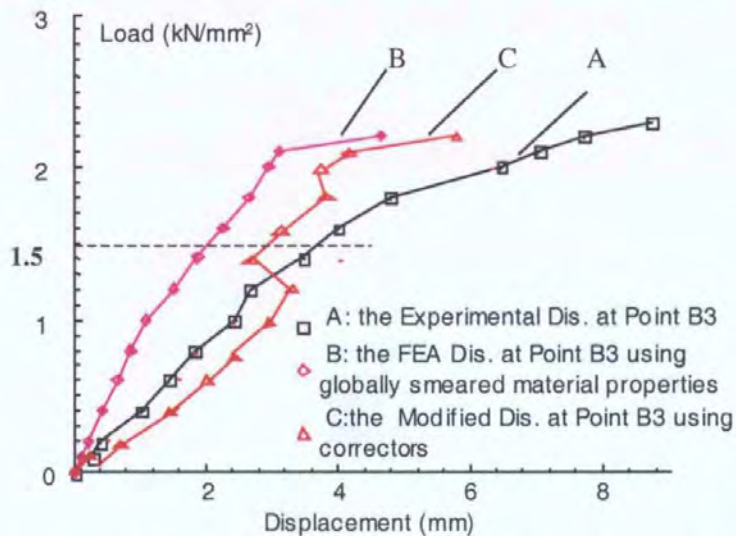
corresponding experimental and the FEA displacements. The CA method developed in Chapter 6 is used to select the correctors from the base panel for the new panels.

Panel SB01 was still used as the base panel of the panels SB02 with an opening, SB05 with d.p.c and SB06 (Chong 1993), because they were constructed of the same material and tested in the same laboratory experimental environment.

Panel SB02 (Figure 7.18) with an opening has the same material properties, boundary conditions and sizes with Panel SB01. For the zone around Point B3 on Panel SB02, its similar zone on the base panel SB01 is the zone around Point A2/A8 on Panel SB01, using the CA method. The FEA displacement of Point B3 on Panel SB02 under globally smeared material properties and individual load increments is then modified using the selected correctors, and the result is shown in Figure 7.19 (Curve C using the correctors at Point A8 on the base panel). Figure 7.19 also shows experimental (Curve A) and the FEA displacements (Curve B). Comparing the three load – displacement curves, it is clear that using correctors to modify masonry properties is a true representative of behaviour of the panel as the result of this analysis is very close to the experimental results. The figure also shows that in the range of normal working load of  $1.5\text{kN/m}^2$ , the displacements modified by the correctors are much closer to the experimental results. The inversion of the load-displacement curves is because in the FEA of the base panel, the initial cracking of the panel occurs at that load value and results in a sudden increase of the FEA displacement of the panel (a sudden increase of the correctors at this load value).



**Figure 7.18** - Panel SB02 with opening



**Figure 7.19** – Load-displacement curves of Point B3 on Panel SB02

Figure 7.20 shows details of another panel SB05 with d.p.c. The CA method matches the similar zones around Point A3 on the both panels. A similar comparison as discussed in the previous example is given in Figure 7.21. Once again, it is clear that the result of the analysis using correctors is much closer to the experimental result. The figure also shows that in the range of normal working load of  $1.5\text{kN/m}^2$ , the displacements modified by the correctors are much closer to the experimental results.

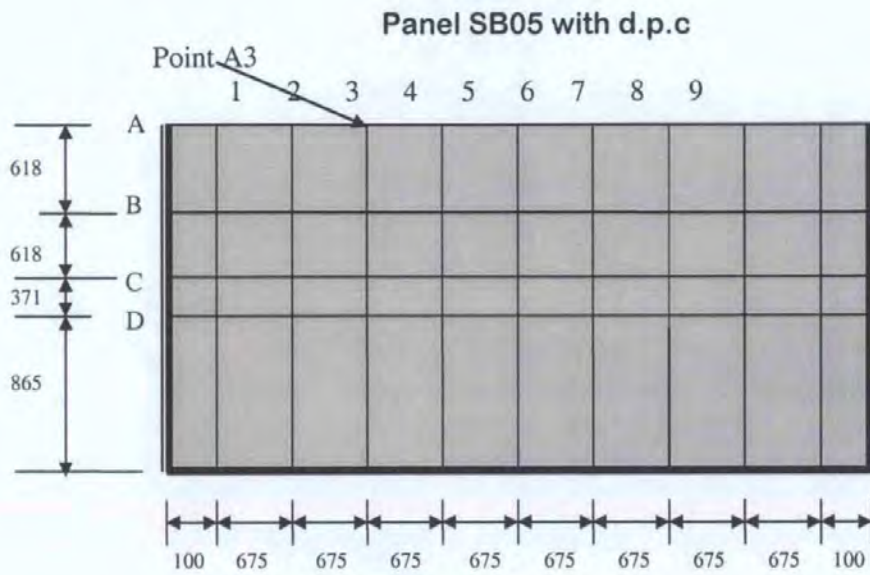


Figure 7.20 - Panel SB05 with d.p.c

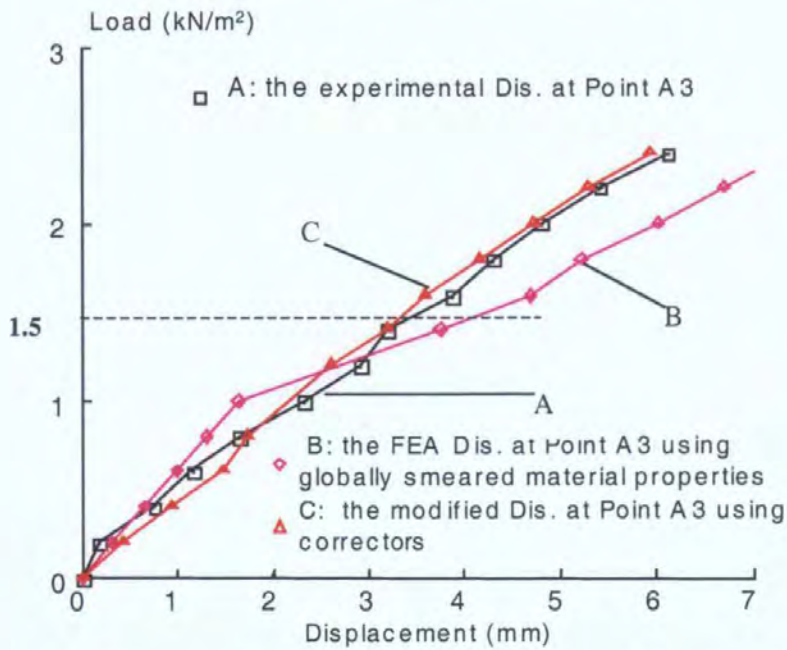


Figure 7.21– Load-displacement curves of Point A3 on Panel SB05

Figure 7.22 shows details of Panel SB06. The zone around Point B2 on the base panel SB01 matches its similar zone around Point C3 on Panel SB06, using the CA method. A similar comparison as discussed in the previous examples is given in Figure 7.23. Once again, it is clear that the displacement modified using the selected correctors is

closer to the experimental result, especially in the range of the normal working load of  $1.5\text{kN/m}^2$ .

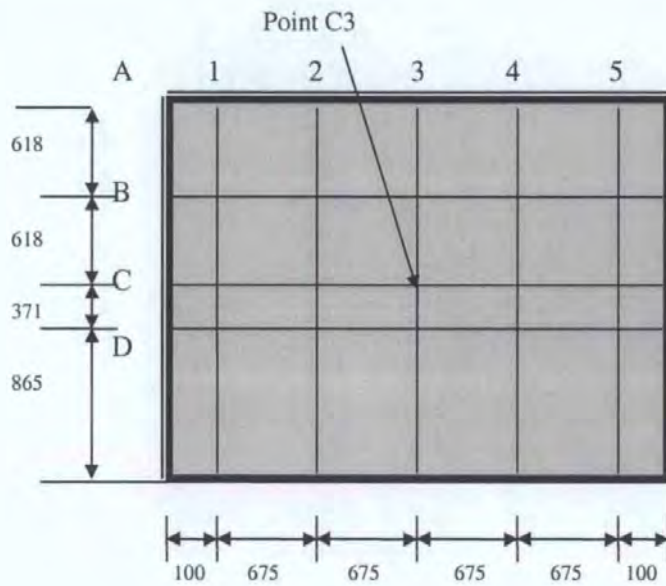


Figure 7.22 – Panel SB06

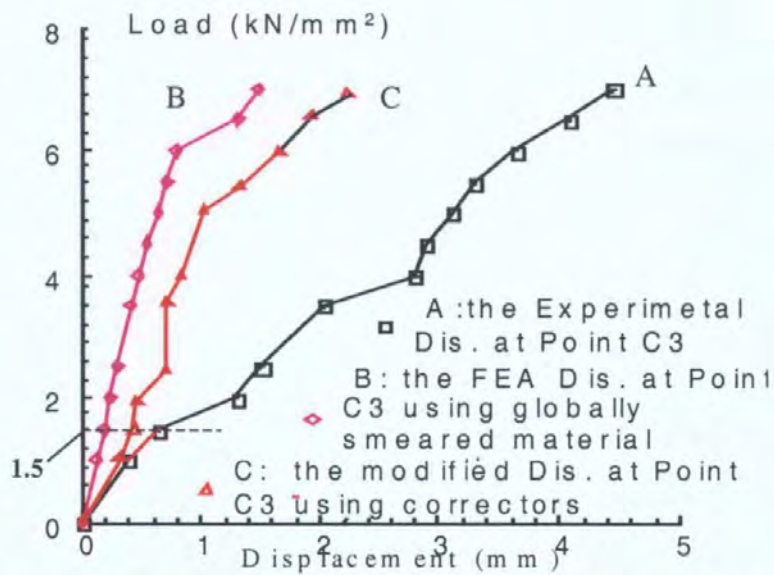


Figure 7.23 – Load-displacement curve of Point C3 on Panel SB06

In the above analysis, all panels are single leaf brick panels. The following analysis is related to two cavity panels, CB01 (Chong 1993) (Figure 7.24) and CAV14 (West 1974) (Figure 7.25). Because the displacements of various points on Panel CB01 were recorded in its test, the panel is used as the base panel here. Both panels have the same boundary conditions, but their sizes are different. For the zones around the



central point F and another point C on Panel CAV14, the CA method matches their similar zones, the zones around Points C5 and C2 on the base panel CB01. The correctors corresponding to the zones around Points C5 and C2 on Panel CB01 are used to modify the FEA displacement of Point F and C. The Load-Displacement curves of Points F and C on Panel CAV14 are shown in Figures 7.26 and 7.27 respectively. Once again, it is clear that the result of the analysis using correctors is much closer to the experimental result.

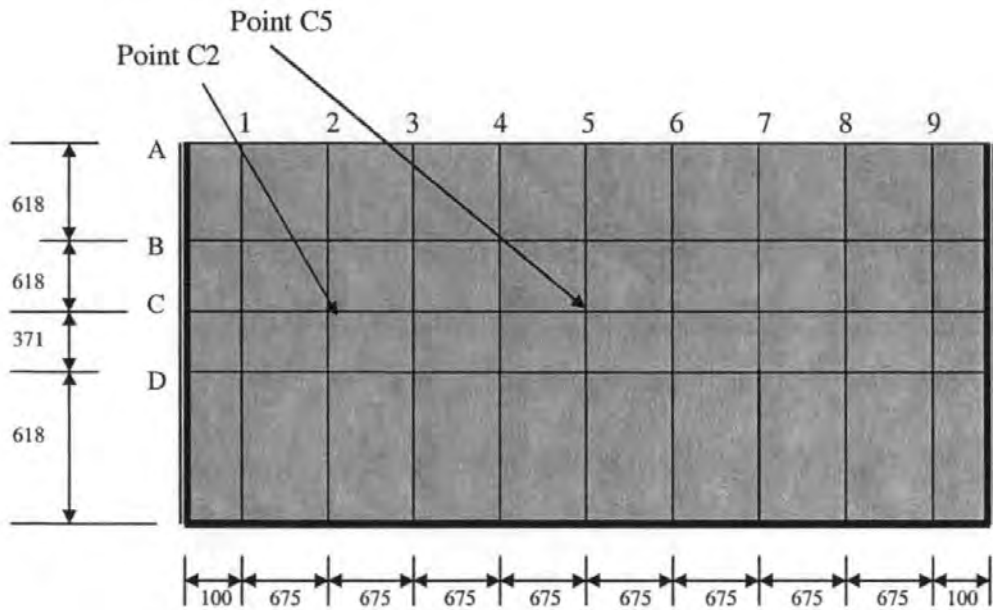


Figure 7.24 - Panel CB01

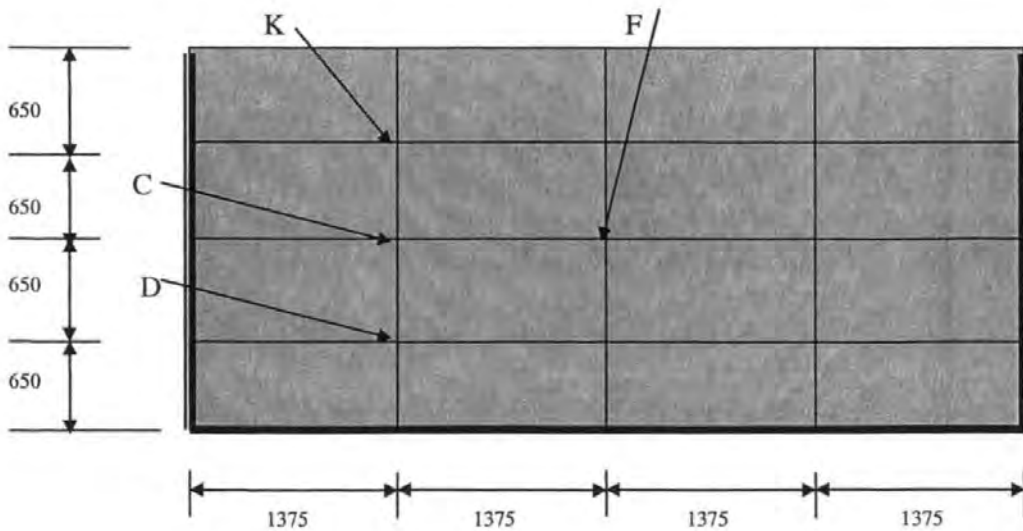


Figure 7.25- Panel CAV14

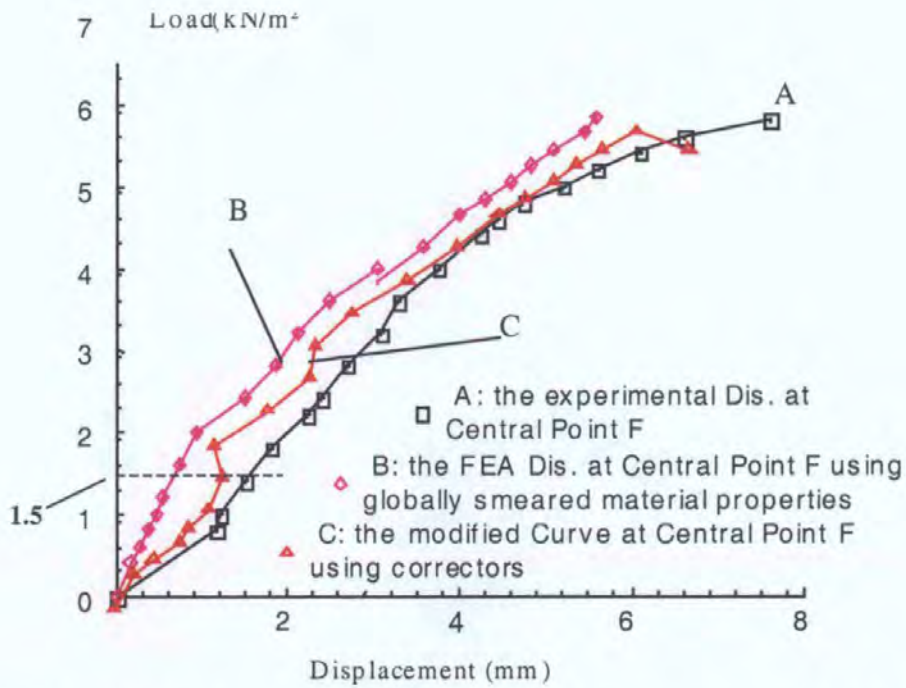


Figure 7.26 – Load-displacement curves of Point F on Panel CAV14

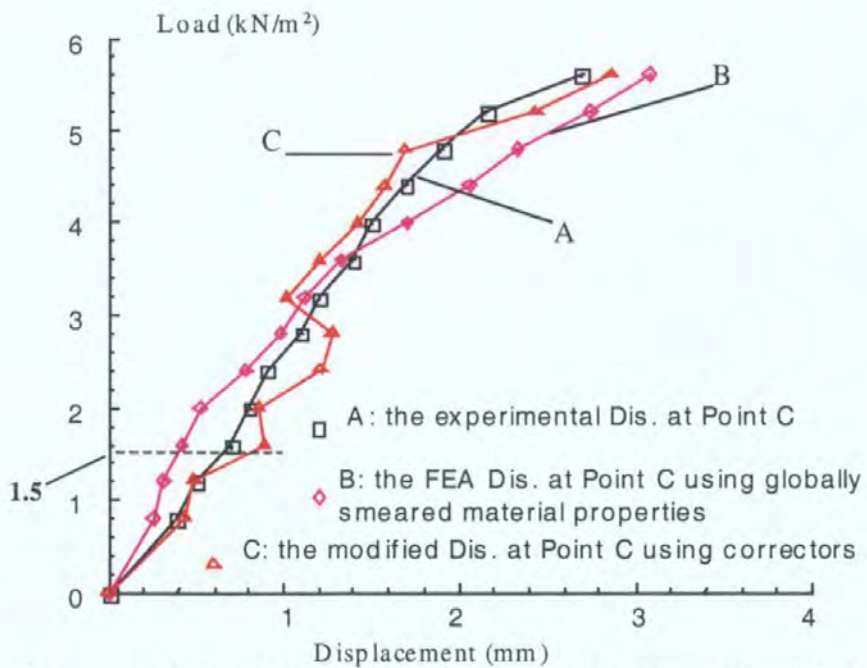


Figure 7.27 – Load-displacement curves of Point C on Panel CAV14

The above examples further indicate that there is similar variation in masonry properties at similar zones within masonry panels which have different boundary conditions and configurations and are constructed of the same masonry material.

Correctors at individual zones within the base panel can back-feed the variation in masonry properties into the similar zones within the new panel. The reason why the above phenomenon exists is considered as:

The failure of laterally loaded masonry panels is mainly from the cracking of the panel. This crack occurs and develops within the linear tension range of masonry material deformation during the working process of the panel. The non-linear property in the FEA process of the panel is from the change of the stiffness matrix caused by the crack. Therefore, in a load increment, the displacement of the panel is still proportional to the modulus  $E$  of the panel so that correctors can effectively back-feed the variation in masonry properties into similar zones within other new panels. The most important is that this analysis has verified that the variation in masonry properties is closely related to the structural factors such as boundary conditions of the panel and locations of zones on the panel.

## **7.6. Summary**

The examples presented in this chapter show that correctors can considerably improve the FEA displacement values at various locations on the panel which in many cases were very close to their experimental results, particularly in the range of normal working load. This proves that using correctors properly models the true behaviour of masonry panels.

As the values of correctors are affected mainly by the boundaries of the panel, the examples give evidence that boundary conditions of panels play a key role in the displacement response of the panel.

Because the displacement analysis of the panel is not the main parameter that governs the design of masonry panels, the results of the investigation, presented in this chapter, were intended to verify whether using correctors, to modify masonry properties at various zones within the panel, could improve the quality of the FEA. The comparison of results for a number of cases clearly demonstrates that using correctorr enables the FEA to more closely model the behaviour of masonry panels.

## **8. CASE STUDY ON PREDICTING FAILURE LOAD AND FAILURE PATTERN OF MASONRY PANELS USING CORRECTORS**

### ***8.1. Introduction***

For the design of masonry panels, it is important to predict the load which causes failure of the panel. However, a reliable and accurate FEA technique should be able to simultaneously estimate both failure load and failure pattern for panels with various boundary conditions and panel configurations. If a FEA technique gives inconsistent results in estimating the failure load and failure pattern of the masonry panel, in comparison with experimental results, these results obtained from the FEA technique can not be reliable. Following the discussion in the previous chapter, on the displacement of the panel, this chapter focuses on the FEA prediction of failure load and failure pattern of laterally loaded masonry panels.

Two FEA softwares, used in the chapter, are specialised FEA programs for non-linear analysis of masonry panels. One of the FEA programs uses the biaxial stress failure criterion (Chong 1993) and the other program uses the homogeneous technique (Lee et al. 1996). The results of the two FEA techniques are compared.

In this chapter, prediction of failure load and failure pattern for each panel is based on corrector values obtained from one single base panel only which is SB01 corresponding to a load increment just before the failure of this base panel (the load value =  $2.4 \text{ kN/m}^2$ ). Correctors for panels with/without openings and with various boundary conditions are obtained both manually and by using the CA method. These

correctors are then used to modify masonry properties at various zones within the panel. On the basis of the FEA results, the failure load and failure pattern for each panel are determined and these are compared with their corresponding experimental results to examine the validity of the proposed methods. These results are also compared with those obtained by conventional FEA results using globally smeared masonry properties.

Therefore in this chapter, the results of the analysis obtained from laboratory experiments on various panels are compared with the predicted failure loads and failure patterns obtained from the FEA of panels using:

1. globally smeared modulus  $E$  and tensile strength  $f$ .
2. globally smeared tensile strength  $f$  but modified modulus  $E'$  in various zones within the panel. The modified modulus  $E'$  was calculated using stiffness correctors obtained by the manual and the CA methods.
3. globally smeared modulus  $E$  but modified strength  $f'$  in various zones within the panel. The modified strength  $f'$  is determined by the strength correctors obtained by the manual and the CA methods.

For the comparison of the results of each panel, along with the FEA predictions, the following information is presented for each panel:

- The experimental failure load and failure pattern of the panel.
- Locations of zones on the “new” panel and their similar zones on the base panel, which are matched by the manual and CA methods respectively.

The aim of the above comparison is to demonstrate the difference between the methodologies proposed in this research with conventional FEA results.

## **8.2. Predicting the Failure Load and Failure Pattern of the Base Panel SB01**


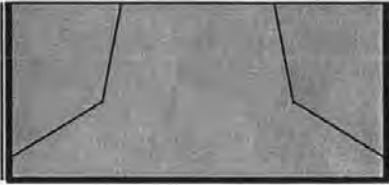
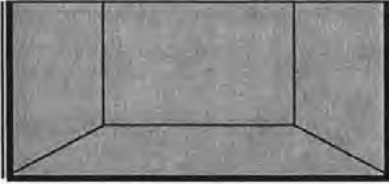

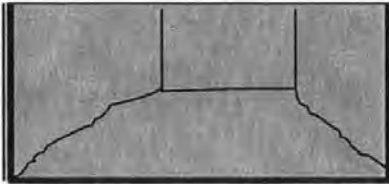
In Chapters 5 and 6, the methodologies for estimating values of correctors were fully discussed. In Chapter 7, corrector values from the base panel SB01 were used for the displacement of all panels. It is essential to demonstrate that modifying the stiffness of various zones within the panel using correctors can improve the FEA results for masonry panels, which leads to an improved and more accurate prediction of failure load and failure pattern. This section verifies the effect of correctors on estimating the failure load and failure pattern of various panels.

### **8.2.1. The FEA Result Using Biaxial Stress Failure Criterion**

In this study, the correctors from the base panel SB01 are those modified as shown in Table 5.2. Panel SB01 was divided into 20 zones (symmetrical half panel, see Figure 6.4) based on the laboratory experimental measurement points on the panel. The correctors are based on a lateral load  $q_m = 2.4\text{kN/m}^2$  (failure load). The panel SB05 has the same dimensions, material properties and boundary conditions as SB01. The only difference between Panels SB01 and SB05 is that Panel SB05 has a d.p.c at its base. The experimental failure loads and failure patterns of both panels are shown in Figures 8.1d and 8.1e. The failure load and failure pattern obtained using the FEA for both Panels SB01 and SB05 are shown in Figure 8.1a, using a globally smeared modulus  $E$  and strength  $f$ .

Figure 8.1b gives the FEA results of both Panels SB01 and SB05, using a globally smeared strength  $f$  but the modified modulus  $E'$ , corresponding to the individual zones on the panel. Figure 8.1c shows the FEA results of the two panels, using

globally smeared modulus  $E$  but the modified strengths  $f'$  corresponding to individual zones.

Case Result	Failure Pattern	Failure Load
(a) Global $E$ and $f$		2.4 kN/m <sup>2</sup>
(b) Global $f$ , but $9 E$ 's		2.2 kN/m <sup>2</sup>
(c) Global $E$ , but $9f$		2.4 kN/m <sup>2</sup>
(d) Experimental Case of SB01		2.7 kN/m <sup>2</sup>
(e) Experimental Case of SB05		2.7 kN/m <sup>2</sup>

**Figure 8.1** – The predicted and experimental failure loads and failure patterns of Panels SB01 and SB05 (the FEA using biaxial stress failure criterion)


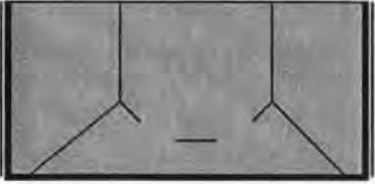
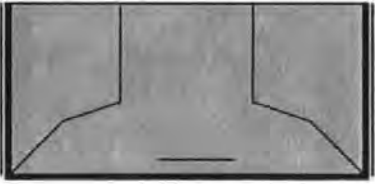
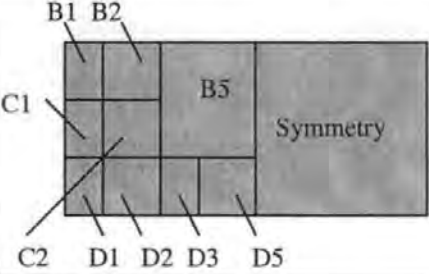


By comparing the FEA results using globally smeared modulus  $E$  and strength  $f$  with those using correctors in different zones within the panel, it is clear that the failure pattern predicted using correctors are closer to the experimental results. The prediction of failure load is also acceptable. Section 8.3 will further show that correctors can considerably improve results of the FEA and bring these results closer to the experimental results.

### **8.2.2. The FEA Result Using Homogeneous Technique**

Figure 8.2 shows the prediction of the failure pattern of Panel SB01 using a FEA calculation program developed in the University of Swansea (STRUMAS 1999). This programme employs the homogenous technique for masonry (Lee et al. 1996). For this analysis, the panel was divided into nine zones as shown in Figure 8.2d. Zones B1, B2, B3, C1, C2, D1, D2, D3 and D5 in Figure 8.2d are the similar zones of the above nine zones manually matched in the base panel SB01. Because the programme does not include the criterion of finding the maximum load capacity of the panel, the analysis here just checks the failure pattern of the panel using the corresponding failure load obtained from the FEA using biaxial stress failure criterion.

Figure 8.2a is the FEA result of the panel SB01 using globally smeared modulus  $E$  and strength  $f$ . Figure 8.2b shows the FEA results of the panel, applying correctors to modify the globally smeared modulus  $E$  in the individual zones within the panel. Figure 8.2c shows the FEA results of the panel, using globally smeared modulus  $E$  but modified strengths  $f$  for each individual zone. These results show that the application of correctors in the FEA using homogenous technique can also improve the FEA prediction closer to the experimental results.

Case Result	Failure Pattern	Lateral Load
(a) Global $E$ and $f$		$2.4 \text{ kN/m}^2$
(b) Global $f$ , but 9 $E$ 's		$2.4 \text{ kN/m}^2$
(c) Global $E$ , but 9 $f$		$2.4 \text{ kN/m}^2$
(d) Divided 9 Zones of Panel SB01		<b>Manual-Selecting Correctors</b>

**Figure 8.2** – The predicted and experimental failure loads and failure patterns of Panel SB01 (the FEA using homogeneous techniques)

### **8.3. Case Study of Predicting Failure Loads and Failure Patterns Using Correctors**

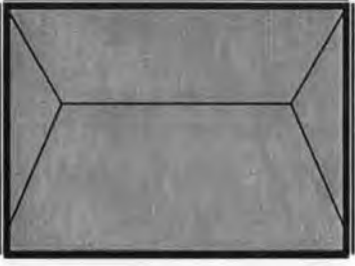
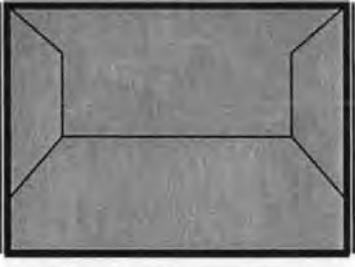
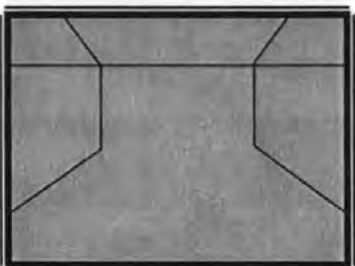
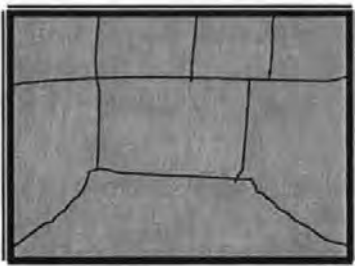
In this section, a number of panels with and without openings with different boundary conditions are analysed. In the FEA of each panel, firstly correctors for individual zones within each panel were determined; secondly values of modified modulus  $E'$  or modified strength  $f'$  corresponding to the individual zones were calculated and then the panel was analysed by the non-linear FEA program using the biaxial stress failure

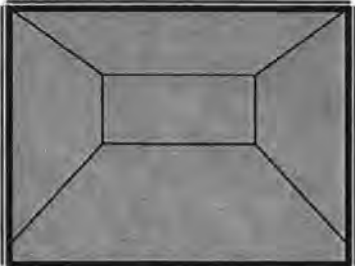
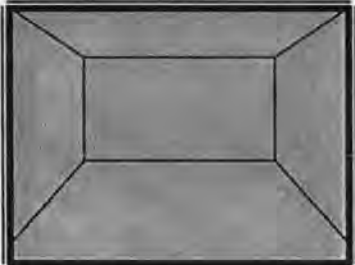
criterion. Correctors for each panel were calculated using the manual method discussed in Section 5.5 and the CA method discussed in Section 6.6. The solid panel SB01 was used as the base panel for all panels analysed in this section. The results for panels with openings, using the panel SB02 with opening, as the base panel have also been presented.

The seven experimental brick panels (Chong 1993) (Edgell) with different configuration are used to verify the validity of correctors in the FEA of the panel. The following sections present the analytical results of these panels.

### **8.3.1. Panel SB06**

Results of the investigation into Panel SB06 (Chong 1993) are presented in Figure 8.3. This panel was a solid brick panel with the size 2800×2475. The bottom edge of this panel was built-in and the other three edges were simply supported. The experimental failure load for this panel was 7.5kN/m<sup>2</sup> and the experimental failure pattern of the panel is shown in Figure 8.3d. The failure pattern prediction obtained using the non-linear FEA is shown in Figure 8.3a using conventionally globally smeared stiffness and strength. The failure load predicted by the FEA using smeared material properties was 9.0kN/m<sup>2</sup>. The conventional FEA result overestimates the failure load of the panel, as it uses globally smeared masonry properties. The predicted failure pattern is also not close to the experimental result.

Case Result	Failure Pattern	Failure Load									
(a) Global $E$ and $f$		9.0 kN/m <sup>2</sup>									
(b) Global $f$ , but 9 $E$ 's		6.0 kN/m <sup>2</sup> (Manual-Selecting Correctors)									
(c) Global $E$ , but 9 $f$		6.0 kN/m <sup>2</sup> (Manual-Selecting Correctors)									
(d) Experi- mental case		7.5 kN/m <sup>2</sup>									
(e) Divided Zones of Panel SB06	<table border="1" data-bbox="363 1592 712 1847"> <tbody> <tr> <td>C1</td> <td>B1</td> <td>C1</td> </tr> <tr> <td>B1</td> <td>B3</td> <td>B1</td> </tr> <tr> <td>D1</td> <td>D3</td> <td>D1</td> </tr> </tbody> </table>	C1	B1	C1	B1	B3	B1	D1	D3	D1	<p>Note: B1, B3, C1, D1 and D3 are the points on the base panel SB01, whose corresponding correctors are applied to improve the FEA of Panel SB06.</p> <p>(Manual-Selecting Correctors)</p>
C1	B1	C1									
B1	B3	B1									
D1	D3	D1									

Case Result	Failure Pattern	Failure Load
(f) Global $f$ , but 9 $E$ 's		6.5 kN/m <sup>2</sup> (CA-Selecting Correctors)
(g) Global $E$ , but 9 $f$		5.5 kN/m <sup>2</sup> (CA-Selecting Correctors)
Note	The result of selecting correctors by the CA method is shown in Appendix C.	

**Figure 8.3** – The FEA and experimental results of Panel SB06

Figure 8.3e shows that the twelve manually-divided zones of Panel SB06 and their similar zones C1, B1, D1, B3 and D3 within Panel SB01 obtained by using the manual matching method. The correctors corresponding to similar zones within the base Panel SB01 are used to modify the global modulus  $E$  or global strength  $f$ . Figure 8.3b shows the failure pattern predicted by the FEA under globally smeared strength  $f$  but different modified stiffness at each zone in this analysis. The corresponding predicted failure load is 6.0kN/m<sup>2</sup>.

Figure 8.3c shows the failure pattern predicted by the FEA under globally smeared modulus  $E$  but different modified strengths  $f$ . The corresponding predicted failure load is 6.0kN/m<sup>2</sup>. Comparing the FEA results in Figures 8.3a, 8.3b, 8.3c and 8.3d, it is

clear that using correctors improves the FEA results considerably. The predicted failure pattern is also much close to the experimental result.

Figure 8.3f shows the failure pattern predicted by the FEA using globally smeared strength  $f$  but different modified modulus  $E'$ . The corresponding failure load is  $6.5\text{kN/m}^2$ . Figure 8.3g shows the failure pattern predicted by the FEA using globally smeared modulus  $E$  but different modified strengths  $f'$ . The corresponding failure load is  $5.5\text{kN/m}^2$ . Comparing the results in Figure 8.3d, the FEA, using modified masonry properties by applying correctors makes the predicted failure pattern closer to the experimental result. It also shows that the predicted failure load by applying modified modulus  $E'$  was much closer to the experimental result than that by different modified strengths  $f'$ . The reason is mainly because correctors are produced by comparing the change of masonry stiffness at individual local zones, see Equation (4.8). Therefore correctors can more effectively reflect the variation in stiffness at local zones within the panel rather than the variation in strength.

### **8.3.2. Wall 1a. Control**

The brick walls analysed in the following sections are the typical experimental walls designed and tested by Edgell (Edgell) in CERAM laboratories. During the experiments on these panels, displacements at a limited number of points were measured, which was not sufficient to be used for the evaluation of correctors. Therefore, Panel SB01 was used as the base panel for these walls as well.



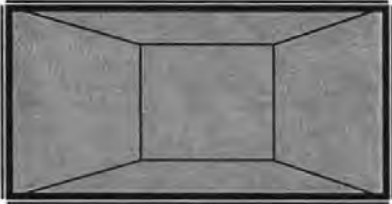

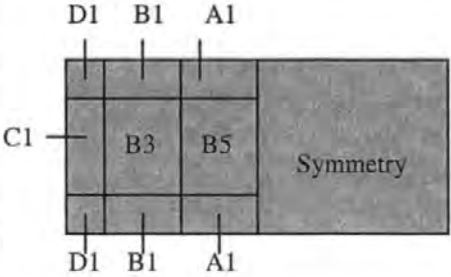
Wall 1a. Control is a brick panel with four sides simply restrained. The size of the wall is  $5500 \times 2600$ . Figure 8.4d shows the experimental failure load of  $2.6\text{kN/m}^2$  and the corresponding failure pattern of the panel. Figure 8.4a represents the failure load

of  $3.0\text{kN/m}^2$  and the corresponding failure pattern predicted by the FEA using globally smeared modulus  $E$  and strength  $f$ . This FEA result overestimates the failure load on the wall when compared with the experimental case, but the predicted failure pattern compares well to the experimental result.

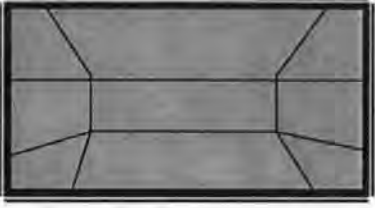
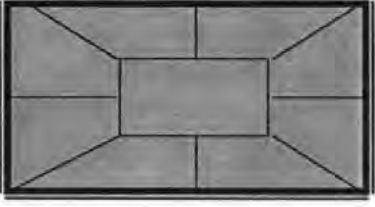
Figure 8.4e shows zones within the symmetrical half of the wall. Using manual selection, the nine zones on the wall are divided to match similar zones on the base panel based on their boundary similarities, as discussed in Chapter 5. Zones A1, B1, B3, B5 and C1 on the base panel were found to be a closer match to respective zones on Wall 1a. Control. Relevant values of the correctors were taken from Table 5.2. Figure 8.4b gives the failure load and failure pattern of the wall predicted using globally smeared strength  $f$  but different modified modulus  $E$ . The predicted failure load is equal to the experimental value and the predicted failure pattern is a better match to the experimental case. This is a much better analytical result than that using globally smeared modulus  $E$  and strength  $f$ . Figure 8.4c gives the failure load and failure pattern of the wall predicted using globally smeared modulus  $E$  but different modified strengths  $f$ . The predicted failure load is quite close to the experimental value, but the predicted failure pattern is not as good as that in Figure 8.4b.

Figure 8.4f shows the failure pattern predicted by the FEA using globally smeared strength  $f$  but different modified modulus  $E'$ . The corresponding failure load predicted in the FEA is  $2.6\text{kN/m}^2$ . Figure 8.4g shows the failure pattern predicted by the FEA using globally smeared modulus  $E$  but different modified strengths  $f$ . The corresponding failure load predicted in the FEA is  $2.0\text{kN/m}^2$ . In the FEA of the above

two cases, cellular automata are used to select and match similar zones between the wall and the base panel SB01

Case Result	Failure Pattern	Failure Load
(a) Global $E$ and $f$		3.0 kN/m <sup>2</sup>
(b) Global $f$ , but 9 $E$ 's		2.6 kN/m <sup>2</sup> (Manual-Selecting Correctors)
(c) Global $E$ , but 9 $f$		2.4 kN/m <sup>2</sup> (Manual-Selecting Correctors)
(d) Experi- mental case		2.6 kN/m <sup>2</sup>
(e) Divided Zones of Wall 1a.		<p>Note: A1, B3, B5, C1 and D1 are the points on the base panel SB01, whose corresponding correctors are applied to improve the FEA of Wall 1a. Control.</p> <p>(Manual-Selecting Correctors)</p>



Case Result	Failure Pattern	Failure Load
(f) 9 $E'$ but Global $f$		2.6 kN/m <sup>2</sup> (CA-Selecting Correctors)
(g) 9 $f'$ but Global $E$		2.0 kN/m <sup>2</sup> (CA-Selecting Correctors)
Note	The result of selecting correctors by the CA method is shown in Appendix C.	

**Figure 8.4** – The FEA and experimental results of Wall 1a.Control

Comparing Figures 8.4d, 8.4f and 8.4g, the FEA result in Figure 8.4f is much better than that in Figure 8.4g. The reason is the same as explained in Section 8.3.1.

### 8.3.3. Wall 2a. Control

Wall 2a. Control (Edgell) in Figure 8.5 is the same as Wall 1a. Control in its material property and size, except that the left edge of this wall is free. The boundaries of the other three edges are same as those of Wall 1a. Control. Figure 8.5d shows the experimental failure pattern and the corresponding failure load was 1.6kN/m<sup>2</sup>.


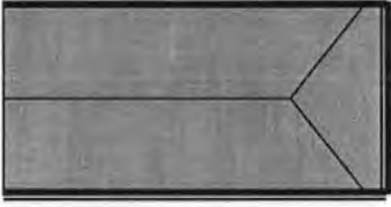
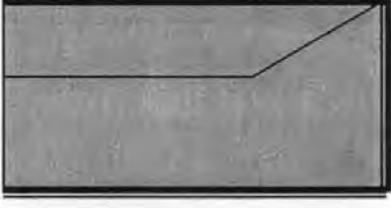
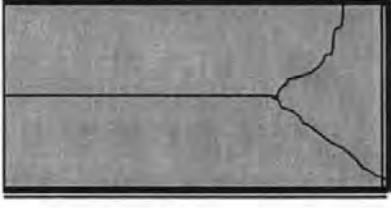
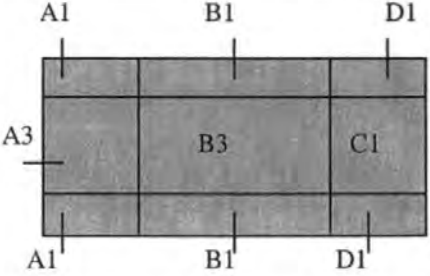
The failure load of 2.2kN/m<sup>2</sup> and the failure pattern predicted by the FEA are shown in Figure 8.5a using conventionally, globally smeared modulus  $E$  and strength  $f$ . The FEA result overestimates the failure load of the wall when compared with the



experimental result and the predicted failure pattern does not correspond to the experimental case.

Figure 8.5e shows the nine zones on the wall. By the manual selection, the similar zones within the base panel SB01 corresponding to these nine zones are Zones A1, A3, B1, B3, C1 and D1. The failure pattern of the wall predicted using globally smeared strength  $f$  but different modified modulus  $E'$  is shown in Figure 8.5b. The corresponding failure load was  $2.0\text{kN/m}^2$ . The predicted failure load was improved when compared with that calculated using conventionally globally smeared modulus  $E$  and strength  $f$  and the predicted failure pattern matches well with the experimental result. The failure pattern of the wall predicted using globally smeared modulus  $E$  but different modified strengths  $f'$  is shown in Figure 8.5c. The corresponding failure load is  $1.8\text{kN/m}^2$ . The predicted failure load is closer to the experimental value, but the predicted failure pattern is not as good as that in Figure 8.5b.

Figure 8.5f shows the failure pattern predicted by the FEA using globally smeared strength  $f$  but different modified modulus  $E'$ . The corresponding failure load is  $2.2\text{kN/m}^2$ . Figure 8.5g shows the failure pattern predicted by the FEA using globally smeared modulus  $E$  but different modified strengths  $f'$ . The corresponding failure load is  $2.0\text{kN/m}^2$ .

The calculation shows that the FEA result using the manual-selecting stiffness correctors is slightly better than that using the CA-selecting stiffness correctors. This is because the manual selection has tried to match similar zones near to boundaries more accurately than can the CA-selection.

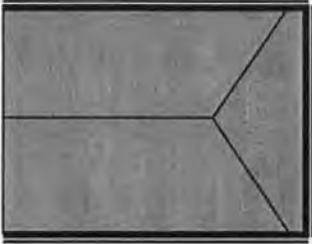
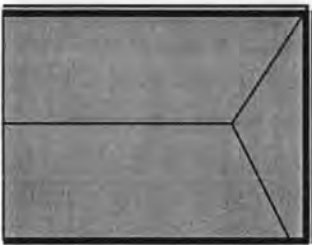
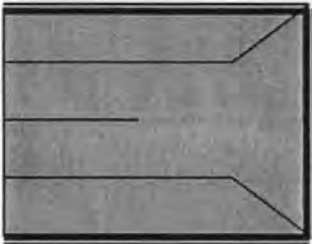
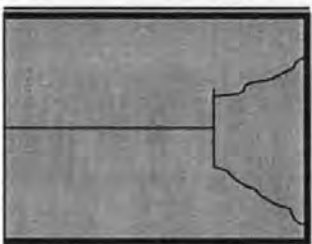
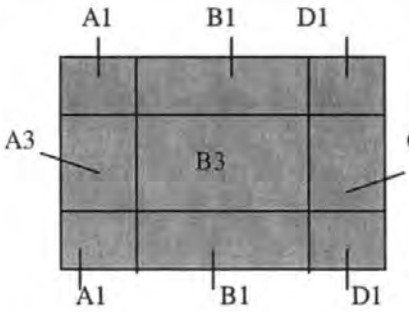
Case Result	Failure Pattern	Failure Load
(a) Global $E$ and $f$		2.2 kN/m <sup>2</sup>
(b) Global $f$ , but 9 $E$ 's		2.0 kN/m <sup>2</sup> (Manual -Selecting Correctors)
(c) Global $E$ , but 9 $f$		1.8 kN/m <sup>2</sup> (Manual -Selecting Correctors)
(d) Experi mental result		1.6 kN/m <sup>2</sup>
(e) Divided Zones of Wall 2 Control.		<p>Note: A1, A3, B1, C1 and D1 are the points on the base panel SB01, whose corresponding correctors are applied to improve the FEA of Wall 2.Control.</p> <p>(Manual-Selecting Correctors)</p>

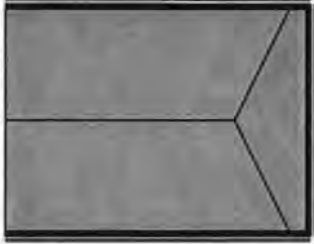

Case Result	Failure Pattern	Failure Load
(f) 9 $E'$ , but Global $f$		2.2 kN/m <sup>2</sup> (CA-Selecting-Correctors)
(g) Global $E$ , but 9 $f_s$		2.0 kN/m <sup>2</sup> (CA-Selecting Correctors)
Note	The result of selecting correctors by the CA method is shown in Appendix C.	

**Figure 8.5** – The FEA and experimental results of Wall 2.Control

#### 8.3.4. Wall Case 7. Control

Wall Case 7. Control (Edgell) in Figure 8.6 is a brick panel with one side free and the other three sides simply-constrained. The size of the wall is 5400mm×4500mm. Figure 8.6d shows the experimental failure pattern of the panel and the corresponding failure load value of 1.5kN/m<sup>2</sup>. The failure pattern predicted by the FEA using conventionally globally smeared stiffness and strength is shown in Figure 8.6a. The corresponding failure load is 1.6kN/m<sup>2</sup>. The FEA result slightly overestimates the failure load of the wall when compared with the experimental case, but the predicted failure pattern is similar to the experimental result.

Case Result	Failure Pattern	Failure Load
(a) Global $E$ and $f$		1.6 kN/m <sup>2</sup>
(b) Global $f$ , but 9 $E$ 's		1.4 kN/m <sup>2</sup> (Manual-Selecting Correctors)
(c) Global $E$ , but 9 $f$		1.6 kN/m <sup>2</sup> (Manual-Selecting Correctors)
(d) Experi- mental case		1.5 kN/m <sup>2</sup>
(e) Divided Zones of Case 7. Control.		<p>Note: A1, A3, B1, C1 and D1 are the points on the base panel SB01, whose corresponding correctors are applied to improve the FEA of Case7.Control</p> <p>(Manual-Selecting Correctors)</p>

Case Result	Failure Pattern	Failure Load
(f) Global $f$ , but 9 $E$ 's		1.4 kN/m <sup>2</sup> (CA-Selecting Correctors)
(g) Global $E$ , but 9 $f$		1.6 kN/m <sup>2</sup> (CA-Selecting Correctors)
Note	The result of selecting correctors by the CA method is shown in Appendix C.	

**Figure 8.6** – The FEA and experimental results of Wall Case 7.Control

Figure 8.6e shows nine zones on the wall. By the manual selection, the similar zones in the base panel SB01 with these nine zones are Zones A1, B1, B3, C1 and D1.

Figure 8.6b shows the failure pattern of the wall predicted using globally smeared strength  $f$  but different modified modulus  $E'$ . The corresponding failure load is 1.4kN/m<sup>2</sup>. The predicted failure load was quite close to the experimental value and the predicted failure pattern was similar to the experimental result.

Figure 8.6c shows the failure pattern of the wall predicted using globally smeared modulus  $E$  but different modified strength  $f'$ . The corresponding failure load is

1.6kN/m<sup>2</sup>. The predicted failure load slightly overestimates the experimental value, but the predicted failure pattern was not as good as that in Figure 8.6b.

Figure 8.6f shows the failure pattern predicted by the FEA using globally smeared strength  $f$  but different modified modulus  $E'$ . The corresponding failure load is 1.4kN/m<sup>2</sup>. Both predicted failure load and failure pattern are quite close to the experimental result.

Figure 8.6g shows the failure pattern predicted by the FEA using globally smeared modulus  $E$  but different modified strengths  $f'$ . The corresponding failure load is 1.6kN/m<sup>2</sup>. The predicted failure load and failure pattern are not as good as those using globally smeared strength  $f$  but different modified modulus  $E'$ . The reason is the same as explained in Section 8.3.1.

### 8.3.5. Wall 1a (ii) with Opening

Wall 1a(ii) with opening (Edgell) is the same as Wall 1a. Control in boundary, size and material property except with central opening size 2800mm×1400mm. For this wall, its FEA results applying correctors are investigated using both the solid panel SB01 and the panel SB02 with opening as the base panel, separately. Correctors from Panel SB01 are listed in Table 5.1. Correctors from Panel SB02 are listed in Table 8.1.

**Table 8.1** – The correctors of Panel SB02 under load  $q = 2.2 \text{ kN/m}^2$

	1	2	3	4	5	6	7	8	9
A	0.55909	0.9006	1.0433	1.0017	0.96026	1.0017	1.0433	0.9006	0.55909
B	0.34293	0.5344	0.6199	0	0	0	0.6199	0.5344	0.34293
C	0.39855	0.6189	0.7024	0	0	0	0.7024	0.6189	0.39855
D	0.26358	0.6836	0.7497	0.6888	0.59486	0.6888	0.7497	0.6836	0.26358

Figure 8.7a shows the FEA result of Wall 1a(ii) using conventionally globally smeared modulus  $E$  and strength  $f$ . When compared with the experimental case of the wall in Figure 8.7d, the failure load was overestimated, but the predicted failure pattern was similar to the experimental result.

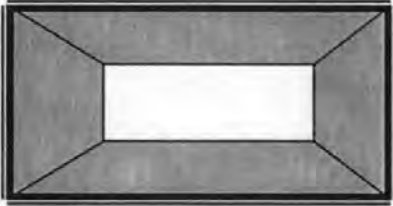
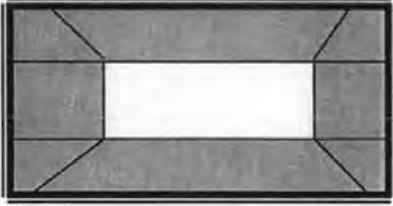
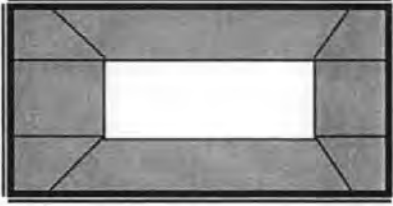
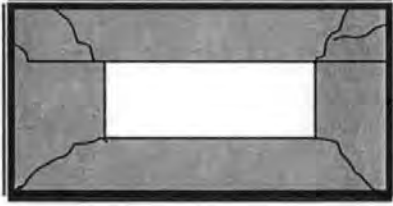
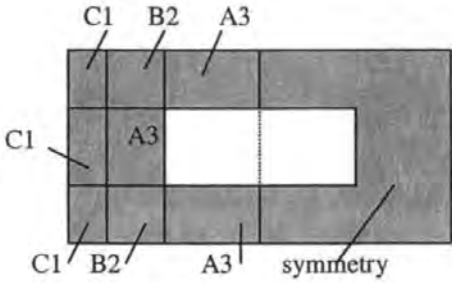
In Figure 8.7e, the divided zones of Wall 1a(ii) match Zones A3, B2 and C1 within the base panel SB01 using the manual-selecting method.

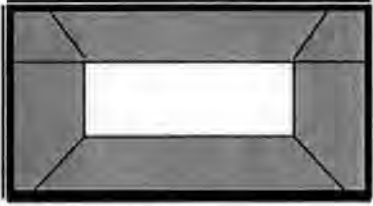
Figure 8.7b shows the failure pattern predicted by the FEA using globally smeared strength  $f$  but different modified modulus  $E'$ . The corresponding failure load was  $1.8\text{kN/m}^2$ . Both predicted failure load and failure pattern were quite close to the experimental result.

Figure 8.7c shows the failure pattern predicted by the FEA using globally smeared modulus  $E$  but different modified strength  $f'$ . The corresponding failure load is  $2.0\text{kN/m}^2$ . Both predicted failure load and failure pattern were quite close to the experimental result.

Figure 8.7f shows the failure pattern predicted by the FEA using globally smeared strength  $f$  but different modified modulus  $E'$ . The corresponding failure load is  $1.8\text{kN/m}^2$ . Both predicted failure load and failure pattern are quite close to the experimental result. The same FEA results were obtained when globally smeared modulus  $E$  but different modified strength  $f'$  were used. The effect of improvement is as good as that taking Panel SB01 as the base panel and manual-selecting correctors from the panel.



Case Result	Failure Pattern	Failure Load
(a) Global $E$ and $f$		2.4 kN/m <sup>2</sup>
(b) Global $f$ , but 9 $E$ 's		1.8 kN/m <sup>2</sup> <b>Manual-Selecting Correctors from SB01</b>
(c) Global $E$ , but 9 $f$		2.0 kN/m <sup>2</sup> <b>Manual-Selecting Corrector from SB01</b>
(d) Experi- mental case		2.0 kN/m <sup>2</sup>
(e) Divided Zones of Wall 1a.		<p>Note: C1, C3, D1, D3 and D5 are the points on the base Panel SB01, whose corresponding correctors are applied to improve the FEA of Wall 1a(ii).</p> <p><b>(Manual- selecting Correctors)</b></p>

Case Result	Failure Pattern	Failure Load
(f) the FEA results		1.8 kN/m <sup>2</sup> (CA-Selecting Correctors From SB02) Global $f$ but 9 $E'$ or Global $E$ but 9 $f'$
Note	The result of selecting correctors by the CA method is shown in Appendix C.	

**Figure 8.7** – The FEA and experimental results of Wall 1a (ii)

### 8.3.6. Wall 2a (i) with Opening

Wall 2a (i) (Edgell) is the same as Wall 2 Control in size, material property and boundary except with central opening 2800mm×1400 mm. The experimental failure load and failure pattern is shown in Figure 8.8d. The FEA result using globally smeared stiffness and strength is shown in Figure 8.8a. In this analytical result, the predicted failure load was overestimated, the failure pattern was in good correlation with the experimental result.

Figure 8.8e shows the zones of Wall 2a(i) and their similar zones A1, A3, B1, C1 and D1 on the base panel SB01 using manual-matching method.

Figure 8.8b shows the failure pattern predicted by the FEA using globally smeared strength  $f$  but different modified modulus  $E'$ . The corresponding failure load is 1.0kN/m<sup>2</sup>. Both predicted failure load and failure pattern are quite close to the experimental result.

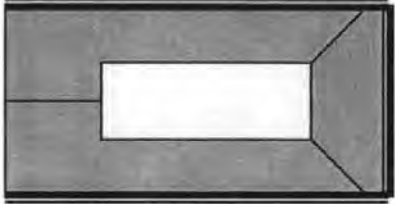
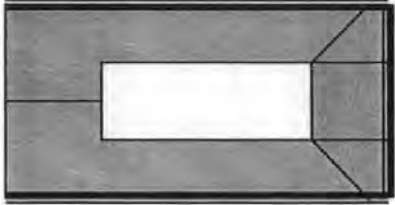
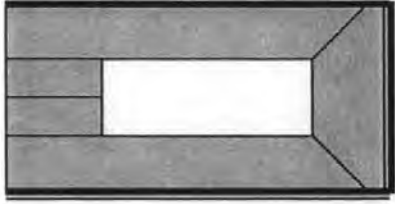
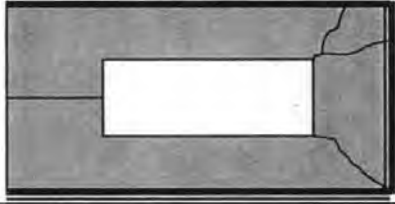
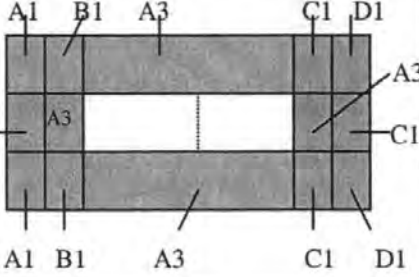
Case Result	Failure Pattern	Failure Load
(a) Global $E$ and $f$		1.2 kN/m <sup>2</sup>
(b) Global $f$ , but 10 $E$ 's		1.0 kN/m <sup>2</sup> (Manual or CA-selecting correctors)
(c) Global $E$ , but 10 $f$		1.2 kN/m <sup>2</sup> (Manual or CA-selecting correctors)
(d) Experi- mental case		0.95 kN/m <sup>2</sup>
(e) Divided Zones of Wall 2a(i)		<p>Note: A1, A3, B1, C1 and D1 are the points on the base panel SB01, whose corresponding correctors are applied to improve the FEA of Wall 2a (i).</p> <p>(Manual-selecting correctors)</p>

Figure 8.8 – The FEA and experimental results of Wall 2a (i)

Figure 8.8c shows the failure pattern predicted by the FEA using globally smeared modulus  $E$  but different modified strength  $f'$ . The corresponding failure load is 1.2 kN/m<sup>2</sup>. Both predicted failure load and failure pattern are close to the experimental result. But the result applying modified strength  $f'$  is not as good as the result applying modified modulus  $E'$ .

### 8.3.7. Panel SB02 with Opening

Panel SB02 (Chong 1993) is the same as the base panel SB01 in size, material property and boundary except with opening. The opening is 2260mm×1125mm in size. The experimental failure load and failure pattern is shown in Figure 8.9d. In this analytical result, the predicted failure load of 1.8kN/m<sup>2</sup> which underestimated the experimental failure load of 2.3 kN/m<sup>2</sup>. However, the predicted failure pattern was in good correlation with the experimental result.

Figure 8.9e shows zones of Panel SB02 and their similar zones A1, A3, A5, B1, B5, C1 and D1 on the base panel SB01 matched using manual-matching method.

Figure 8.9b shows the failure pattern predicted by the FEA using globally smeared strength  $f$  but different modified modulus  $E'$ . The predicted failure pattern was in good correlation with the experimental result. The corresponding predicted failure load is 1.6kN/m<sup>2</sup> which underestimates the experimental failure load.

Figure 8.9c shows the failure pattern predicted by the FEA using globally smeared modulus  $E$  but different modified strength  $f'$ . The corresponding failure load is 1.8 kN/m<sup>2</sup>. Both predicted failure load and failure pattern are the same as those predicted using globally smeared stiffness and strength.

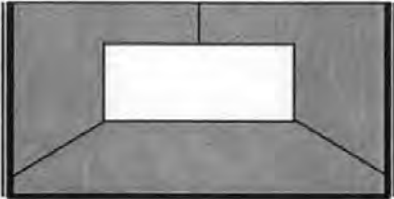
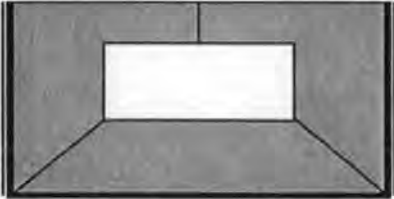
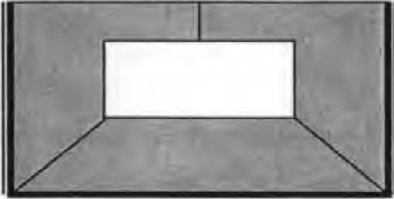
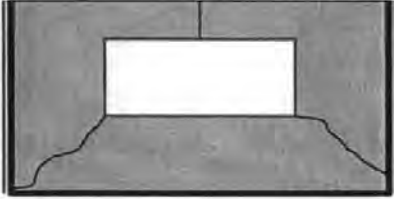
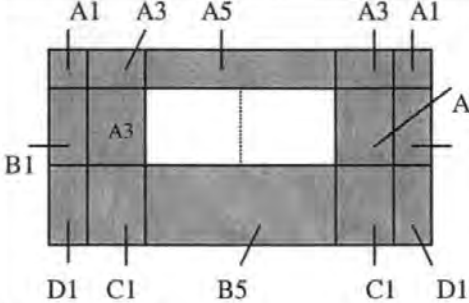
Case Result	Failure Pattern	Failure Load
(a) Global $E$ and $f$		$1.8 \text{ kN/m}^2$
(b) Global $f$ , but $10 E$ 's		$1.6 \text{ kN/m}^2$ (Manual or CA-selecting correctors)
(c) Global $E$ , but $10 f$ '		$1.8 \text{ kN/m}^2$ (Manual or CA-selecting correctors)
(d) Experi- mental case		$2.3 \text{ kN/m}^2$
(e) Divided Zones of SB02		Note: A1, A3, A5, B1, B5, C1 and D1 are the points on the base Panel SB01, whose corresponding correctors are applied to improve B1 the FEA of Panel SB02.  (Manual-selecting correctors)

Figure 8.9 – The FEA and experimental results of Panel SB02

#### 8.4. Homogeneous Technique

In this section, two panels, which have been calculated by the FEA technique using the biaxial stress failure criterion, are used to further verify the validity of correctors

in the FEA technique using homogeneous technique proposed by Lee et al. (1996). In this investigation, correctors are based on the base panel SB01.

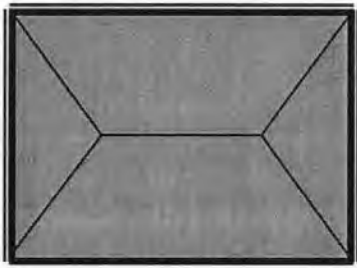
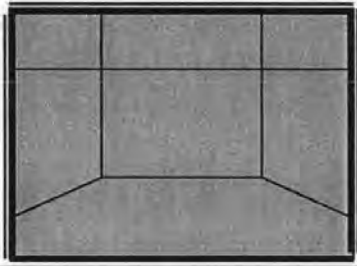
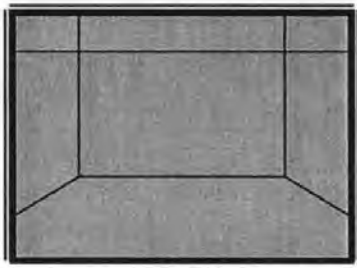
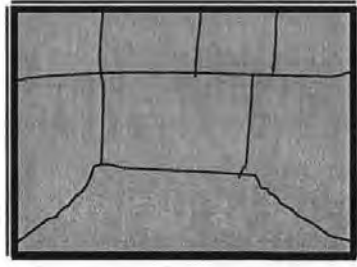
Table 8.2 shows the modified correctors whose original values were produced by the experimental displacements and the corresponding displacements from the FEA using homogeneous technique. Comparing the correctors in Table 5.1 (obtained using the biaxial stress failure criterion) and the modified correctors in Table 8.2, two tables have around 0.1 errors at zones adjacent and close to simply supported and built-in edges. In the following FEA of the three panels, the correctors in Table 8.2 are used to improve the FEA calculation.

**Table 8.2 – The correctors of Panel SB01**

q=2.4kN/m <sup>2</sup>	The FEA using Homogeneous Technique								
Measured Points	1	2	3	4	5	6	7	8	9
A	0.796	0.968	1.32	1.289	1.3	1.289	1.32	0.968	0.796
B	0.624	0.841	0.995	0.965	1	0.965	1.03	0.841	0.624
C	0.8	0.848	0.934	1.002	1.07	1.002	0.934	0.848	0.8
D	0.563	0.76	0.852	1.079	1.04	1.137	0.852	0.76	0.563

#### 8.4.1. Panel SB06

As mentioned in Section 8.2.2, the analysis here just checks the failure pattern of the panel using the corresponding failure load obtained from the FEA using the biaxial stress failure criterion. Figure 8.10a shows that the failure pattern and failure load predicted using globally smeared modulus  $E$  and tensile strength  $f$ . When compared with the experimental failure pattern, as shown in Figure 8.10d, the predicted failure pattern is not very good.

Case Result	Failure Pattern	Lateral Load									
(a) Global $E$ and $f$		11.0kN/m <sup>2</sup>									
(b) Global $f$ , but 9 $E$ 's		7.0 kN/m <sup>2</sup> (Manual or CA-Selecting Correctors)									
(c) Global $E$ , but 9 $f$		7.0 kN/m <sup>2</sup> (Manual or CA-Selecting Correctors)									
(d) Experi- mental case		7.5 kN/m <sup>2</sup>									
(e) Divided Zones of Panel SB06	<table border="1" data-bbox="362 1599 709 1853"> <tbody> <tr> <td>C1</td> <td>B1</td> <td>C1</td> </tr> <tr> <td>B1</td> <td>B3</td> <td>B1</td> </tr> <tr> <td>D1</td> <td>D3</td> <td>D1</td> </tr> </tbody> </table>	C1	B1	C1	B1	B3	B1	D1	D3	D1	<p>Note: B1, B3, C1, D1 and D3 are the points on the base panel SB01, whose corresponding correctors are applied to improve the FEA of Panel SB06.</p> <p>(Manual-Selecting Correctors)</p>
C1	B1	C1									
B1	B3	B1									
D1	D3	D1									

**Figure 8.10** – The failure load and failure pattern of Panel SB06 (the FEA using homogeneous techniques)

Figure 8.10b shows the failure pattern predicted under globally smeared tensile strength  $f$  but the different modified modulus  $E'$ . The corresponding predicted failure load was  $q_m = 7.0\text{kN/m}^2$ . The predicted failure load was quite accurate and the predicted failure pattern was closer to the experimental result.

Figure 8.10c shows the failure pattern predicted by the FEA under globally smeared modulus  $E$  but the different modified tensile strengths  $f'$ . The corresponding predicted failure load was also  $q_m = 7.0\text{kN/m}^2$ . The predicted failure load was quite accurate and the predicted failure pattern was also closer to the experimental result.

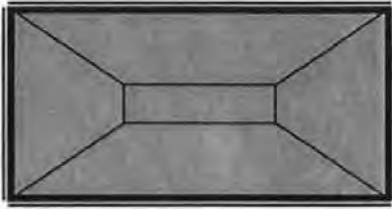

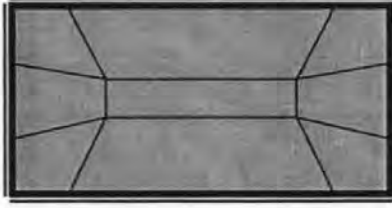

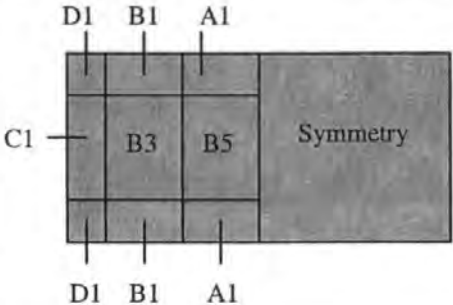
When compared with the result (Figure 8.3) predicted by the FEA using the biaxial stress failure criterion, the result (Figure 8.10) obtained by the FEA using homogeneous technique was slightly better.

#### **8.4.2. Wall 1a. Control**

Figure 8.11a shows that the failure pattern and failure load predicted using globally smeared modulus  $E$  and tensile strength  $f$ . When compared with the experimental failure pattern, as shown in Figure 8.11d, the predicted failure pattern was good. The predicted failure load was also quite close to the experimental failure load.

Figure 8.11b shows the failure pattern predicted under the global tensile strength  $f$  but different modified modulus  $E'$ . The corresponding predicted failure load was  $2.4\text{kN/m}^2$ . The predicted failure load is quite accurate and the predicted failure pattern was much closer to the experimental result.



Case Result	Failure Pattern	Lateral Load
(a) Global $E$ and $f$		2.5 kN/m <sup>2</sup>
(b) Global $E$ , but $9f$ 's		2.4 kN/m <sup>2</sup> (Manual or CA-Selecting Correctors)
(c) Global $f$ , but $9E$ 's		2.4 kN/m <sup>2</sup> (Manual or CA-Selecting Correctors)
(d) Experi- mental case		2.6 kN/m <sup>2</sup>
Divided Zones of Wall 1a.		<p>Note: A1, B3, B5, C1 and D1 are the points on the base panel SB01, whose corresponding correctors are applied to improve the FEA of Wall 1a. Control.</p> <p>(Manual-Selecting Correctors)</p>

**Figure 8.11** – The failure load and failure pattern of Wall 1a. Control (the FEA using homogeneous techniques)

Figure 8.11c shows the failure pattern predicted under globally smeared modulus  $E$  but different modified tensile strength  $f$ . The corresponding predicted failure load

was also  $2.4\text{kN/m}^2$ . The predicted failure load was also quite accurate, but the predicted failure pattern is not as good as that obtained using globally smeared tensile strength  $f$  but different modified modulus  $E'$ .

When compared with the result (Figure 8.4) predicted by the FEA using the biaxial stress failure criterion, the result (Figure 8.11) obtained by the FEA using homogeneous technique is basically same.

### **8.5. Summary**

Application of correctors in the FEA using biaxial stress failure criterion or using homogeneous technique shows:

- (1) Generally, the conventional FEA which uses a globally smeared masonry property overestimates the failure loads, for instance, the average percentage of the overestimated parts of failure loads to the corresponding experimental failure loads was 21% for the seven out of the eight walls. In this investigation, this percentage of 21% was reduced to 3% because of application of correctors in the FEA.
- (2) Prediction of failure patterns for most of the walls (the six out of the eight walls) was improved using correctors.
- (3) The investigation proved that even using a single solid panel (Panel SB01) as the base panel for new panels with and without openings can give reasonable results.
- (4) The CA process can replace the manual process to match similar zones and to select correctors from the base panels for the FEA of new panels. In some cases, this CA method gives slightly better results than the manual method.

(5) The investigation shows that in the FEA using the biaxial stress failure criterion, using the modified flexural rigidity obtained by correctors can give a slightly better result than using the modified tensile strength obtained by correctors. However, in the FEA using homogeneous technique, using the modified tensile strength obtained by correctors can give a slightly better result than using the modified flexural rigidity obtained by correctors

## **9. CONCLUSIONS AND PROPOSALS FOR FUTURE RESEARCH**

### ***9.1. Conclusions***

The research outcome presented in this thesis has shown that boundary constraint is the main factor which greatly affects the behaviour of laterally loaded masonry panels. In the past research, variation in masonry properties at various zones within the panel was related to random factors from nature and workman. In this thesis, the author discovered the structural characteristics of variation in masonry properties. In other words, the variation in masonry properties was governed by boundary conditions of the panel and was related to the positions of various zones within the panel.

By introducing a stiffness/strength corrector, for the first time, this research has quantified the variation in masonry properties at various zones within the panel. Correctors were derived from comparison of the FEA and laboratory experimental results of various points on the panel. Correctors include factors such as natural variation in material properties, geometrical properties and boundary conditions as well as variation in the manufacturing process and the quality of site workmanship and so on. It was found that the values of correctors were closely related to positions of individual nodes/zones within the panel and boundary types governing these zones. It was also shown that zones close to boundaries are more sensitive to changes in masonry properties in comparison to zones away from the boundaries. Thus using the correctors the global flexural rigidity or strength at various zones within the panel was modified at each zone within the panel, based on the laboratory experimental results.

These new masonry properties were then used in non-linear FEA of the masonry panel.

In this study, limited information, based on laboratory test results on full-scale panels, was utilised to derive corrector values. After extensive investigation on the behaviour of masonry panels with and without openings and implementing the CA technique, it became clear that it was possible to use only one panel, SB01 (Chong 1993), as the base panel to derive values of correctors for single wall leaf panels with/without openings and with different boundary conditions. It is worth mentioning that the accuracy of the corrector values depends on the quality of the test data. Unfortunately, current test data available from laboratory tests do not cover a sufficient number of points near to all boundary types. Therefore, more tests would be needed to cover this shortcoming.

This research has also found that regions with similar corrector distribution are mainly governed by similar boundary conditions. Based on this finding, zones with the same corrector value and adjacent to the similar boundary conditions were called similar zones. Based on the definition of zone similarity, appropriate rules for matching zone similarity within panels were introduced. The proposed rules for matching similar zones between panels were used to match similar zones between a base panel and a new panel, to select correctors from the base panel for the FEA of the new panel. At first a manual operation method was proposed for matching similar zones, but it was found that this method was not easy to use because it needed an in-depth understanding on how to divide the panel into zones to correctly reflect the boundary effect on the zone. Thus in this thesis, an automatic technique for dividing the panel

into zones, matching similar zones between a base panel and a new panel and selecting the corresponding correctors for the FEA of the new panel was developed using cellular automata (CA) technique.

The CA model introduced in the thesis and the results of a comprehensive studies show that it was capable of correctly propagating the effect of all boundaries into the various zones within the panel. The CA method uses the behaviour of the surrounding zones to calculate the value of the corrector for any particular zone. A number of rules were proposed for matching similar zones using the “state values” of zones and their neighbouring zones. The rules include that state values of a zone and its four neighbourhood zones on the new panel are respectively compared with state values of every zone and its four neighbourhood zones on the base panel, together with consideration on orientations of similar regions on the new panel and the base panel. This information was used to locate similar zones on the base panel that correspond to zones on a new panel.

The results of extensive parametric study proved that the CA method, introduced in this thesis, was able to effectively match similar zones between new panels and the base panel using the following parameter values: transition efficient  $\eta$  of 0.2, initial state values for the free boundary type of 0.0, the simply-supported boundary type of 0.2 and the built-in boundary type of 0.4.

The application of correctors to the FEA techniques for masonry greatly improved the predicted results of both failure load and failure pattern of the panel. For the FEA technique using the biaxial stress failure criterion, applying the modified flexural

rigidity  $D'$  in every zone within the panel gave much better predicted results than applying the modified tensile strength  $f'$  in corresponding zones. However, for the FEA technique using the homogeneous technique, applying the modified tensile strength  $f'$  in corresponding zones can give a better prediction than applying the modified flexural rigidity  $D'$  in corresponding zones. In any case, both methods showed an improvement in the FEA results. The FEA results of the eight panels show that dividing the panel into nine to twelve zones can usually provide the accurate prediction results.

From the FEA results of eight typical brick panels, analysed in this thesis, it was discovered that by using correctors an average improvement of 18% in the prediction of failure loads was achieved. If the better test data on the panels with measuring points close to boundaries was available, the accuracy of the results would have been further improved.

In conclusion, it can be claimed that using corrector factors more accurately models true behaviour of masonry panels and reflects the effect of panel boundaries more realistically. Using corrector values to modify masonry properties, a much better prediction of failure load and failure pattern of the panel is achieved, and the predicted results, especially in the range of the normal working-load of  $1.5 \text{ kN/m}^2$ , are also much closer to their experimental results.

## **9.2. Proposals for Future Research**

There are many areas that need further investigation in order to develop methodologies identified in this thesis. The research in this thesis was only focused on the analysis of single leaf brick panels. To generalise these methodologies, it would

be necessary to extend this research to cavity walls and walls made of concrete blocks. The use of correctors should also be extended to reinforced brick masonry panels.

Although the experiment of using Panel SB01 provides useful information on deriving correctors which have greatly improved the FEA results of the typical single leaf brick panels, experimental data on other typical full-scale masonry panels with different boundary conditions and sizes is needed to obtain more reliable and accurate data for the improvement of corrector values. New experiments should include data for all typical zones in the panel, particularly those close to boundaries of the panel which have not been measured in the past.

The application of correctors to the existing FEA techniques for masonry needs to be further developed to include variation in masonry material in both flexural rigidity and strength, because variation in masonry material in fact coexists with stiffness and strength.

The CA methods used to match similar zones between panels need to be further verified and developed to further investigate the effect of the transition function for boundary effect, "state values" of zones and the accuracy of the rules for matching similarity between zones in the panel.

A combination of cellular automata with neural networks seems to be able to create a simulative experimental environment for masonry panels to replace some expensive masonry experiments, based on the FEA results using correctors. This simulative



experimental environment should be able to predict both failure load and failure pattern with consideration of variation in masonry properties at various zones within the panel. All the important factors relevant to variation in masonry properties should be included in this simulative experiment environment.

The further study for application of correctors should be extended to other load types such as in-plane vertical or lateral load as well as other masonry structures such as masonry arches popular both in the UK and in the world.

The method for applying correctors to the FEA should be extended to panels constructed using other masonry materials, because correctors are different for the base panels built with different masonry materials.

In this thesis, correctors were derived from ratios between the experimental displacements and the corresponding FEA displacements. It would be useful if this technique is extended to use of other properties such as tensile stress/strain.

The development of an integrated software package with a powerful front end interface and a powerful graphic interface would greatly enhanced a better understanding of the panel behaviour.

## References

- Anderson, C. (1984). Transverse Laterally Loaded Tests on Single Leaf and Cavity Walls. *CIB Third International Symposium on Wall Structures*. Warsaw.
- Anderson, C. (1985a). Tests on Walls subjected to Uniform Lateral Loading and Edge Loading. In: McNeilly, T. and Screveiner, J.C., ed. *7th IBMaC.*, Melbourne, BDRI.
- Anderson, C. (1985b). *Tests on Treasure Laterally Loaded Masonry Walls*. Int. Reports/053, South Bank Polytechnic, London.
- Anderson, C. (1987). Lateral Strength From Full-Sized Tests Related to the Flexural Properties of Masonry. *Masonry International*, Vol. 1, No. 2.
- Baker, L.R. (1972). Brickwork Panels subject to Face Wind Loads. Thesis (M. Eng. Sc.). University of Melbourne.
- Baker, L.R. (1973). Structural Action of Brickwork Panels subject to Wind Loads. *Journal Australian Ceramic Society*, Vol. 9, No. 1.
- Baker, L.R. (1980). Lateral Loading of Masonry Panels. *Structural Design of Masonry*, Cement and Concrete Association of Australia, Sydney.
- Baker, L.R. (1982a). An Elastic Principal Stress Theory for Brickwork Panels in Flexure. *Proc. 6th IBMaC*, Rome.
- Baker, L.R. (1982b). A Principal Stress Failure Criterion for Brickwork in Bi-Axial Bending. *Proc. 6th IBMaC*, Rome.
- Brinker, R. (1984). Yield-Line Theory and Materials Properties of Laterally Loaded Masonry Walls. *Masonry Inst.*, No. 1.
- BSI, British Standards Institution. (1970). *CP111; Part 1. Code of Practice for Structural Use of Masonry, Part 1*. London.
- BSI, British Standards Institution. (1970). *CP111; Part 2. Loading: Wind Loads. C.P. 3: Chapter V: Part 2*. London.
- BSI, British Standards Institution (1985). *BS 5268: Part 1. Code of Practice for use of Masonry. Part 1. Structural Use of Unreinforced Masonry*. UK.
- Brooks, J.J. and AbuBaber, B.H. (1998). The Modulus of Elasticity of Masonry. *Masonry International*, Vol. 12, No.2, 58-63.

- Cajdert, A. and Losberg, A. (1976). Lateral Strength of Reinforced Brick Walls.-Design for Wind Loads. *Proc. 4th IBMaC*, Bruques.
- Cajdert, A. (1980). Laterally Loaded Masonry Walls. *Publication 80:5*, Chalmers University of Technology, Goteborg.
- Candy, C.C.E. (1983). The Energy Line Method for Predicting Ultimate Lateral Pressure on Masonry Wall Panels. *Proc. 8th, IBMaC*, Ireland.
- Cheng R. (1996). *Design load tables for laterally loaded masonry panels TO BS 5628 1 AND 2*. Thomas Telford Publishing.
- Chong, V. L. (1993). *The Behaviour of Laterally Loaded Masonry Panels with Openings*. Thesis (Ph.D). University of Plymouth, UK.
- Davey, N. and Thomas, F.G. (1950). The Structural Uses of Brickwork. *Structural and Building Paper, Inst. of Civil Engineering*, No. 24.
- de Vekey, R.C. (1992). Current Masonry Research and Development at BRE. *Masonry International*, Vol. 5, No. 3.
- Duarte, R. B. (1998). The Design of Unreinforced Brickwork Panels with Openings under Lateral Pressure. *Masonry International*, Vol. 11, No. 3.
- Edgell G. *The experimental results of laterally loaded masonry wall panels*. CERAM Building Technology.
- Edward, R. (1989). *Exploring the geometry of nature – computer modeling of chaos, fractal, cellular automata and neural networks*. Blue Ridge Summit, PA: Windcrest Books.
- Eissler, W. et al. (1992). Cellular automata simulation of flow around chains of cylinders. *International Journal for Numerical Methods in Engineering*, 34, 773-791.
- Essawy, A.S., Drysdale, R.G. and Mirza, F.A. (1985). Nonlinear microscopic finite element model for masonry walls. *Proc. of New Analysis Techniques for Structural Masonry, ASCE Structures Congress' 85*, Chicago, Illinois, 19-45.
- Fishburn, C.C. (1961). Effect of Mortar Properties on Strength of Masonry. *National Bureau of Standards*, Monograph 36, Washington.
- Fried, A.N. (1989). *Laterally Loaded Masonry Panels-The Significance of Analytical Methods and Material Properties*. Thesis (Ph.D), South Bank Polytechnic, London.
- Gairns, D.A. (1983). *Flexural Behaviour of Concrete Blockwork Panels*. Master of Building Science Thesis, University of Melbourne, Victoria, Australia.

Ghali A. and Neville, A.M. (1997). *Structural Analysis*. London SE1, 8HN, UK. Published by E & FN Spon, an imprint of Thomson Professional.

Goles, Eric and Mari'nez, Sevet. (1990). *Neural and Automata Networks: Dynamical Behavior and Applications*. Boston, Kluwer Academic Publishers.

Grenley, D.G., Cattaneo, L.E. and Pfrang, E.O. (1969). *Effect of Edge Load on Flexural Strength of Clay Masonry Systems Utilizing Improved Mortars*. 'Designing, Engineering and Constructing with Masonry Products'. F.B. Johnson. Houston, Texas, Gulf Publishing.

Halpern, P. (1989). Sticks and stones: a guide to structurally dynamic cellular automata. *American Journal of Physics Teachers*, 57 (5).

Haseltine, B.A. and Hodgkinson, H.R. (1973). Wind Effects on Brick Panel Walls-Design Information. *Proc. 3rd IBMac*, Essen.

Haseltine. B.A. and West, H.W.H. (1976). *Design of laterally Loaded Wall Panels: Part 2*. Technical Note, No. 248, The British Ceramic Research Association.

Hedstorm, R.O. (1961). Load Tests of Patterned Concrete Masonry Walls. *Journal of the A.C.I.*, Proceedings Vol. 57, No. 10.

Hendry, A.W. (1973). The Lateral Strength of Unreinforced Brickwork. *The Structural Engineer*, Vol. 51, No. 2.

Hendry, A.W. and Kheir, A.M.A. (1976). The Lateral Strength of Certain Brickwork Panels. *Proc. 4th IBMaC*, Bruques.

Hendry, A. W. (1996). Masonry Research in the UK 1960-95. *Masonry International*, Vol 9, No 3, 71-74.

Hendry, A.W. (1997). The Future of Masonry Research in the UK. *Masonry International*, Vol. 10, No. 3.

Hendry A.W., Sinha B. P. and Dacies, S. R. (1997). *Design of Masonry Structures*. E & FN SPON, An Imprint of Chapman & Hall.

Hendry A. W. (1998). *Structural Masonry*. Second Edition, MACNILLAN PRESS LTD.

James, J. A. (1978). *An Investigation of the lateral Load Resistance of Walls of Unreinforced Brickwork without Precompression*. Report W/LAT/1, Building Development Laboratories, Perth.

Lawrence, S. J. (1980). *Design of Masonry Panels for Lateral Loading. Some Interim Recommendations*. Technical Record No. 460, Experimental Building Station, Chatswood, NSW.

Lawrence, S. J. (1983). *Behaviour of Brick Masonry Walls under Lateral Loading. Vols 1 and 2*. Thesis (Ph.D), University of New South Wales, UK.

Lawrence, S. J. and Lu, J. P. (1991). An Elastic Analysis of Laterally Loaded Masonry Walls with Openings. *International Symposium on Computer Methods in Structural Masonry*, 39-48, Swansea, UK.

Lawrence, S. J. (1994). Out-of-Plane Lateral Load Resistance of Clay Brick Panels. *Australia Structural Engineering Conference*, Sydney, Australia.

Lawrence, S. J. (1995). The Behaviour of Masonry in Horizontal Flexure. *Seventh Canadian Masonry Symposium*. Canada.

Lawrence, S. J. and Marshall, R. J. (1998). The New AS3700 Approach to Lateral Load Design. *5th Australia Masonry Conference*, Gladstone, Queensland, Australia.

Lee, J. S., Pande, G. N., Middleton, J. and Kralj. (1996). Numerical Modelling of Brick Masonry Panels Subject to Lateral Loadings. *Computer and Structures*, Vol. 61, No. 4, 735-745.

Losberg, A. and Johansson, S. (1964). Sideway Pressure on Masonry Walls of Brickwork. *CIB Symp. on Loadbearing Walls*, Warsaw.

Ma, S. Y. A. and May, I. M. (1984). *Masonry Panels under Lateral Loads*. Report No. 3. Dept of Engineering, University of Warwick.

Mathew A., Kumar B., Sinha B. P. and Pedreschi R. F. (1999). Analysis of Masonry Panel under Biaxial Bending Using ANNs and CBR. *Journal of Computing in Civil Engineering*, 170-177.

May, I.M. and Ma, S.Y.A. (1986). Design of Masonry Panels under Lateral Load. *Proc. Brit. Mas. Soc., 1st Int. Mas. Conf.*, 118-120.

Moffatt, K. R. and Lim, P. T. K. (1976). Finite element analysis of composite box girder bridge having complete or incomplete interaction. *Proc. Inst. Civil Eng. Part 2*, Vol. 61, 1-22.

Monk, C. B. and Allen, M. H. (1967). *Compressive, Transverse and Racking Strength Tests of 4-in. Structural Clay Facing Tile Walls. Res. Rep. 11, 1967*. Structural Clay Products Research Foundation.

Pietruszczak, S. and Niu, X. (1993). On the description of localized deformation. *Int. J. Numer. Anal. Mech. Geomech.* 17, 791-805.

Plumer, H. C. and Blume, J. A. (1953). *Reinforced Brick Masonry and Lateral Force Design*. Structural Clay Products Institute, 131, Washington.

Plummer, H. C. (1962). *Brick and Tile Engineering*. Structural Clay Products Institute, Washington.

Rots, J. G. (1997). *Structural Masonry. An Experimental/ Numerical Basis for Practical Design Rules*. Netherlands. A. A. BALKEMA/ROTTERDAM/BROOKFIELD/1997.

Rucker, Rudy. (1989). *CA Lab (Exploring Cellular Automata) – Rudy Rucker's Cellular Automata Laboratory*. Autodesk Inc., Sausalito, CA.

Samarasinghe, W., Page, A. W. and Hendry A. W. (1983). A finite element model for the inplane behaviour of brickwork. *Proc. Inst. Civ. Engrs. Part 2*, vol 73.

Shin. H. S. (1999). *STRUMAS for the analysis of structural masonry* [software]. Department of Civil Engineering, University of Swansea.

Sinha, B. P. (1978). A Simplified Ultimate Load Analysis of Laterally Loaded Model Brickwork Panels of Low Tensile Strength. *The Structural Engineer*, Vol. 56B, No. 4.

Soschinske, K. A. (1997). *Cellular Automata Simulation of Resin Flow Through a Fiber Reinforcement*. UMI Dissertation Service.

SAA, Standards Association of Australia. (1969). *S.A.A. Brickwork Code*. CA 47-1969.

Structural Clay Products Institute. (1969). *Building Code Requirements for Engineered Brick Masonry*. S.C.P.I.

Tellett, J. (1984). Pocket-type reinforced brickwork retaining walls. Thesis (Ph.D). Uni. of Bradford, Apr01.

Thomas, F. G. (1953). The Strength of Brickwork. *The Structural Engineer*, Vol. 31, No. 2.

West, H. W. H., Hodgkinson, H. R. and Webb, W. F. (1971). *The Resistance of Clay Brick Walls to Lateral Loading*. Technical Note, No. 176, The British Ceramic Research Association.

West, H. W. H., Hodgkinson, H. R. and Webb, W. F. (1973). Lateral Loading Tests on Walls with different Boundary Conditions. *Proc. 3rd IBMac*, Essen.

West, H. W. H., Hodgkinson, H. R. and Webb, W. F. (1974). *The Resistance of Clay Brick Walls to Lateral Loading, Part 2*. Technical Note, No. 226, The British Ceramic Research Association.

West, H. W. H., Hodgkinson, H. R. and Haseltine, B. A. (1975). *Design of lateral Loaded Wall Panels*. Technical Note, No. 242, The British Ceramic Research Association.

West, H. W. H. (1976). *The Flexural Strength of Clay Masonry Determined from Wallettes Specimens*. Technical Note, No. 247, The British Ceramic Research Association.

West, H. W. H., Hodgkinson, H. R. and Haseltine, B. A. (1979a). The Lateral Resistance of Walls with one Free Vertical Edge. *Vth IBMaC*, Washington.

West, H. W. H., Hodgkinson, H. R., Goodwin, J. F. and Haseltine, B. A. (1979b). The Resistance to Lateral Loads of Walls Built of Calcium Silicate Bricks. *Vth IBMaC*, Washington.

West, H. W. H. (1998). The Development of Masonry. *Masonry International*, Vol. 11, No. 3.

Zienkiewicz, O. C. (1982). *The Finite Element Method*. Third Edition, McGRAW-HILL Book Company (UK) Limited.

## APPENDIX A: THE CORRECTOR DATA AND LOAD-CORRECTOR DIAGRAMS DERIVED FROM THE BASE PANEL SB01

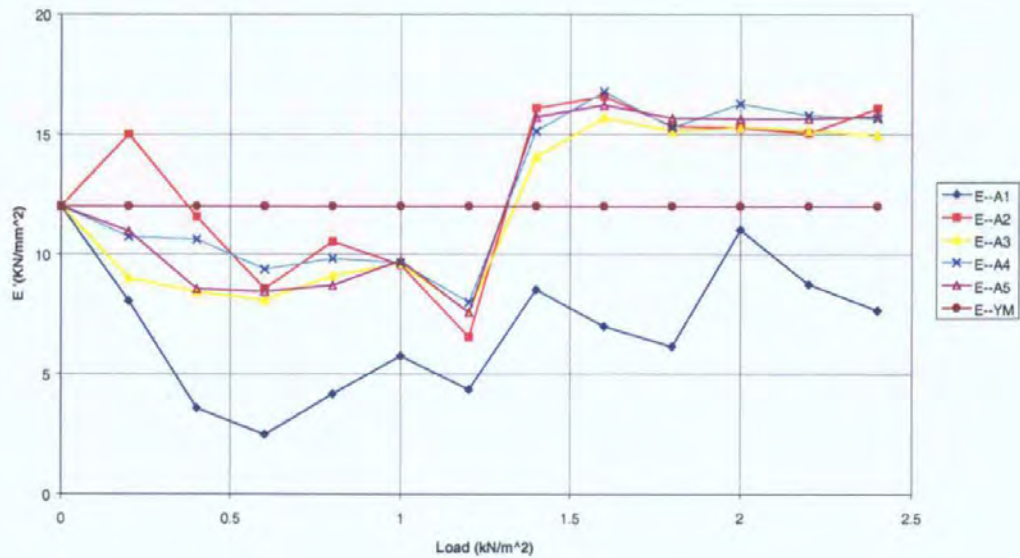
Correctors of the Base panel SB01 at individual load increments and individual zones around the measured points on the panel.									
Load	D1-SP	D2-SP	D3-SP	D4-SP	D5-SP	D6-SP	D7-SP	D8-SP	D9-SP
0.2	-0.01	-0.09	0.29	1.18	0.34	0.45	0.20	0.43	0.05
0.4	-0.17	-4.78	0.27	0.57	0.46	0.28	0.81	0.64	0.09
0.6	0.08	0.62	0.29	1.05	0.40	0.50	0.93	0.45	0.20
0.8	-1.33	-0.53	0.42	1.22	0.55	0.92	0.39	0.52	0.27
1	-0.10	1.84	0.59	1.10	0.88	0.80	0.68	0.63	0.20
1.2	-0.13	0.51	0.54	1.05	0.75	0.61	0.59	0.48	0.10
1.4	-0.31	9.13	0.88	1.19	2.38	1.18	1.09	0.89	0.51
1.6	1.15	8.73	0.97	1.99	1.78	1.30	1.62	0.76	0.86
1.8	0.44	2.78	1.01	1.20	1.59	1.29	1.43	0.66	0.26
2	0.42	1.31	0.78	1.04	1.07	1.19	0.51	0.28	0.23
2.2	0.35	0.83	0.97	1.08	1.19	1.04	1.12	0.81	0.09
2.4	0.55	2.44	0.99	1.31	1.29	1.38	0.60	0.34	0.37
Load	C1-SP	C2-SP	C3-SP	C4-SP	C5-SP	C6-SP	C7-SP	C8-SP	C9-SP
0.2	-0.03	-0.25	0.31	0.82	5.83	0.30	0.36	0.13	0.19
0.4	2.25	5.45	0.37	0.69	0.58	0.55	0.27	0.22	0.23
0.6	0.11	0.58	0.36	0.60	0.46	0.50	0.62	0.23	0.15
0.8	0.90	4.67	0.50	0.77	0.58	0.55	0.52	0.33	0.20
1	-0.43	0.73	0.60	0.73	0.67	0.55	0.64	0.35	5.64
1.2	-1.96	0.47	0.58	0.78	0.69	0.57	0.63	0.37	0.10
1.4	-7.67	2.02	0.92	1.15	1.48	1.01	1.10	0.66	0.33
1.6	0.55	1.53	0.98	1.37	1.18	1.01	1.21	0.57	0.40
1.8	0.36	1.25	0.97	1.09	1.21	1.00	1.13	0.60	0.27
2	3.94	1.24	0.98	1.28	1.15	1.14	1.10	0.81	0.35
2.2	0.00	1.01	1.02	1.07	1.12	1.05	1.08	0.75	0.39
2.4	0.72	1.39	0.99	1.15	1.26	1.13	1.16	0.79	0.67
Load	B1-SP	B2-SP	B3-SP	B4-SP	B5-SP	B6-SP	B7-SP	B8-SP	B9-SP
0.2	-0.08	-7.00	0.43	0.54	1.10	0.34	0.29	0.12	0.10
0.4	0.21	0.74	0.42	0.58	0.52	0.39	0.48	0.20	0.27
0.6	0.12	0.51	0.41	0.60	0.47	0.49	0.48	0.24	0.09
0.8	0.27	0.72	0.51	0.62	0.54	0.56	0.47	0.30	0.14
1	0.68	0.55	0.57	0.61	0.63	0.54	0.51	0.61	0.31
1.2	0.52	0.49	0.60	0.68	0.64	0.57	0.57	0.37	0.09
1.4	1.00	1.18	0.91	1.04	1.19	0.95	0.94	0.62	0.28
1.6	0.40	1.01	0.90	1.09	1.05	0.91	0.95	0.59	0.31
1.8	0.32	0.94	0.91	0.98	1.03	0.91	0.90	0.58	0.24
2	0.85	0.96	0.93	1.05	1.02	1.02	0.95	0.71	0.32
2.2	0.84	0.91	0.97	1.01	1.02	0.96	0.97	0.70	0.35
2.4	0.57	1.09	0.97	1.06	1.09	1.02	1.00	0.73	0.51
Load	A1-SP	A2-SP	A3-SP	A4-SP	A5-SP	A6-SP	A7-SP	A8-SP	A9-SP
0.2	-0.67	4.93	0.75	0.89	0.91	0.53	0.49	0.14	0.12
0.4	0.30	0.96	0.70	0.88	0.71	0.59	0.66	0.23	0.19
0.6	0.21	0.71	0.67	0.78	0.70	0.70	0.66	0.26	0.13
0.8	0.35	0.88	0.76	0.82	0.72	0.76	0.67	0.34	0.17
1	0.48	0.80	0.80	0.80	0.81	0.74	0.70	0.38	0.23
1.2	0.49	0.74	0.86	0.91	0.86	0.81	0.77	0.44	0.17
1.4	0.77	1.45	1.27	1.37	1.42	1.26	1.22	0.72	0.31
1.6	0.55	1.31	1.23	1.32	1.28	1.21	1.19	0.70	0.33
1.8	0.51	1.27	1.25	1.27	1.30	1.20	1.16	0.71	0.28



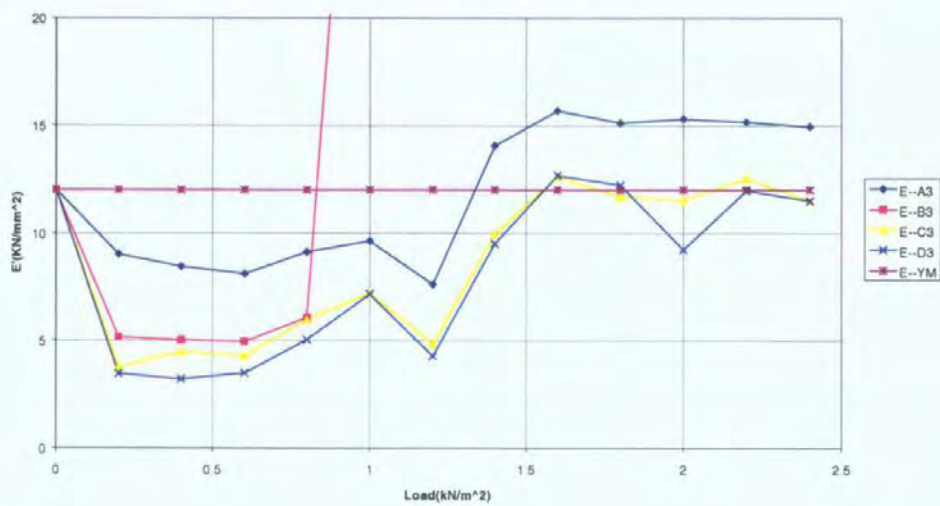
2	0.93	1.29	1.29	1.37	1.32	1.31	1.22	0.81	0.33
2.2	0.72	1.23	1.24	1.29	1.28	1.24	1.19	0.80	0.33
2.4	0.66	1.38	1.28	1.34	1.35	1.30	1.23	0.84	0.39

### E'-Load Curves

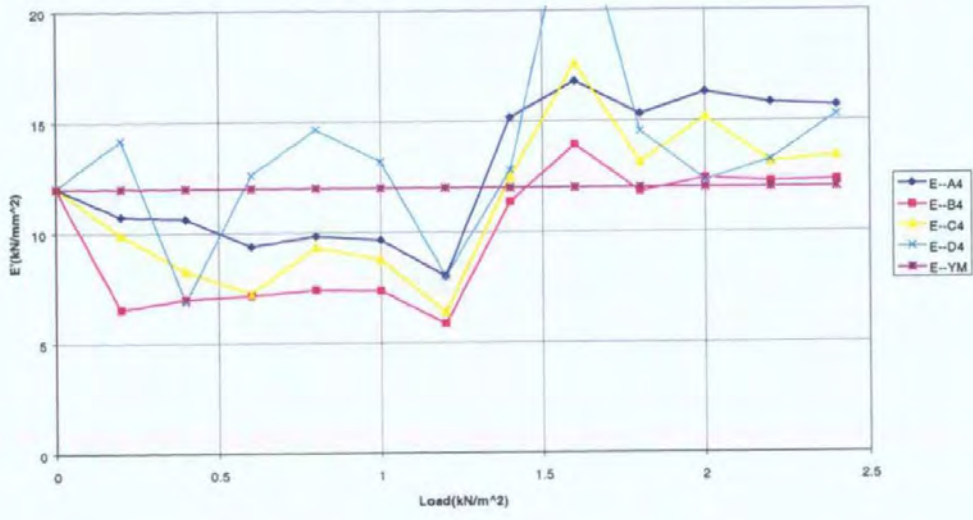
E'-Load curves of Points A1-A5



E'-Load curves of Points A3-D3

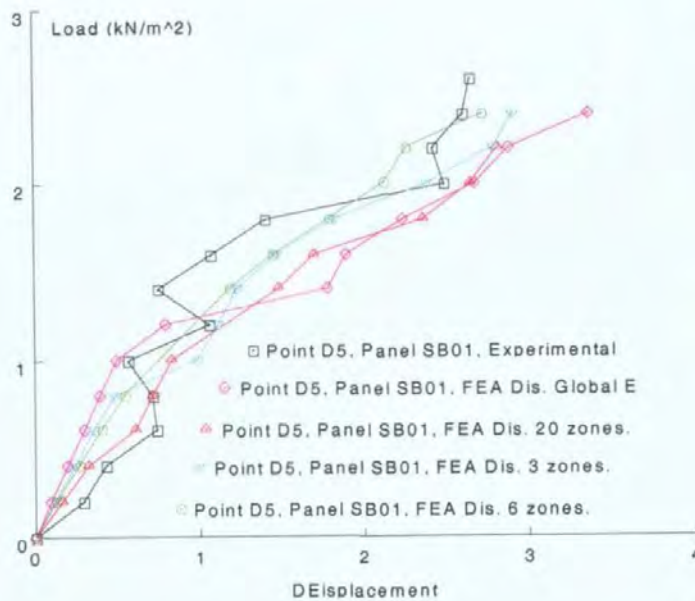
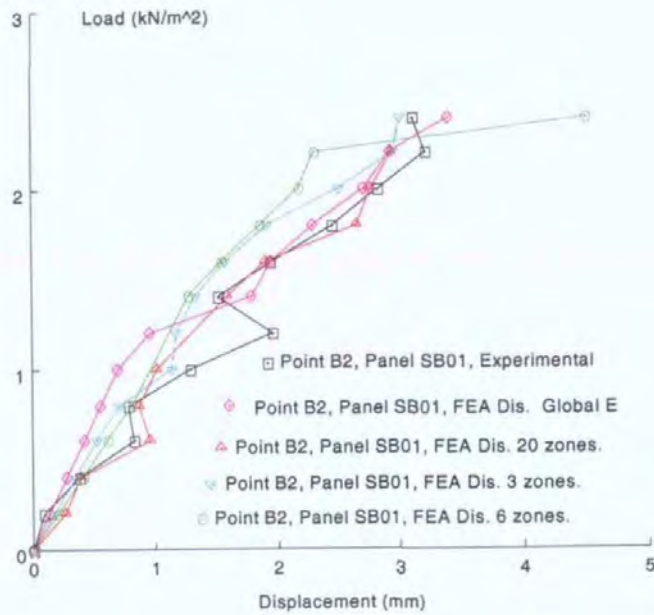


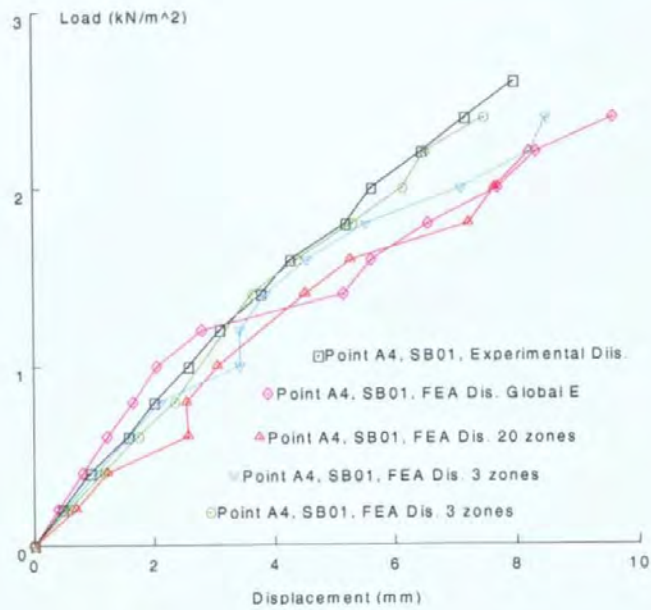
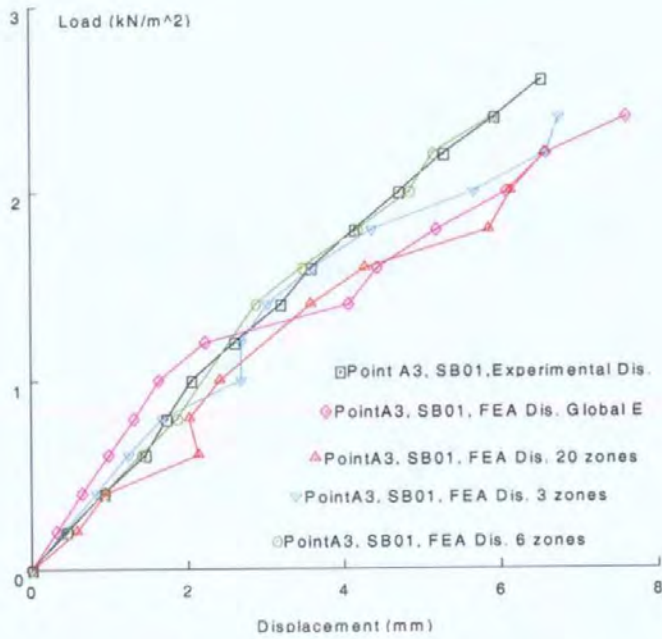
E'-Load curves of Points A4-D4

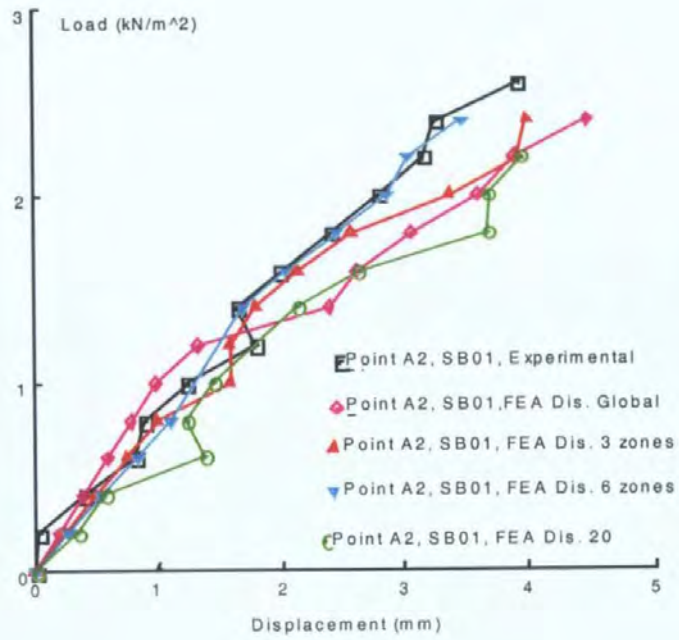
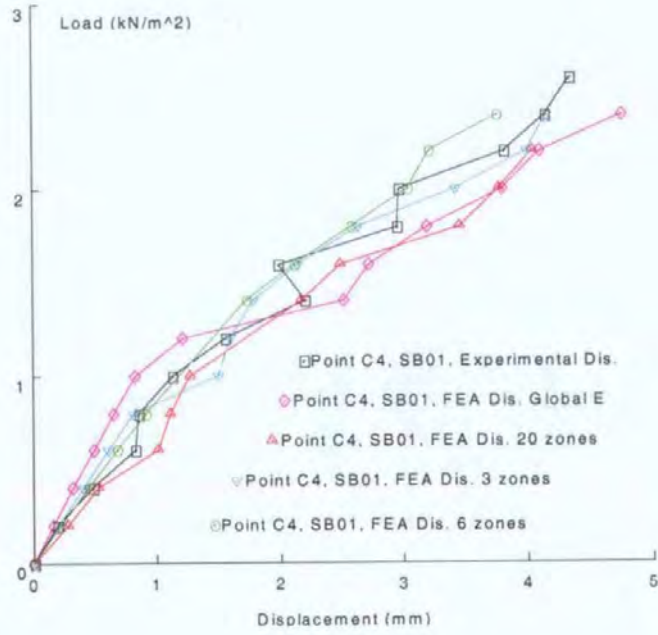


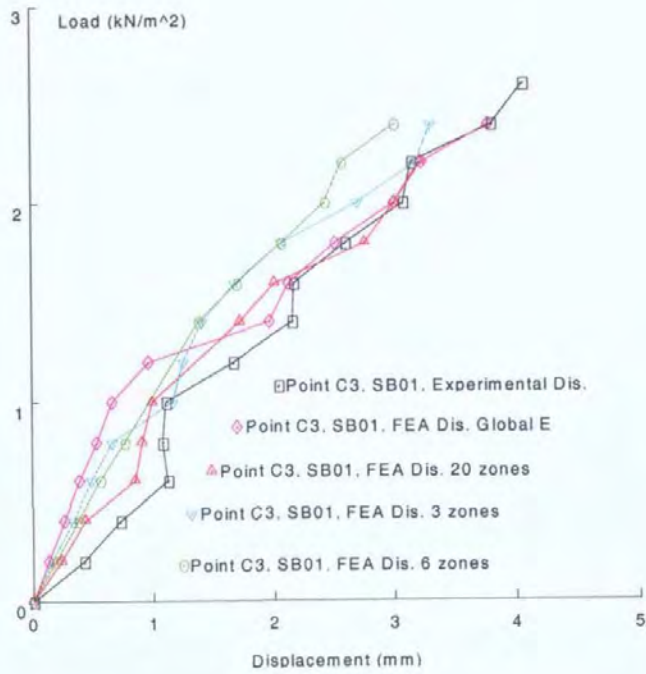
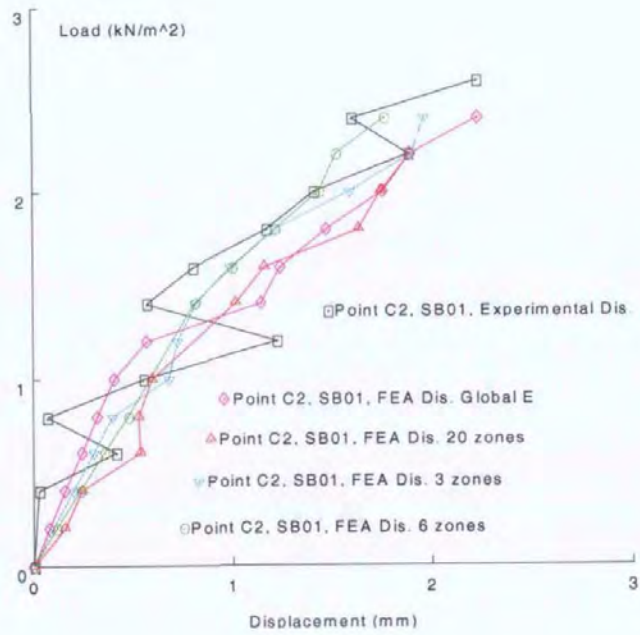
## APPENDIX B: LOAD-DISPLACEMENT CURVES

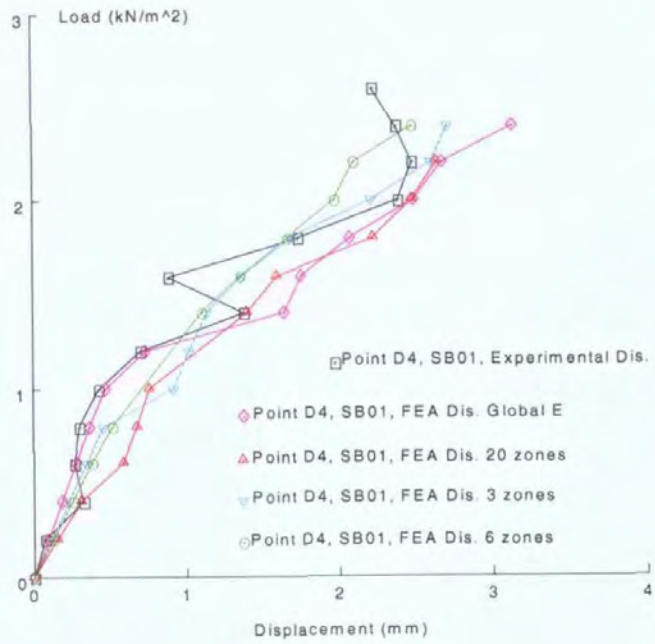
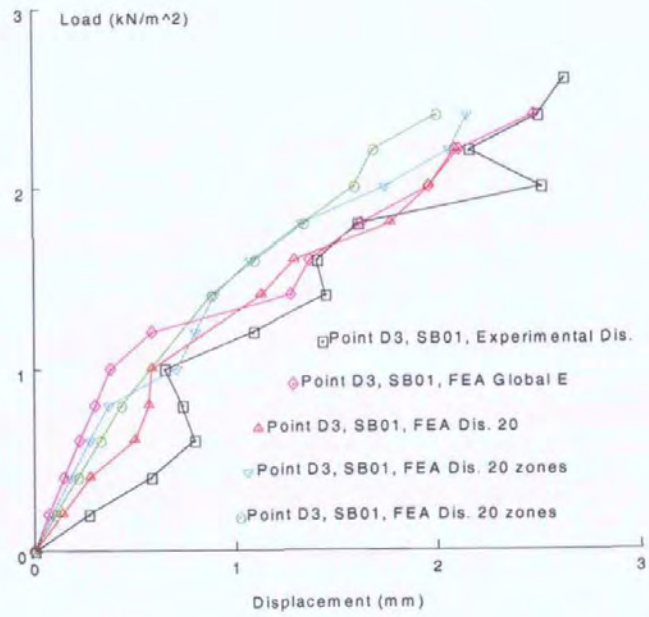
### The FEA Displacement Curves Using Correctors

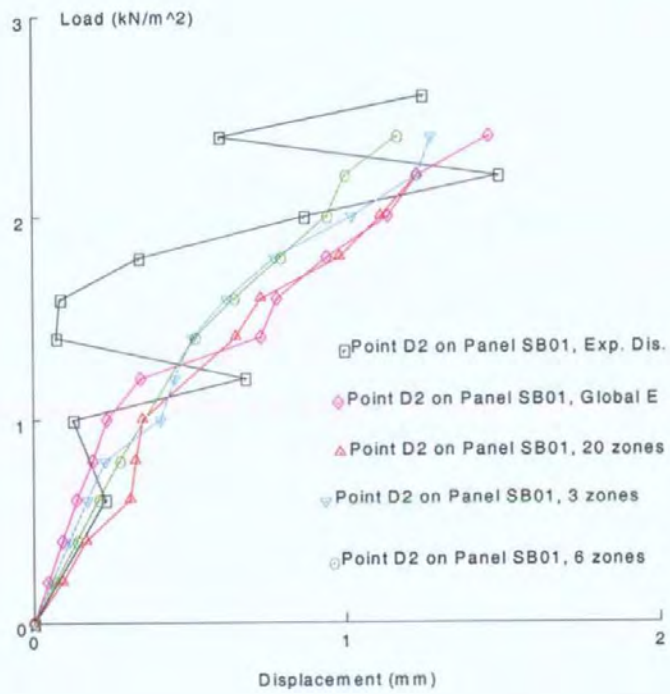








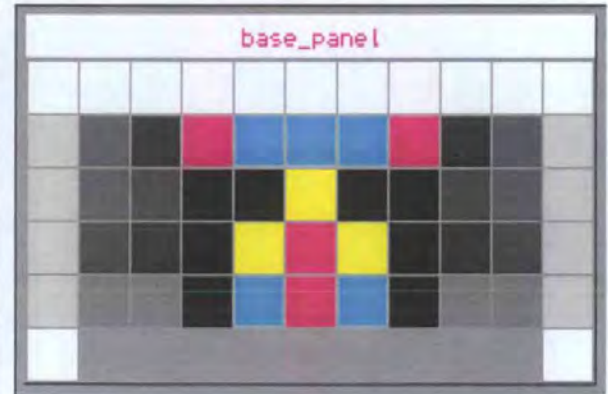
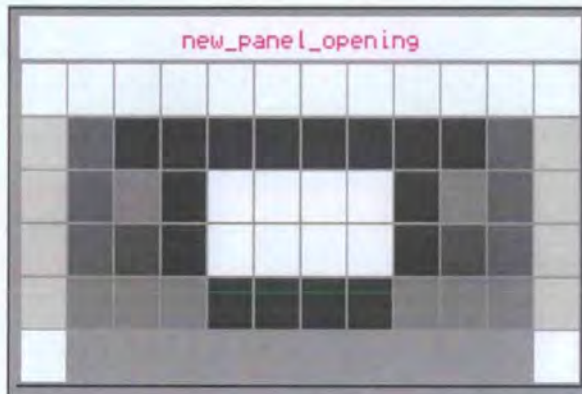






## APPENDIX C: CORRECTORS SELECTED BY THE CA

### 1. Panel SB02 with opening:



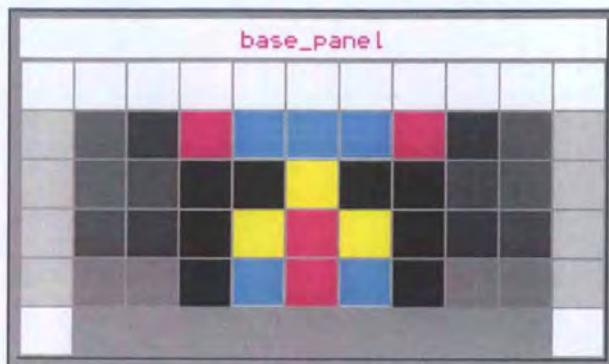
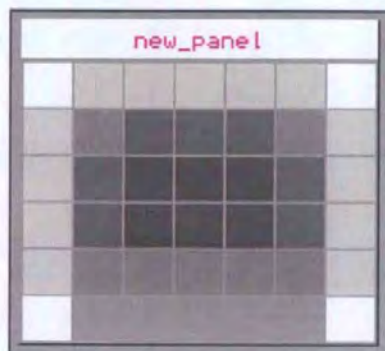
Note: Similar zones have the same colour.

new_panel_opening												
0.000	0.000	0.000	0.000	0.000	0.000	0.000	0.000	0.000	0.000	0.000	0.000	0.000
0.200	0.640	0.820	0.820	0.820	0.820	0.820	0.820	0.820	0.820	0.820	0.640	0.200
0.200	0.550	0.540	0.820	0.000	0.000	0.000	0.000	0.000	0.820	0.540	0.550	0.200
0.200	0.550	0.710	0.820	0.000	0.000	0.000	0.000	0.820	0.710	0.550	0.200	0.200
0.200	0.530	0.540	0.540	0.820	0.820	0.820	0.820	0.540	0.540	0.530	0.200	0.200
0.000	0.400	0.400	0.400	0.400	0.400	0.400	0.400	0.400	0.400	0.400	0.400	0.000

base_panel												
0.00	0.00	0.00	0.00	0.00	0.00	0.00	0.00	0.00	0.00	0.00	0.00	0.00
0.20	0.64	0.82	1.20	1.26	1.31	1.26	1.20	0.82	0.64	0.20	0.20	0.20
0.20	0.55	0.71	0.93	1.03	1.06	1.03	0.93	0.71	0.55	0.20	0.20	0.20
0.20	0.69	0.76	0.96	1.11	1.22	1.11	0.96	0.76	0.69	0.20	0.20	0.20
0.20	0.53	0.54	0.92	1.27	1.25	1.27	0.92	0.54	0.53	0.20	0.20	0.20
0.00	0.40	0.40	0.40	0.40	0.40	0.40	0.40	0.40	0.40	0.40	0.40	0.00

Note: Similar zones have the same corrector value. The parameter values in the cells adjacent to the four sides are the boundary parameter values. Free Edge = 0.0, Simply Support = 0.2 and Built-in Edge = 0.4.

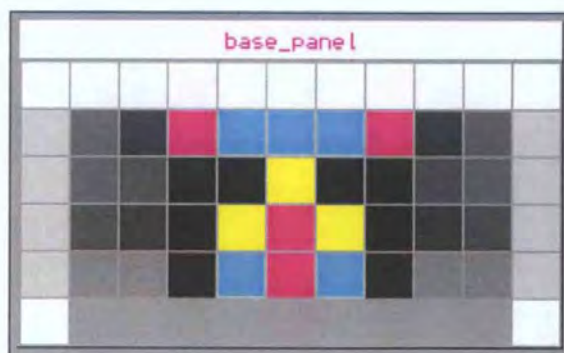
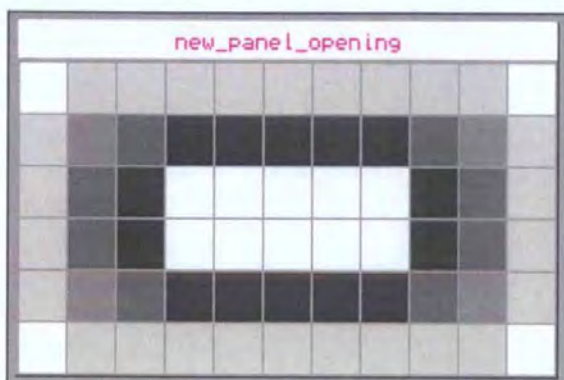
## 2. Panel SB06:



new_panel									
0	000	200	200	200	200	200	200	00	00
0	200	530	550	550	550	550	530	20	20
0	200	550	710	710	710	710	550	20	20
0	200	550	710	710	710	710	550	20	20
0	200	530	540	540	540	540	530	20	20
0	000	400	400	400	400	400	400	00	00

base_panel									
0	00	0	00	0	00	0	00	0	00
0	20	0	64	0	82	1	20	1	26
0	20	0	55	0	71	0	93	1	03
0	20	0	69	0	76	0	96	1	11
0	20	0	53	0	54	0	92	1	27
0	00	0	40	0	40	0	40	0	40

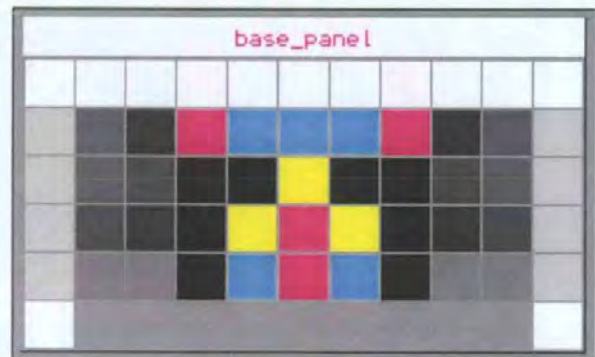
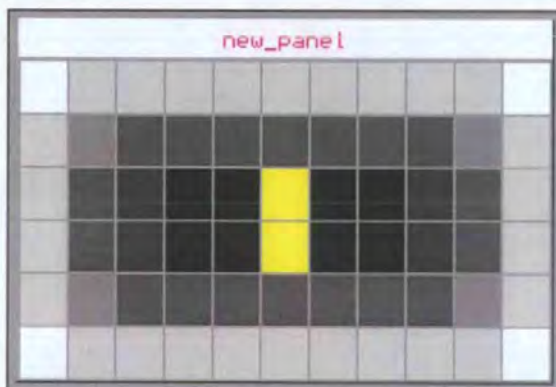
## 3. Wall 1a(ii) with opening:



new_panel_opening																			
0	00	0	20	0	20	0	20	0	20	0	20	00							
0	20	0	53	0	55	0	82	0	82	0	82	0	55	0	53	0	20		
0	20	0	55	0	82	0	00	0	00	0	00	0	00	0	82	0	55	0	20
0	20	0	55	0	82	0	00	0	00	0	00	0	00	0	82	0	55	0	20
0	20	0	53	0	55	0	82	0	82	0	82	0	82	0	55	0	53	0	20
0	00	0	20	0	20	0	20	0	20	0	20	0	20	0	20	0	00		

base_panel																					
0	00	0	00	0	00	0	00	0	00	0	00	00									
0	20	0	64	0	82	1	20	1	26	1	31	1	26	1	20	0	82	0	64	0	20
0	20	0	55	0	71	0	93	1	03	1	06	1	03	0	93	0	71	0	55	0	20
0	20	0	69	0	76	0	96	1	11	1	22	1	11	0	96	0	76	0	69	0	20
0	20	0	53	0	54	0	92	1	27	1	25	1	27	0	92	0	54	0	53	0	20
0	00	0	40	0	40	0	40	0	40	0	40	0	40	0	40	0	40	0	00		

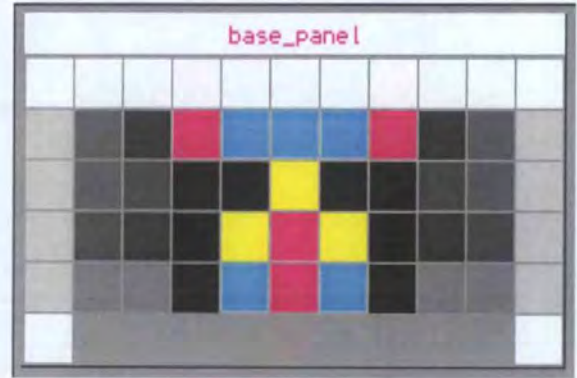
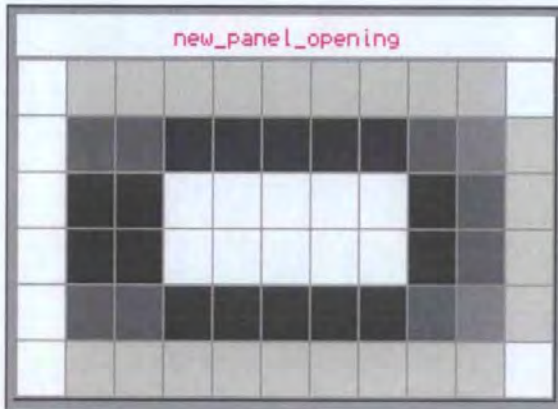
#### 4. Wall 1a. Control:



new_panel																					
0	00	0	20	0	20	0	20	0	20	0	20	00									
0	20	0	53	0	69	0	69	0	69	0	69	0	69	0	53	0	20				
0	20	0	69	0	76	1	03	0	96	1	11	0	96	1	03	0	76	0	69	0	20
0	20	0	69	0	76	1	03	0	96	1	11	0	96	1	03	0	76	0	69	0	20
0	20	0	53	0	69	0	69	0	69	0	69	0	69	0	69	0	53	0	20		
0	00	0	20	0	20	0	20	0	20	0	20	0	20	0	20	0	00				

base_panel																					
0	00	0	00	0	00	0	00	0	00	0	00	00									
0	20	0	64	0	82	1	20	1	26	1	31	1	26	1	20	0	82	0	64	0	20
0	20	0	55	0	71	0	93	1	03	1	06	1	03	0	93	0	71	0	55	0	20
0	20	0	69	0	76	0	96	1	11	1	22	1	11	0	96	0	76	0	69	0	20
0	20	0	53	0	54	0	92	1	27	1	25	1	27	0	92	0	54	0	53	0	20
0	00	0	40	0	40	0	40	0	40	0	40	0	40	0	40	0	40	0	00		

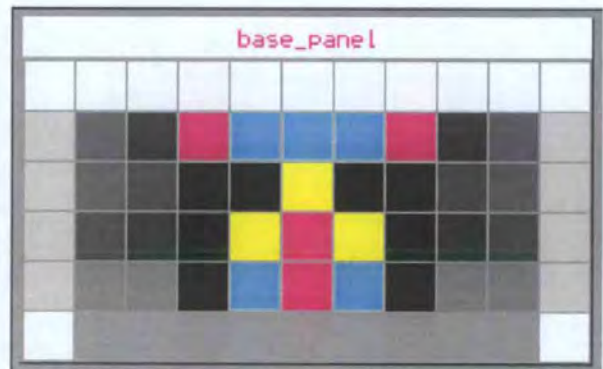
### 5. Wall 2a(i) with opening:



new_panel_opening																			
0	00	0	20	0	20	0	20	0	20	0	00								
0	00	0	64	0	55	0	82	0	82	0	53	0	20						
0	00	0	82	0	82	0	00	0	00	0	00	0	82	0	55	0	20		
0	00	0	82	0	82	0	00	0	00	0	00	0	00	0	82	0	55	0	20
0	00	0	64	0	55	0	82	0	82	0	82	0	82	0	55	0	53	0	20
0	00	0	20	0	20	0	20	0	20	0	20	0	20	0	20	0	20	0	00

base_panel																					
0	00	0	00	0	00	0	00	0	00	0	00	0	00	0	00	0	00	0	00		
0	20	0	64	0	82	1	20	1	26	1	31	1	26	1	20	0	82	0	64	0	20
0	20	0	55	0	71	0	93	1	03	1	06	1	03	0	93	0	71	0	55	0	20
0	20	0	69	0	76	0	96	1	11	1	22	1	11	0	96	0	76	0	69	0	20
0	20	0	53	0	54	0	32	1	27	1	25	1	27	0	32	0	54	0	53	0	20
0	00	0	40	0	40	0	40	0	40	0	40	0	40	0	40	0	40	0	40	0	00

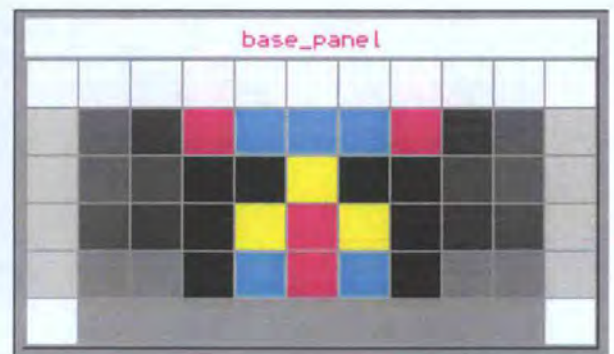
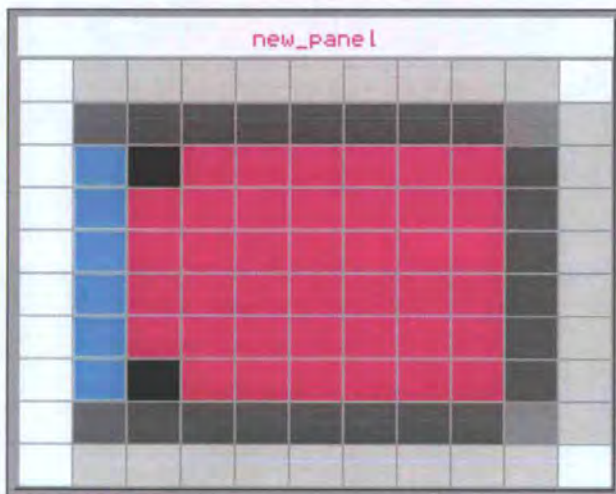
### 6. Wall 2a. Control:



new_panel										
0.000	0.200	0.200	0.200	0.200	0.200	0.200	0.200	0.200	0.200	0.000
0.000	0.640	0.550	0.550	0.690	0.690	0.690	0.690	0.550	0.530	0.200
0.000	0.820	0.710	0.710	0.761	0.091	0.090	0.760	0.710	0.550	0.200
0.000	0.820	0.710	0.710	0.761	0.091	0.090	0.760	0.710	0.550	0.200
0.000	0.640	0.550	0.550	0.690	0.690	0.690	0.690	0.550	0.530	0.200
0.000	0.200	0.200	0.200	0.200	0.200	0.200	0.200	0.200	0.200	0.000

base_panel										
0.000	0.000	0.000	0.000	0.000	0.000	0.000	0.000	0.000	0.000	0.000
0.200	0.640	0.821	1.201	1.261	1.311	1.261	1.200	0.820	0.640	0.200
0.200	0.550	0.710	0.991	1.091	1.061	1.090	0.990	0.710	0.550	0.200
0.200	0.690	0.760	0.961	1.111	1.221	1.110	0.960	0.760	0.690	0.200
0.200	0.530	0.540	0.921	1.271	1.251	1.270	0.920	0.540	0.530	0.200
0.000	0.400	0.400	0.400	0.400	0.400	0.400	0.400	0.400	0.400	0.000

### 7. Wall Case 7. Control:



new_panel										
0.000	0.200	0.200	0.200	0.200	0.200	0.200	0.200	0.200	0.200	0.000
0.000	0.640	0.690	0.690	0.690	0.690	0.690	0.690	0.690	0.530	0.200
0.000	1.261	1.091	1.221	1.221	1.221	1.221	1.221	1.221	0.690	0.200
0.000	1.311	1.221	1.221	1.221	1.221	1.221	1.221	1.221	0.690	0.200
0.000	1.311	1.221	1.221	1.221	1.221	1.221	1.221	1.221	0.690	0.200
0.000	1.311	1.221	1.221	1.221	1.221	1.221	1.221	1.221	0.690	0.200
0.000	1.311	1.221	1.221	1.221	1.221	1.221	1.221	1.221	0.690	0.200
0.000	1.261	1.091	1.221	1.221	1.221	1.221	1.221	1.221	0.690	0.200
0.000	0.640	0.690	0.690	0.690	0.690	0.690	0.690	0.690	0.530	0.200
0.000	0.200	0.200	0.200	0.200	0.200	0.200	0.200	0.200	0.200	0.000

base_panel										
0.000	0.000	0.000	0.000	0.000	0.000	0.000	0.000	0.000	0.000	0.000
0.200	0.640	0.821	1.201	1.261	1.311	1.261	1.200	0.820	0.640	0.200
0.200	0.550	0.710	0.991	1.091	1.061	1.090	0.990	0.710	0.550	0.200
0.200	0.690	0.760	0.961	1.111	1.221	1.110	0.960	0.760	0.690	0.200
0.200	0.530	0.540	0.921	1.271	1.251	1.270	0.920	0.540	0.530	0.200
0.000	0.400	0.400	0.400	0.400	0.400	0.400	0.400	0.400	0.400	0.000